Failure Mode Transition for Rock Cutting: Theoretical, Numerical and Experimental Modelling

by

Xianqun He

A thesis submitted for the degree of
Doctor of Philosophy

School of Civil, Environmental and Mining Engineering
Faculty of Engineering, Computer and Mathematical Sciences
The University of Adelaide

Dedication

This work is dedicated to my beloved parents.

Failure Mode Transition for Rock Cutting: Theoretical, Numerical and Experimental Modelling

By:

Xianqun He

Supervised by:

Associate Professor Chaoshui Xu, *Ph.D.,*
School of Civil, Environmental & Mining Engineering,
The University of Adelaide
and

Associate Professor Abdul Sheikh, *Ph.D.,*
School of Civil, Environmental & Mining Engineering,
The University of Adelaide

Thesis submitted in fulfillment of the requirements for the degree of
Doctor of Philosophy
School of Civil, Environmental & Mining Engineering
Faculty of Engineering, Computer and Mathematical Sciences
The University of Adelaide
North Terrace, Adelaide, SA 5005, Australia
Tel: +61(8) 8303 4323
Fax: +61(8) 8303 4359
Email: xianqun.he@adelaide.edu.au

Abstract

Rock cutting involves removing the rock material in front of the cutter when it moves against the rock at certain penetrating depth. The responses of rocks under cutting are influenced by rock properties such as mineral constituents, strength and fracture properties, as well as the operational parameters such as the depth of cut, cutting velocity and the back rake angle. A common approach to characterise the interaction between rock and cutter is to model the cutting forces. When the depth of cut is small, cutting forces show a linear relationship against the depth of cut, indicating a ductile-dominant failure mode. As the depth of cut increases, the rock cutting failure shifts from ductile-dominant mode to brittle-dominant mode and the cutting forces gradually deviate from the linear relationship. The depth of cut at which the dominant failure mode changes is termed the critical transition depth in rock cutting. The challenge lies in developing a generalised model for cutting force prediction based on rock properties and various complex cutting conditions while incorporating both ductile and brittle failure regimes.

In this thesis, the discrete element method (DEM) was employed to investigate the key rock properties that influence the failure pattern in rock cutting. It was demonstrated that rock (Brazilian) tensile strength (BTS) is as important as the uniaxial compressive strength (UCS) in the determination of the critical transition depth. The mineral grain size is also an important factor. Experiments were then carried out on two types of rock, namely Savonnières and Tuffeau limestone, to study changes in failure modes under different operational parameters of cutting velocity, back rake angle and depth of cut. Bažant’s size effect law was used for in-depth analysis of the cutting data, which performs exceptionally well in the quantification of the critical failure mode transition depth. These derived transition depths were then incorporated into the established generalised cutting force prediction model, which uses a more realistic assumption that the cutting failure is neither purely ductile nor purely brittle, but a combination of both.

It was demonstrated that the generalised cutting force prediction model captures reasonably well the cutting responses and failure mechanisms for the rock under various cutting conditions. The insights presented in this study will help in the understanding of rock cutting failure mechanisms and rock cutting mechanics and will be beneficial to the optimisation of tool design and rock cutting operations.

Statement of Originality

I, **Xianqun He**, hereby declare that this work contains no material which has been accepted for the award of any other degree or diploma in any university or other tertiary institution in my name and, to the best of my knowledge and belief, contains no material previously published or written by another person, except where due reference has been made in the text. In addition, I certify that no part of this work will, in the future, be used in a submission in my name, for any other degree or diploma in any university or other tertiary institution without the prior approval of the University of Adelaide and where applicable, any partner institution responsible for the joint-award of this degree.

I give consent to this copy of my thesis when deposited in the University Library, being made available for loan and photocopying, subject to the provisions of the Copyright Act 1968.

The author acknowledges that copyright of published works contained within this thesis resides with the copyright holder(s) of those works.

I also give permission for the digital version of my thesis being made available on the web, via the University's digital research repository, the Library catalogue, the Australian Digital Thesis Program (ADTP) and also through web search engines, unless permission has been granted by the University to restrict access for a period of time.

Signed: ……………………………………………Date: …………………..

Acknowledgments

This thesis marks a milestone on my road of research which was made possible via collaborations and supports of various persons, to whom I would like to express my gratitude. Many of them have accompanied and helped me in one way or the other when I was working on my project. Without their supports and encouragements, the production of this thesis would not be possible.

Firstly, I would like to express my gratitude to my principle supervisor Associate Professor Chaoshui Xu for the opportunity to work in the Deep Exploration Technologies Cooperative Research Centre at the University of Adelaide, for encouraging me to take steps towards my individual development and for granting me great flexibility and freedom in exploring the realms beyond the predetermined research paths. My gratitude also goes to my co-supervisor Associate Professor Abdul Hamid Sheikh, for his comments and feedback during my study.

I am highly indebted to those who helped me in many different aspects and made my time in Adelaide unforgettable. It was my pleasure to meet Dr Liang Huang, Dr Jinzhe Gong, Mr Adam Schwartzkopff, Ms Nimasha, Ms He Shi, Ms Qian Feng and Ms Zhiyuan Hu, just to name a few, for their friendship, ideas and patience in coping with all the ups and downs. Their companionship was a memorable part of my life at the University of Adelaide.

The financial supports from the Deep Exploration Technologies CRC and the University of Adelaide are greatly appreciated. The work has been supported by the Deep Exploration Technologies Cooperative Research Centre whose activities are funded by the Australian Government's Cooperative Research Centre Programme. This is DET CRC Document 2015/751.

Many thanks go to Luiz Franca for his generous support and constructive suggestions and Luis Mariano and Stephen Banks for their assistance in the sample preparation and the data collection during the laboratory testing at CSIRO's research centre in Perth. I am also very thankful to laboratory staff, Mr. Simon Golding, Mr. Adam Ryntjes and Mr. Ian Cates at the University of Adelaide for their assistance with the experimental works in Adelaide. Special thanks are given to Mr. Adam Ryntjes for his helpful discussions, excellent cooperation and patience.

My special thanks go to Mr Shaojin Yu, Mrs Chunlian He and Mr Yiping Zhang for their endless supports and inspirations, which keep me moving on.

Finally I am especially grateful to my parents for their love, understanding and endurance during my years away from home. Surely I would not be able to reach where I am standing now without their constant support and love throughout my life.

Table of Contents

List of Tables

List of Figures

Chapter 1

Introduction

1.1 Research background

Understanding the mechanics of rock cutting and developing a realistic modeling tool are extremely important for drill bit design and drilling optimisation. In the mining industry, one of the most significant challenges worldwide is to find new resources to replace those currently being mined. Inevitably the future for minerals exploration and mining is going to involve increasingly deep drill holes and deep mines as most of the accessible surface resources become depleted. While operations are forced to mine from deeper locations, the radical deterioration of drilling conditions due to the extreme depth gives rise to current deficiencies in the understanding of the drilling mechanism and in the optimization of the drilling operation under complex conditions. The problem is further compounded by the inability to meaningfully observe the drilling process and the bit-rock interaction in real time, as well as the unpredictable heterogeneity of the rock material being drilled. The whole bit drilling model can be extrapolated from the superimposition of the contributions made by each single cutter element. Thus, the key to a successful characterisation of the drilling process for the whole bit requires a better understanding of the rock failure and cutting mechanics under the consideration of the cutter-rock interaction mechanisms with a single cutter element.

In modelling rock cutting, the majority of efforts have been given to describe the interaction between rocks and various cutters, involving theoretical analysis, numerical simulations and experimental validations. Inspired by the cutting theory for metal cutting first proposed by Merchant (1944), various rock cutting theories have been developed analytically to make prediction for the cutting forces at the cutter-rock interface. Some focus on the relationship between the cutting forces and stress status induced by the forces (Conway and Kirchner 1980; Shah and Wong 1997); some try to correlate cutting forces with rock strengths (compression, tension and shear) and geometrical parameters under different cutting conditions (Evans 1958; Evans 1984; Fairhurst and Lacabanne 1957; Goktan and Gunes 2005); and on the other hand, some make cutting force predictions in terms of energy dissipation and utilisation (Bao et al. 2011; Detournay and Defourny 1992; Detournay et al. 2008; Rånman 1985).

In addition to these analytical models, the rock cutting mechanisms have also been investigated experimentally by single cutter cutting/scratching tests (Hogan et al. 2012; Richard et al. 2012; Tanovic et al. 2009; Wang and Clausen 2002) and numerically (Huang et al. 1999; Rojek et al. 2011; Stavropoulou 2006; Su and Akcin 2011). Recently, a variety of experiments have been done to explore the intrinsic dependences of cutting forces on rock mechanical properties (Huang and Detournay 2008; Richard et al. 2012; Schei et al. 2000). In addition, Wang and Clausen (2002) demonstrated that the material removal process in marble cutting by single point cutting tool is dominated by plastic deformation as well as brittle chipping. Hogan et al. (2012) studied the fracture behaviours of albite and quartz under cutting by a single diamond and they concluded that the material removal process can be associated with material properties, such as fracture toughness, hardness and melting temperature of rocks.

In terms of numerical simulations, preliminary two-dimensional studies of rock cutting using DEM demonstrated that DEM model could reproduce the behaviours that feature brittle and ductile failures observed in experiments using cutting tools of simple geometry (Huang et al. 1999; Rizo 2010; Stavropoulou 2006). Subsequent research expanded the study to include variations in cutting tool geometry, such as the work completed by Rojek et al. (2011) who used a pick commonly found on various tunnelling machines, and Labra et al. (2008) who modelled pick designs implemented on road headers. The three-dimensional numerical modelling of rock cutting is only possible due to the advance in computer technology but there are still limited published results. Currently the 3D model is mostly based on the 2D modelling of cutting picks commonly used in tunnelling machines and road headers, but with the addition of the third dimension. The idealised planar picks could now be represented with their true conical shape in numerical models (Rojek et al. 2010; Su and Akcin 2011). These numerical models in general aim to reproduce what are observed in laboratory tests and to serve as a supplementary tool to study the insight mechanisms of some cutting scenarios that are difficult to deal with using existing laboratory techniques.

Based on the results obtained from experiments and numerical simulations, various aforementioned analytical formulations were proposed to characterise the interaction between rock and cutting tool. Despite some great improvements in the analytical models, different models often generate significantly different prediction results based on different rock properties and varying cutting conditions (Su and Akcin 2011). In particular, most of these models were developed for material cutting in a strength-driven process, which are not in general applicable to rocks undergoing brittle mode cutting where the cutting action becomes mainly a fracturing-dominated process. Based on large amount of experimental tests, it is demonstrated that there are two failure modes observed during rock cutting: ductile failure, occurring at shallow cutting depths, characterised by crushing of particles at the tip of the cutting tool and shearing of rocks in front of the tool; and brittle failure, featured by the development and propagation of macroscopic cracks ahead of the cutting tool when cutting at greater depths (Richard et al. 2012). Due to the differences between these two failure modes, the force prediction model based on the ductile failure mode (the strength-driven model) fails to estimate the cutting forces correctly when the cutting is actually in the brittle-dominant failure regime.

Therefore, the validity of using these models should be evaluated carefully based on relevant cutting mechanisms. A more robust modelling tool would be one that has more comprehensive views on different cutting mechanisms and considers different failure modes accordingly based on rock properties and different cutting conditions.

1.2 Research objectives

The focus of this thesis is to derive a generalised model for cutting force prediction by considering the coexistence of ductile failure and brittle failure modes commonly observed in rock cutting for different rock properties and cutting parameters. In order to achieve this goal, the research involved both experimental tests and numerical simulations. The detailed research objectives are summarised below.

1. ***Identify the key factors influencing the responses of rocks subjected to various cutting conditions***. This objective was addressed by rock cutting numerical simulations using DEM on two types of synthetic rock specimens with nearly identical UCS but different brittleness (defined as the ratio of UCS to BTS) (Chapter 2). The numerical model was quantitatively validated against experimental results obtained from laboratory cutting tests (Chapter 4).

2. ***Determine the role of rock properties and cutting operational parameters on the failure transition behaviour of rock specimens***. This objective was addressed experimentally by investigating the individual impact of cutting velocity, back rake angle and depth of cut on the cutting mode transition. A specific cutting energy transition model was established to study the relationship between these parameters and the failure mechanisms (Chapter 3).

3. ***Investigate the effect of back rake angle on the critical failure transition depth***. This objective was addressed experimentally by

conducting cutting tests on two types of rocks with three different back rake angles. The depth of cut was increased gradually to ensure the presence of brittle chippings. The size effect law was then introduced to determine the specific value for the critical transition depth. The results derived from the size effect law were compared with those from the specific cutting energy transition model developed in Chapter 3. Visual inspection of the cut surface was used to assess the validity of these two approaches for the quantitative determination of the critical transition depth (Chapter 4)

4. ***Devise a generalised force prediction model for various cutting scenarios, in which both ductile failure and brittle failure are incorporated***. This objective was addressed by the development of a framework where the total energy is regarded to be dissipated proportionally in ductile-regime failure and brittle-regime failure. For the ductile failure, the cutting force is dependent on rock UCS while for the brittle failure it is associated with the rock fracture toughness. In addition, this proposed model also incorporates the influence of cutting operational parameters such as the back rake angle and the depth of cut (Chapter 5).

1.3 Thesis overview

This thesis consists of six chapters and is in the format of a thesis by publication. In addition to this Introduction chapter, the main part of the thesis (Chapters 2 to 5) presents the research contributions and outcomes, which are reported and prepared in the format for academic journal publication. Each chapter contains its own introduction and literature review. Therefore, background materials on cutting force modelling, rock cutting failure regimes and effects of rock properties and operational parameters on the cutting force responses are described as needed in Chapters 2 to 5.

Chapter 2 presents numerical simulations on ductile failure mode cutting versus brittle failure mode cutting using the distinct element method (DEM). Two types of synthetic rocks were used to simulate the rock cutting process: one uses conventional synthetic rock generation process that produces an unrealistic strength ratio while the other uses a proposed cluster approach that can result in a more realistic strength ratio matching the values of some real rocks. The details of the force responses of the synthetic rock under cutting are recorded, including the force profile and the events of fracturing, to demonstrate the effect of tensile strength on the cutting failure regime transition. The numerical results are then compared with the fracture patterns of available cutting experiments. This chapter was published in the *International Journal for Numerical and Analytical Methods in Geomechanics* (Xianqun He and Chaoshui Xu, 2015a).

Chapter 3 investigates experimentally the ductile to brittle failure mode transition and its influencing factors including rock properties and cutting operational parameters, such as the cutting velocity, the depth of cut and the back rake angle. The cutting/scratching techniques were explained and a comprehensive set of cutting tests were carried out on two types of rocks and 140 combinations of different cutting parameters for each type of rock. A new model to identify the critical failure mode transition depth, termed the specific cutting energy transition model, was developed based on the evolution of the specific cutting energy. Discussions on the critical transition depth at which the dominant failure mode changes with respect to different rock properties and cutting parameters are presented. This chapter was submitted to *Rock Mechanics and Rock Engineering* and is currently published online (Xianqun He and Chaoshui Xu, 2015b).

Chapter 4 further discusses the effect of the back rake angle on the failure mode transition since it is a key operational parameter affecting the critical transition depth, as suggested in Chapter 3. The depth of cut in experiments was set to be large enough to ensure the occurrence of failure transition at different transition depths for different rocks and different back rake angles.

The application of size effect law in failure mode transition analysis is then introduced. A comparison study in terms of the reliability in determining the critical failure transition depth using the size effect law and the specific cutting energy transition model proposed in Chapter 3 is presented. This chapter has been submitted to the *Journal of the Mechanics and Physics of Solids* (Xianqun He and Chaoshui Xu, 2015c).

Chapter 5 describes a generalised model for predicting the rock cutting forces arising from the interaction between cutter and rock. The model considers rock properties and cutting geometry for cases where the brittle failure and ductile failure modes coexists. This force prediction model is established based on the principle of energy balance. It is assumed that the total energy, dissipated in plastic flow as well as brittle fracturing, is the product of the tangential component of the cutting force and cutting distance and that at the critical transition depth the energy consumed in ductile failure is equal to that in brittle failure. The performance of this new generalised cutting force model is then compared with other models based on either purely ductile failure mechanism or purely brittle failure mechanism and it is demonstrated that the proposed model is able to give much better predictions compared with existing models. This chapter has been submitted to the *International Journal of Rock Mechanics and Mining Sciences* (Xianqun He and Chaoshui Xu, 2015d).

Chapter 6 summarises the main contributions and conclusions. In addition, the limitations of this research are discussed together with some recommendations for future works.

References

Bao RH, Zhang LC, Yao QY, Lunn J (2011) Estimating the Peak Indentation Force of the Edge Chipping of Rocks Using Single Point-Attack Pick. Rock Mechanics and Rock Engineering 44:339-347 doi:10.1007/s00603-010-0133-2

Conway JC, Kirchner HP (1980) The mechanics of crack initiation and propagation beneath a moving sharp indentor. Journal of Materials Science 15:2879-2883 doi:10.1007/bf00550558

Detournay E, Defourny P (1992) A phenomenological model for the drilling action of drag bits. International Journal of Rock Mechanics and Mining Sciences & Geomechanics Abstracts 29:13-23 doi:10.1016/0148-9062(92)91041-3

Detournay E, Richard T, Shepherd M (2008) Drilling response of drag bits: Theory and experiment. International Journal of Rock Mechanics and Mining Sciences 45:1347-1360 doi:10.1016/j.ijrmms.2008.01.010

Evans I (1958) Theoretical aspects of coal ploughing. Mechanical Properties of Non-Metallic Brittle Materials:451

Evans I (1984) A theory of the cutting force for point-attack picks. International Journal of Mining Engineering 2:63-71 doi:10.1007/bf00880858

Fairhurst C, Lacabanne W (1957) Hard rock drilling techniques. Mine and Quarry Engineering 23:157-161

Goktan R, Gunes N (2005) A semi-empirical approach to cutting force prediction for point-attack picks. JS Afr Inst Min Metall 105:257-263

Hogan JD, Rogers RJ, Spray JG, Boonsue S (2012) Fracture and fragmentation of quartz and albite during single-diamond sliding-point contact. Engineering Fracture Mechanics doi:10.1016/j.engfracmech.2012.07.020

Huang H, Detournay E (2008) Intrinsic length scales in tool-rock interaction. International Journal of Geomechanics 8:39-44

Huang H, Detournay E, Bellier B (1999) Discrete element modeling of rock cutting. Rock Mechanics for Industry

Labra C, Rojek J, Oñate E, Zarate F (2008) Advances in discrete element modelling of underground excavations. Acta Geotechnica 3:317-322 doi:10.1007/s11440-008-0071-2

Merchant ME (1944) Basic mechanics of the metal cutting process. Journal of Applied Mechanics 11:168-175

Rånman K (1985) A model describing rock cutting with conical picks. Rock Mechanics and Rock Engineering 18:131-140 doi:10.1007/bf01019602

Richard T, Dagrain F, Poyol E, Detournay E (2012) Rock strength determination from scratch tests. Engineering Geology 147-148:91-100 doi:10.1016/j.enggeo.2012.07.011

Rizo JAM (2010) Modeling rock cutting using dem with crushable particles. University of Pittsburgh

Rojek J, Labra C, Oñate E Discrete element simulation of rock cutting processes. In, 2010. pp 1040-1044

Rojek J, Oñate E, Labra C, Kargl H (2011) Discrete element simulation of rock cutting. International Journal of Rock Mechanics and Mining Sciences 48:996-1010 doi:10.1016/j.ijrmms.2011.06.003

Schei G, Fjær E, Detournay E, Kenter CJ, Fuh GF, Zausa F (2000) The Scratch Test: An Attractive Technique for Determining Strength and Elastic Properties of Sedimentary Rocks. Paper presented at the SPE

Annual Technical Conference and Exhibition, Dallas, Texas, 1-4 October 2000

Shah KR, Wong TF (1997) Fracturing at contact surfaces subjected to normal and tangential loads. International Journal of Rock Mechanics and Mining Sciences 34:727-739 doi:10.1016/s1365-1609(97)00007-7

Stavropoulou M (2006) Modeling of small-diameter rotary drilling tests on marbles. International Journal of Rock Mechanics and Mining Sciences 43:1034-1051 doi:10.1016/j.ijrmms.2006.03.008

Su O, Akcin NA (2011) Numerical simulation of rock cutting using the discrete element method. International Journal of Rock Mechanics and Mining Sciences 48:434-442 doi:10.1016/j.ijrmms.2010.08.012

Tanovic LJ, Bojanic P, Puzovic R, Klimenko S (2009) Experimental Investigation of Microcutting Mechanisms in Marble Grinding. Journal of Manufacturing Science and Engineering-Transactions of the Asme 131 doi:10.1115/1.4000619

Wang CY, Clausen R (2002) Marble cutting with single point cutting tool and diamond segments. International Journal of Machine Tools and Manufacture 42:1045-1054 doi:10.1016/s0890-6955(02)00032-9

Chapter 2

Discrete element modelling of rock cutting: from ductile to brittle transition

(Paper 1)

Xianqun He and Chaoshui Xu

Deep Exploration Technologies Cooperative Research Centre, School of Civil, Environmental and Mining Engineering, the University of Adelaide, Australia

Publication:

He X. and Xu C. (2015a) Discrete element modelling of rock cutting: from ductile to brittle transition. *International Journal for Numerical and Analytical Methods in Geomechanics* 39: 1331-1351 doi:10.1002/nag.2362.

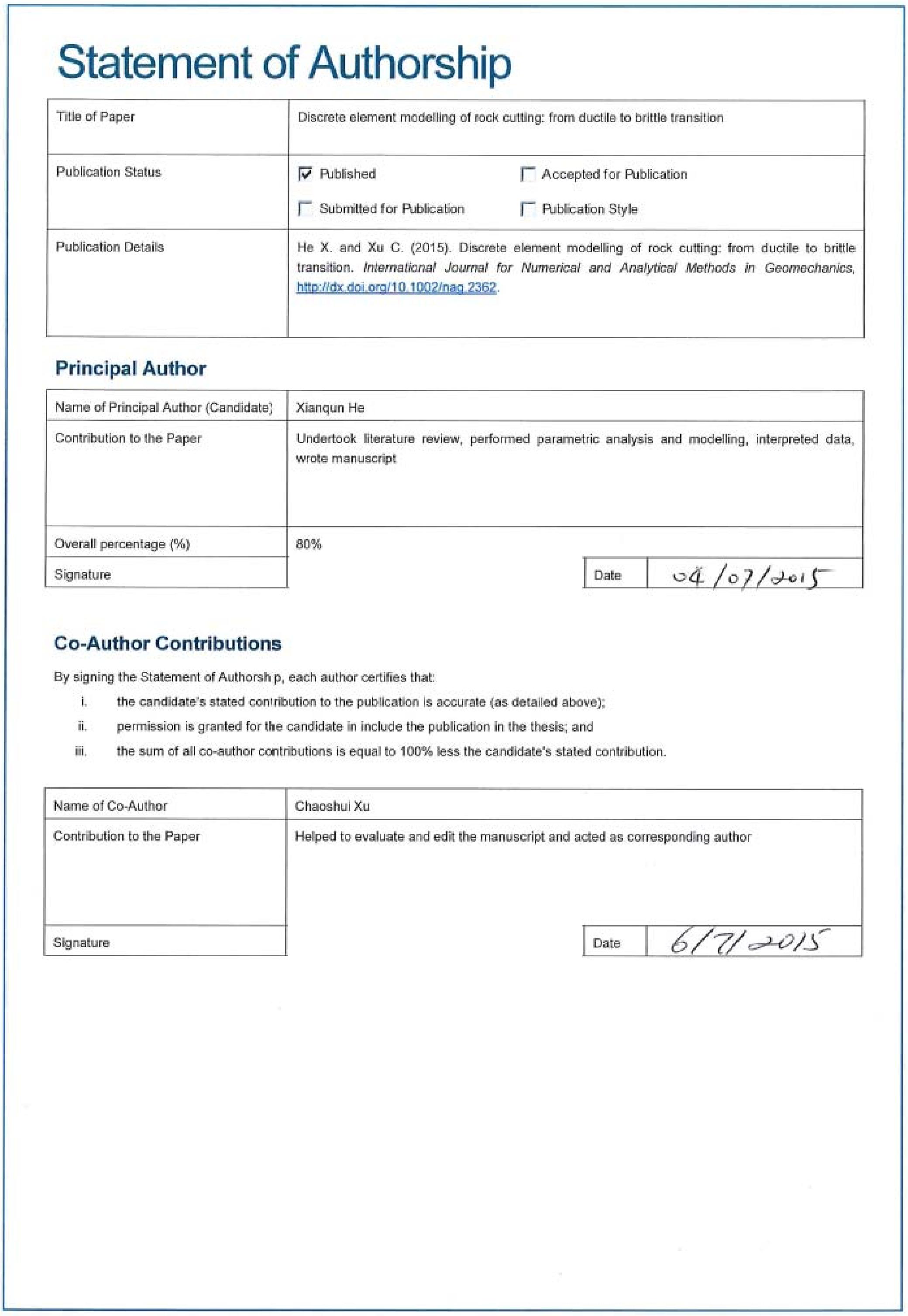

Statement of Authorship

Title of Paper	Discrete element modelling of rock cutting: from ductile to brittle transition
Publication Status	☑ Published ☐ Accepted for Publication ☐ Submitted for Publication ☐ Publication Style
Publication Details	He X. and Xu C. (2015). Discrete element modelling of rock cutting: from ductile to brittle transition. *International Journal for Numerical and Analytical Methods in Geomechanics*, http://dx.doi.org/10.1002/nag.2362.

Principal Author

Name of Principal Author (Candidate)	Xianqun He		
Contribution to the Paper	Undertook literature review, performed parametric analysis and modelling, interpreted data, wrote manuscript		
Overall percentage (%)	80%		
Signature		Date	04/07/2015

Co-Author Contributions

By signing the Statement of Authorship, each author certifies that:

i. the candidate's stated contribution to the publication is accurate (as detailed above);

ii. permission is granted for the candidate in include the publication in the thesis; and

iii. the sum of all co-author contributions is equal to 100% less the candidate's stated contribution.

Name of Co-Author	Chaoshui Xu		
Contribution to the Paper	Helped to evaluate and edit the manuscript and acted as corresponding author		
Signature		Date	6/7/2015

Abstract

It is well accepted that there is a transition of failure mode from ductile to brittle with increasing depth of cut during rock cutting process. Rock failure modes affect cutting efficiency and knowledge of the failure transition is essential to the determination of optimum cutting parameters. The critical transition depth can be linked with rock properties. In this study, an attempt was made to model rock cutting process and to check the dependence of the critical failure mode transition depth on the brittleness of rock. For this purpose, dimensional analysis was first performed to establish the correlations between rock macro-properties and micro-parameters for discrete element simulations. Following the specimen calibration procedure, two types of synthetic rocks having approximately the same uniaxial compressive strength were generated as the synthetic specimens for simulating the rock cutting process. The first specimen was created using conventional model construction method with identical bond strengths between particles, giving rise to undesirably high indirect tensile strength. The second specimen was created using a proposed clustering algorithm such that the ratio between the tensile and compressive strength matches reasonably well with that of real rocks. The results of rock cutting simulations demonstrate that failure mode transition took place in both models, but for the clustered model the transition emerged at a shallower cutting depth. A further exploration was made to derive the critical depth for this transition based on the simulations performed on the clustered models. The derived relationship indicates that the critical transition depth decreases as strength ratio or brittleness of the rock increases. This provides a very useful tool for predicting the critical transition depth which can be used to help cutting tool design and cutting parameter optimisations.

***Keywords*:** rock cutting; failure mode; brittleness; strength ratio; fracture toughness

2.1 Introduction

Mechanical rock cutting in various forms is widely used in mining and civil engineering in areas such as drilling (Franca and Lamine 2010), tunnelling (Moon and Oh 2012) and grinding (Tanovic et al. 2009). To understand the rock cutting mechanism, laboratory rock cutting tests have been the most direct and reliable source. Experimental studies of rock cutting enables better understanding of rock-tool interactions and their outcomes can be used to establish the relationships between cutting forces and various influencing factors (Bilgin et al. 2006; Che et al. 2012). However, experiments are in general expensive and sometimes they are difficult to be carried out or to provide reliable results. As an alternative, numerical modelling, using either finite element method (FEM) or discrete element method (DEM), can provide a faster and cheaper method of investigating the cutting process. A number of numerical investigations on rock cutting have been implemented based on FEM (e.g., (Liu et al. 2002; Liu et al. 2008; Menezes et al. 2014)), but the analysis, in many cases, can only model the major chip formation and is unable to deal with the post-failure bahaviour. On the other hand, DEM provides a more suitable platform to simulate rock failure under cutting as it allows the simulation of damage, chip formation and crack initiation, propagation and coalescence (Ledgerwood 2007; Rojek et al. 2011; Stavropoulou 2006; Su and Akcin 2011). DEM is also the tool used in this study.

Most experimental, analytical and numerical models from the literature aimed to characterise the forces arising from the tool-rock contact under different configurations. Richard et al. (1998), however, focused particularly on rock failure mode transition during cutting and they concluded that there are two distinct failure modes in rock cutting. One is ductile failure (Fig. 2.1a) occurring at shallow cutting depths typically less than 1 mm for sandstones, characterised by crushing of particles at the tip of the cutting tool and shearing of rock in front of the tool. The other one is brittle failure (Fig. 2.1b) when cutting at greater depths, characterised by the development and propagation of macroscopic cracks ahead of the cutting tool. In terms of cutting forces, Richard et al. (1998) further argued conceptually that: for the failure mode in the ductile regime, the cutting force is related to the uniaxial compressive strength σ_c as $F_d \propto \sigma_c W d$, where W is the cutting width and d the cutting depth, and, in the brittle regime, the cutting force is related to the mode I fracture toughness as $F_b \propto K_{IC} W \sqrt{d}$. Using $F_d = F_b$, the transition of failure mode from ductile to brittle can be found to take place at a critical depth of $d_c \propto \left(K_{IC}/\sigma_c\right)^2$. In rock cutting, one important indicator for rock cuttability and cutting efficiency is specific energy (Yaşar et al. 2011). Different cutting modes are associated with different specific energy (Richard et al. 1998) as the brittle-mode cutting obviously has lower specific energy due to the large cutting volume. The selection of a suitable cutting tool for optimal cutting performance, to a great extent, is associated with the correct identification of the cutting mode at various cutting arrangements with different rocks. It is therefore important to understand the cutting mode transition under different conditions.

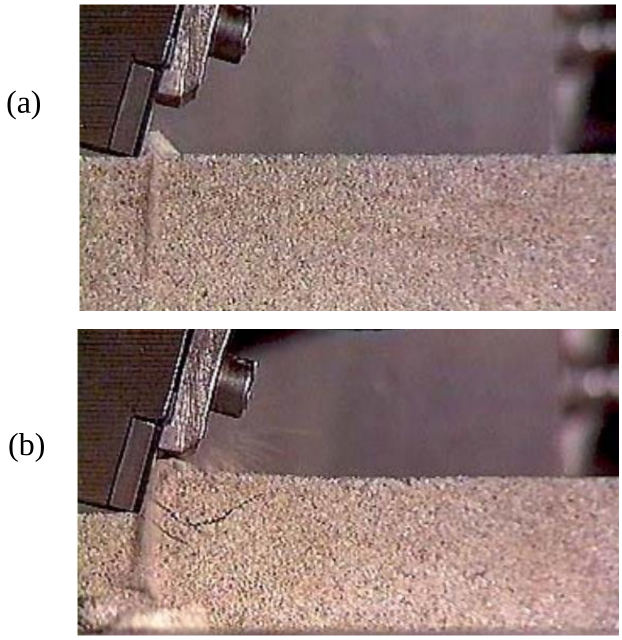

Fig. 2.1 Material removal in (a) ductile mode at a depth of cut d =0.3 mm and (b) brittle mode at d =3 mm during cutting tests on slab sample of Vosges sandstone (after Richard (1999)).

In terms of numerical investigations dealing with failure mode transition, the first one was reported by Huang (1999) using two dimensional Particle Flow Code (PFC2D). The code was further successfully employed by Huang and Detournay (2008) to simulate the transition of failure from ductile to brittle regime with increasing depth of cut. They used the term of "intrinsic length scale" to describe the ratio between K_{IC} and σ_c, expressed as $l_{in} = \left(K_{IC}/\sigma_c\right)^2$, which is proportional to the critical depth of cut d_c as discussed above. However, the simulation results indicated the ratio of d_c/l_{in} is approximately 12 compared with the experimental values of 2 ~ 3. This overestimation was considered to be caused by the low ratio between compressive and tensile strengths of the synthetic rock samples used for the numerical simulations (Huang et al. 2013).

In fact, the ratio of uniaxial compressive strength σ_c to tensile strength σ_t, known as strength ratio, plays a significant role in characterising the brittleness of rocks. Although the definition for brittleness varies for different applications (Atici and Ersoy 2009; Hucka and Das 1974; Kahraman 2002; Yarali and Kahraman 2011), in this study the rock brittleness is defined as $B = \sigma_c/\sigma_t$ considering the fact that the discrepancy between σ_c and σ_t increases with brittleness (Göktan 1991). Despite the dominant usage of σ_c as a rock strength parameter in engineering practice, it is well known that rocks can easily have brittle failure under tension (Hucka and Das 1974). It is surprising how little is done with regard to the calibration of a realistic strength ratio σ_c/σ_t when using DEM to model rock cutting processes. Most studies consider only the calibration of σ_c (Ledgerwood 2007; Mendoza et al. 2011; Stavropoulou 2006) while some others who did consider the ratio only used unrealistically low values (Huang and Detournay 2008; Moon and Oh 2012). These problems are mainly due to the limitations of the conventional DEM configuration which cannot guarantee the matching of both σ_c and σ_t to those of a rock simultaneously (Scholtès and Donzé 2013).

In this research, we propose the use of DEM assemblies composed of clusters by bonding fine particles to generate synthetic rock samples so that more realistic strength ratios of σ_c/σ_t can be obtained. Note clusters used here are different to clumps in DEM. Clumps are commonly used in DEM to model irregularly shaped particles by bonding together a collection of circular (2D) or spherical (3D) particles which are not breakable regardless of the forces acting upon them (Cho et al. 2007). Clustered particles proposed here can break once the stress acting on the bond exceeds its strength.

In our work, numerical simulations of uniaxial compressive strength (UCS) and Brazilian tensile strength (BTS) tests on clustered specimens are carried out to investigate the feasibility of the strength ratio improvement. Once a suitable set of micro-mechanical parameters to achieve the desired strength ratio are obtained, a series of rock cutting simulations are performed on the clustered particle assemblies (CPA) to establish a more realistic prediction of the critical depth of cut for the failure mode transition. As a comparison, rock cutting simulations are also performed on synthetic samples using non-clustered particle assemblies (NCPA).

2.2 Determination of rock model parameters

DEM was initially proposed by Cundall (1971) to represent rock masses as “blocky rock systems”. The constituent discrete components (termed particles or balls) of the assembly are either rigid discs in 2D or rigid spheroids in 3D. When the system is subjected to mechanical actions, these particles can overlap or detach and the movement of particles follows Newton’s law of motion whilst the interaction of particles is described via contact laws. Contact force between particles arises whenever two particles come into contact and thus is related to the degree of overlaps (simulating the particle deformations) and the contact stiffness, see a general view of ball-ball contact depicted in Fig. 2.2. The contact force (F^i) has a normal (F_n^i) and a shear

(F_s^i) component at each contact point (x_i) which is defined by a unit normal vector n_i. The normal and shear contact force vectors are determined by Eqs. (2.1) and (2.2), respectively (Potyondy and Cundall 2004):

$$F_n^i = k_n U_n n_i \tag{2.1}$$

$$\Delta F_s^i = -k_s \Delta U_s \tag{2.2}$$

where k_n and k_s are the normal and shear stiffness at the contact, U_n is the overlap between two particles in the normal direction, ΔF_s^i is the shear contact force increment and ΔU_s is shear displacement increment.

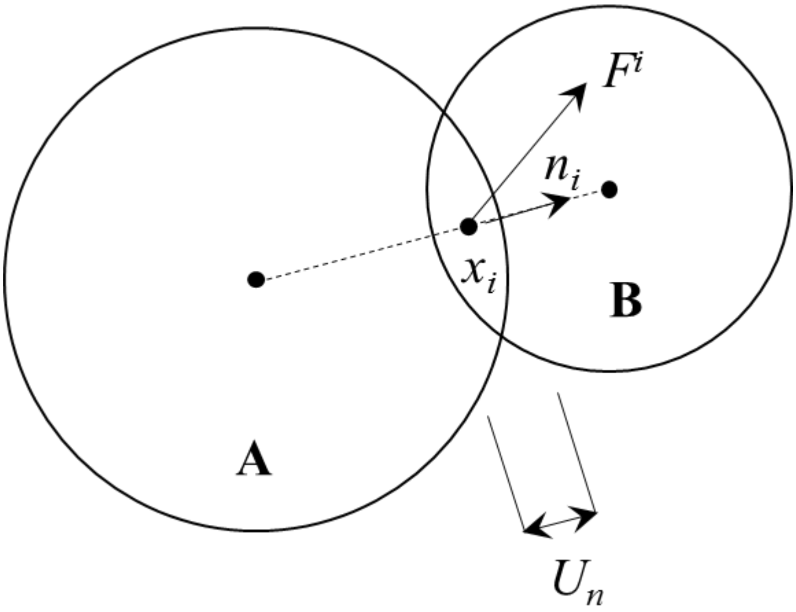

Fig. 2.2 Schematic view describing a ball-ball contact (after Potyondy and Cundall (2004)).

Note that k_n is a secant stiffness which relates normal force to total overlap owing to relative position change between particles whereas the shear stiffness k_s is a tangent value and thus the shear contact force vector is calculated in an incremental manner. F_s^i is initialized to 0 when a contact is formed. Each subsequent relative shear displacement increment ΔU_s is accumulated to calculate the shear force vector F_s^i.

Due to its discontinuous nature, DEM is capable of dealing with the initiation and propagation of micro-cracks inside heterogeneous media and therefore provides a suitable tool to study the fracture behaviour of brittle materials. However, a serious limitation lies in the fact that a high σ_c/σ_t ratio, representative of brittle rock materials, cannot be achieved for synthetic specimen created using only individual particles regardless of the micromechanical parameters used (Potyondy and Cundall 2004). As a preliminary approach to address the issue, discrete models considering the interlocking effect between particles were introduced by clustering particles to form complex-shaped larger particles to study how the cluster size affects the strength envelope and the σ_c/σ_t values (Cho et al. 2007; Potyondy and Cundall 2004). Despite of these encouraging works, in these clustered models, the intra-cluster bonds were assigned with extremely high strengths and therefore cracking was only allowed to occur along the cluster boundaries where a much lower inter-cluster bond strength is used (the white dots in the enlarged view in Fig. 2.3, see below). As a consequence, grain crushing phenomenon, commonly observed in laboratory cutting experiments, could not be reproduced in these numerical models. Another approach to address the issue of unrealistic σ_c/σ_t ratio is to enhance the microstructure of a particle assemblage by increasing the number of bonds associated with each particle. Other similar DEM simulations with regard to the study of the strength ratio include Fakhimi (2004), Scholtès and Donzé (2013) and Donze et al. (1997).

In this study, we use the bonded-particle model (BPM) proposed in Potyondy and Cundall (2004). BPM allows particles to be bonded together at contacts and to separate when either the normal or shear stress exceeds the corresponding bonding strength. In BPM, there are two types of bonds, namely contact bond and parallel bond. A contact bond has no contact area and can only resist forces acting at the contact point. A parallel bond, however, assumes a bonded area between particles. The key difference is that parallel bonds can resist moment acting across the contact. For the purpose of forming the particle clusters, the contact bond is used in this study, keeping force-displacement behaviour of contacts consistent with that described in Huang et al. (2013). The contact bond also simplifies the dimensional relationships proposed below as only two parameters (normal and shear strengths) are needed to define a contact bond, compared to five for a parallel bond (Potyondy and Cundall 2004). Within this context, a NCPA can be regarded as a special case of CPA with identical bonding strength assigned to all inter-cluster and intra-cluster contacts within the assembly.

Determination of suitable model parameters is essential for the successful implementation of DEM. For the current study, the methodology developed by Huang (1999) was applied to determine the micromechanical parameters, based on the combination of dimensional analysis and numerical simulations of standard laboratory tests for rocks such as UCS test and BTS test. To describe the motion and interaction between particles in BPM for non-clustered and clustered assemblies, the following three sets of parameters are required (Huang et al. 2013; Stavropoulou 2006):

(a) Geometrical and physical parameters:

$\overline{R}$ $[L]$ = average particle radius;

ρ $[F{\cdot}L^{-4}{\cdot}T^{2}]$ = density of particles;

n [–] = porosity of the non-clustered assembly.

S [–] = size of cluster, i.e., the number of particles in a cluster.

(b) Constitutive parameters for contacts between particles:

k_n $[F{\cdot}L^{-1}]$ = ball-ball contact normal stiffness;

k_s $[F{\cdot}L^{-1}]$ = ball-ball contact shear stiffness;

T_n $[F{\cdot}L^{-1}]$ = normal bonding strength for non-clustered assembly;

T_s $[F{\cdot}L^{-1}]$ = shear bonding strength for non-clustered assembly;

T_n^{in} $[F{\cdot}L^{-1}]$ = intra-cluster normal bonding strength for clustered assembly;

T_s^{in} $[F{\cdot}L^{-1}]$ = intra-cluster shear bonding strength for clustered assembly;

T_n^{bt} [$F \cdot L^{-1}$] = inter-cluster normal bonding strength for clustered assembly;

T_s^{bt} [$F \cdot L^{-1}$] = inter-cluster shear bonding strength for clustered assembly;

μ [–] = ball-ball contact friction coefficient.

(c) Loading condition parameters:

L [L] = characteristic dimension of the model;

V [$L \cdot T^{-1}$] = loading velocity,

where $\left[L, F, T\right]$ represent the primary dimensions of length, force and time respectively.

2.2.1 Dimensionless micro parameters

Here we search for functions that associate the microscopic parameters with the macroscopic properties of rocks including the phenomenological elastic constants (Young's modulus E, Poisson's ratio ν), uniaxial compressive strength σ_c and tensile strength σ_t. Dimensional analysis is performed based on Buckingham π theorem (Yang et al. 2006) which describes that a physically meaningful equation $\varphi(q_1, q_2 ..., q_n) = 0$, where q_i are n physical variables, can be restated as $\Phi(\pi_1, \pi_2 ..., \pi_{n-k}) = 0$, where π_i are dimensionless parameters, if they are expressed in terms of k independent physical units. According to the abovementioned micro parameters, the number of relevant parameters is 10 for non-clustered assembly and 13 for clustered assembly. Since $\left[L, F, T\right]$ act as the three independent physical units in this study, there are 7 dimensionless parameters for non-clustered assembly and 10 for clustered assembly.

Choice of the dimensionless parameters is not unique. Our study is based on the following sets: non-clustered assembly includes a set of $\left\{\mu, n, k_s/k_n, T_n/k_n, T_s/T_n, \bar{R}/L, V\Big/\sqrt{k_n/(\rho\bar{R})}\right\}$ and clustered assembly is given as $\left\{\mu, n, S, k_s/k_n, T_n^{bt}/k_n, T_s^{bt}/T_n^{bt}, T_n^{in}/T_n^{bt}, T_s^{in}/T_s^{bt}, \bar{R}/L, V\Big/\sqrt{k_n/\left(\rho\bar{R}\right)}\right\}$. Since the loading condition is quasi-static, the number of independent dimensionless parameters can be reduced by removing $V\Big/\sqrt{k_n\Big/\left(\rho\overline{R}\right)}$. In addition, μ and $\overline{R}/L$ can also be removed considering that the friction coefficient mainly influences the post-failure behaviour and the particle size $\overline{R}$ is much smaller than the macroscopic characteristic length of the assembly ($L \gg \bar{R}$) (Rojek et al. 2011). Therefore these two sets of dimensionless parameters are reduced to $\left\{n, k_s/k_n, T_n/k_n, T_s/T_n,\right\}$ and $\left\{n, S, k_s/k_n, T_n^{bt}/k_n, T_s^{bt}/T_n^{bt}, T_n^{in}/T_n^{bt}, T_s^{in}/T_s^{bt}\right\}$ respectively.

2.2.1.1 Dimensionless relationships of micro-macro parameters for non-clustered assembly

According to DEM formulations in PFC2D, the elastic constants are determined in the elastic regime where no failure occurs (Potyondy and Cundall 2004). Thus, we can only consider two dimensionless parameters $\left\{n, k_s/k_n\right\}$ for the elastic constants. The following phenomenological dimensionless equations linking macro- and micro-parameters can be established for a non-clustered DEM model, cf. Huang (1999):

$$\frac{E}{k_n} = \Phi_E^{nc}(\frac{k_s}{k_n}, n) \tag{2.3}$$

$$\nu = \Phi_\upsilon^{nc}(\frac{k_s}{k_n}, n) \tag{2.4}$$

$$\frac{\sigma_c \overline{R}}{T_n} = \Phi_c^{nc}(\frac{T_n}{k_n}, \frac{T_s}{T_n}, \frac{k_s}{k_n}, n) \tag{2.5}$$

$$\frac{\sigma_t \overline{R}}{T_n} = \Phi_t^{nc}(\frac{T_n}{k_n}, \frac{T_s}{T_n}, \frac{k_s}{k_n}, n) \tag{2.6}$$

where Φ_E^{nc}, Φ_υ^{nc}, Φ_c^{nc} and Φ_t^{nc} are functions relating E, ν, σ_c and σ_t to the micro dimensionless parameters for non-clustered assembly respectively.

2.2.1.2 Dimensionless relationships of micro-macro parameters for clustered assembly

A clustered assembly differs from a non-clustered one in the inclusion of two additional types of contact bond strength, namely the inter- and intra-cluster strength. The dimensionless functional relationships are similar to the previous case and are given by:

$$\frac{E}{k_n} = \Phi_E^{cl}(\frac{k_s}{k_n}, n, S) \tag{2.7}$$

$$\nu = \Phi_\upsilon^{cl}(\frac{k_s}{k_n}, n, S) \tag{2.8}$$

$$\frac{\sigma_c \overline{R}}{T_n^{bt}} = \Phi_c^{cl}(\frac{T_n^{bt}}{k_n}, \frac{T_s^{bt}}{T_n^{bt}}, \frac{T_n^{in}}{T_n^{bt}}, \frac{T_s^{in}}{T_n^{in}}, \frac{k_s}{k_n}, n, S) \tag{2.9}$$

$$\frac{\sigma_t \overline{R}}{T_n^{bt}} = \Phi_t^{cl}(\frac{T_n^{bt}}{k_n}, \frac{T_s^{bt}}{T_n^{bt}}, \frac{T_n^{in}}{T_n^{bt}}, \frac{T_s^{in}}{T_n^{in}}, \frac{k_s}{k_n}, n, S) \tag{2.10}$$

where Φ_E^{cl}, Φ_υ^{cl}, Φ_c^{cl} and Φ_t^{cl} are functions relating E, ν, σ_c and σ_t to the micro dimensionless parameters for clustered assembly respectively.

2.2.2 Parametric study on macro-mechanical parameters

Unlike continuum based numerical codes such as FEM where the macro-mechanical properties of the specimen can be directly specified, DEM suffers from the disadvantage of an additional numerical calibration procedure, i.e., the determination of micro-scale parameters given a set of macro-mechanical properties, such as Young's modulus E, Poisson's ratio ν, uniaxial compressive strength σ_c and tensile strength σ_t. Young's modules, uniaxial compressive strength and Poisson's ratio are normally derived by simulating the unconfined compression test and the tensile strength by simulating the indirect tension (Brazilian) test.

Note it is not the intention in this work to establish the complete relationships between micro- and macro-mechanical parameters. The focus of the current research is to obtain a suitable relationship between the inter-cluster strength and intra-cluster bond strength to derive a more realistic σ_c/σ_t ratio that can be used to study the transition of the cutting regime. For general discussions about the effect of micro-mechanical parameters on macro-mechanical properties, readers are referred to Huang (1999) and Yang et al. (2006).

2.2.2.1 Parametric study for non-clustered particle assembly (NCPA)

As shown in Fig. 2.3a, a rectangular sample of 37.5 × 75mm for UCS test containing 1902 randomly compacted particles with their radii uniformly distributed between 0.5 mm and 0.75 mm was generated by using the cluster algorithm proposed in Potyondy and Cundall (2004). The BTS sample of 37.5 mm in diameter was generated by cutting a disk out of the UCS specimen and it contains 754 particles in this case. The porosity of these specimens is approximately $n \approx 0.17$. As stated in Huang et al. (2013), the ratio T_n/k_n has little effect on the macro-properties σ_c and σ_t. Therefore, we mainly examined the variation of macro-properties under various micro elastic contact-stiffness ratios and bond strength ratios.

Simulations of both the UCS and the BTS test were conducted by varying the k_s/k_n ratio in the range 0.1-2.0 given $k_n = 52$ N/m, $T_n = 80$ N/m and $T_s/T_n = 10$. Preliminary simulation results are listed in

Table 2.1 and are plotted in Fig. 2.4. As shown in Fig. 2.4a, both curves follow the patterns similar to those reported in Huang et al. (2013) where it was claimed that each curve corresponding to the scaled Young's modulus E and Poisson's ratio ν respectively can be fitted by a function in the form of $(1+ax)/(b+cx)$. On the other hand, the contact stiffness ratio hardly affects the strength properties although there are some mild variations when its value is smaller than 2.0 (Fig. 2.4b).

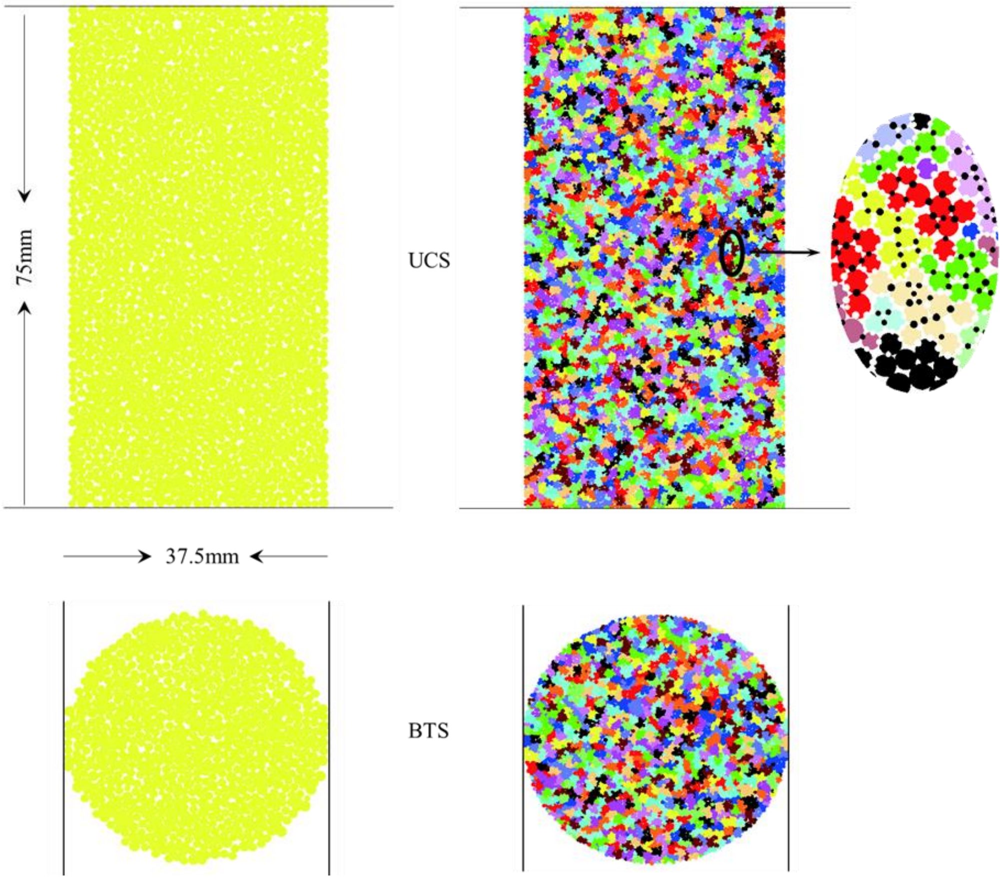

(a) (b)

Fig. 2.3 Two dimensional numerical specimens for UCS and BTS tests comprising (a) NCPA and (b) CPA. For CPA, clusters are shown in different colours, white dots in the detailed view are inter-cluster bonds and black dots are intra-cluster bonds.

Strength properties were then investigated by varying the T_s/T_n ratio ranging from 0.1 to 5 assuming $T_n = 80$ N/m, $k_n = 52$ N/m and $k_s/k_n = 0.48$. The modelling results for elastic constants and strength properties are summarised in Table 2.2. Dependence of the scaled Young's modulus E and Poisson's ratio ν on the bond strength ratio T_s/T_n is plotted in Fig. 2.5 based on the results listed in Table 2.2. The T_s/T_n ratio has little effect on Young's modules and Poisson's ratio (Fig. 2.5a), but the strength parameters (UCS σ_c and BTS σ_t) both increase as the bond strength ratio T_s/T_n increases (Fig. 2.5b). The increasing trend ceases after $T_s/T_n \geq 1.5$.

Table 2.1 Results of UCS and BTS tests for non-clustered assemblage with varying contact stiffness ratio

k_s/k_n	E (GPa)	ν	σ_c (MPa)	σ_t (MPa)	$\sigma_c\bar{R}/T_n$	$\sigma_t\bar{R}/T_n$	σ_c/σ_t
0.10	10.4	0.34	120.6	28.0	9.42E-04	2.19E-04	4.3
0.13	11.3	0.32	126.6	29.8	9.89E-04	2.33E-04	4.2
0.20	13.6	0.28	136.0	32.0	1.06E-03	2.50E-04	4.3
0.33	16.2	0.22	152.7	33.8	1.19E-03	2.64E-04	4.5
0.40	17.2	0.20	156.5	34.5	1.22E-03	2.70E-04	4.5
0.48	18.2	0.18	153.9	36.0	1.20E-03	2.81E-04	4.3
0.59	19.2	0.17	156.6	31.8	1.22E-03	2.48E-04	4.9
0.67	19.9	0.16	151.1	41.6	1.18E-03	3.25E-04	3.6
0.83	20.9	0.13	131.4	39.1	1.03E-03	3.05E-04	3.4
1.00	22.1	0.11	167.5	46.2	1.31E-03	3.61E-04	3.6
1.43	23.8	0.04	157.4	48.1	1.23E-03	3.76E-04	3.3
2.00	25.4	0.02	167.7	40.8	1.31E-03	3.19E-04	4.1

Table 2.2 Results of UCS and BTS tests for non-clustered assemblage with varying bond strength ratio

T_s/T_n	E (GPa)	ν	σ_c (MPa)	σ_t (MPa)	$\sigma_c\bar{R}/T_n$	$\sigma_t\bar{R}/T_n$	σ_c/σ_t
0.1	18.2	0.17	16.7	4.3	1.30E-04	3.36E-05	3.9
0.2	17.8	0.18	29.7	8.1	2.32E-04	6.33E-05	3.7
0.4	17.9	0.18	54.6	15.2	4.27E-04	1.19E-04	3.6
0.6	18.0	0.18	79.4	21.2	6.20E-04	1.66E-04	3.7
0.8	18.1	0.18	95.5	24.0	7.46E-04	1.88E-04	4.0
1.0	18.2	0.18	116.2	28.8	9.08E-04	2.25E-04	4.0
1.5	18.2	0.19	141.2	33.2	1.10E-03	2.59E-04	4.3
2.0	18.2	0.18	155.5	36.0	1.21E-03	2.81E-04	4.3
3.0	18.2	0.18	153.9	36.0	1.20E-03	2.81E-04	4.3
5.0	18.2	0.18	153.9	36.0	1.20E-03	2.81E-04	4.3
10.0	18.2	0.18	153.9	36.0	1.20E-03	2.81E-04	4.3

Table 2.3 Results of UCS and BTS tests for clustered assemblage with varying inter-cluster to intra-cluster bond strength ratio

T_n^{in}/T_n^{bt}	E (GPa)	ν	σ_c (MPa)	σ_t (MPa)	$\sigma_c\bar{R}/T_n^{bt}$	$\sigma_t\bar{R}/T_n^{bt}$	σ_c/σ_t
1.0	19.1	0.01	46.3	10.4	1.45E-03	3.25E-04	4.5
2.0	19.4	0.01	67.8	12.6	2.12E-03	3.94E-04	5.4
4.0	18.9	0.09	95.9	17.2	3.00E-03	5.38E-04	5.6
6.0	18.2	0.19	126.6	16.5	3.96E-03	5.16E-04	7.7
8.0	18.0	0.18	151.1	16.5	4.72E-03	5.16E-04	9.2
10.0	18.2	0.18	155.4	16.5	4.86E-03	5.16E-04	9.4
12.0	17.9	0.18	159.7	16.5	4.99E-03	5.16E-04	9.7
15.0	17.8	0.18	172.5	16.5	5.39E-03	5.16E-04	10.5

2.2.2.2 Parametric study for clustered assembly (CPA)

Identical sample dimensions were used for the clustered assemblage and the porosity was also kept at 0.17. There are a total of 1830 clusters within the clustered assembly for UCS modelling. Fig. 2.3b illustrates the interlocking effect between crystals (shown in different colours) in real rocks. This interlocking effect can be represented in DEM models by specifying different inter- and intra-cluster bond strengths. For the clustered assembly, it has been demonstrated that an increase in cluster size, i.e., the maximum number of particles in a cluster, could lead to a significant increase in the σ_c/σ_t ratio (Cho et al. 2007). The mean particle radius however was reduced such that a number of fine particles could be used to form a cluster to represent a big irregular shape crystal grain in rock material. The fine particle radii were designed to follow a uniform distribution as used in the NCPA assembly. The cluster size *S* was set at 10 in this study and therefore smaller particles with the average radius of 0.0625 mm were used to construct clusters to make the average cluster size approximately equal to the single particle size of non-clustered assemblage. Likewise, the clusters can be regarded to follow a uniform distribution as well.

As stated above, many specifications of the clustered assemblage are identical to those of the non-clustered assemblage and they differ from each other only in terms of bonding strength between discrete elements. Therefore, the influences of k_s/k_n , T_n^{bt}/k_n , T_s^{bt}/T_n^{bt} and T_s^{in}/T_n^{in} ratios on the macro-mechanical properties in the case of clustered assemblage are expected to be similar to those described in Section 2.2.1.1. The only micro-scale parameter left in the scaling relationships (2.7)-(2.10) that need to be examined is the T_n^{in}/T_n^{bt} ratio. The corresponding simulation results are listed in Table 2.3 and shown in Fig. 2.6. It can be seen that the σ_c/σ_t ratio for the clustered assemblage increases considerably from 4.5 when $T_n^{in}/T_n^{bt}=1$ to 9.2 when $T_n^{in}/T_n^{bt}=8$ and it continues to increase gently afterwards. Note the σ_c/σ_t ratio is constant at approximately 4.0 for the non-clustered assemblage (see Table 2.2 and Fig. 2.5b),

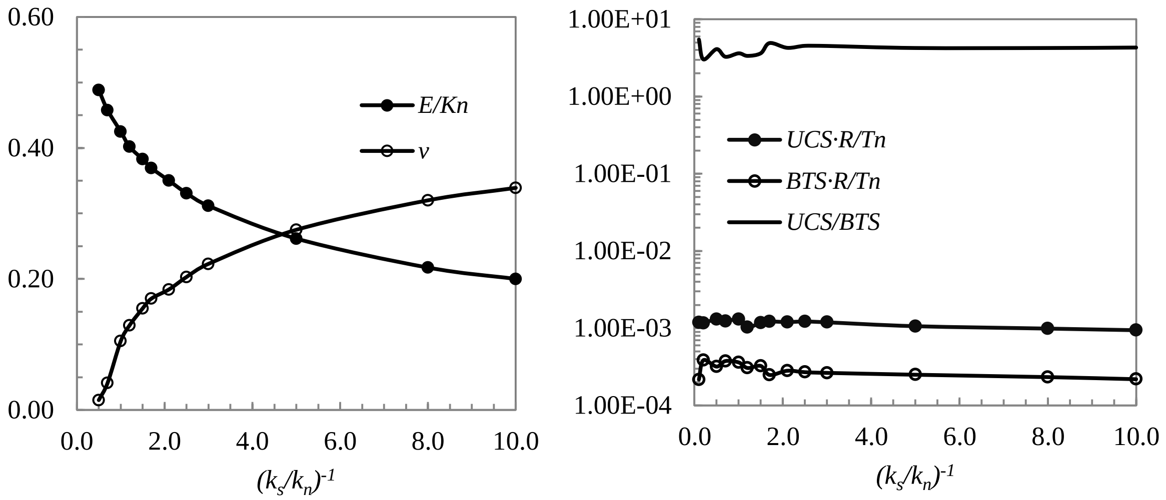

(a) (b)

Fig. 2.4 Dependence of macroscopic properties on k_s/k_n ratio for non-clustered assembly.

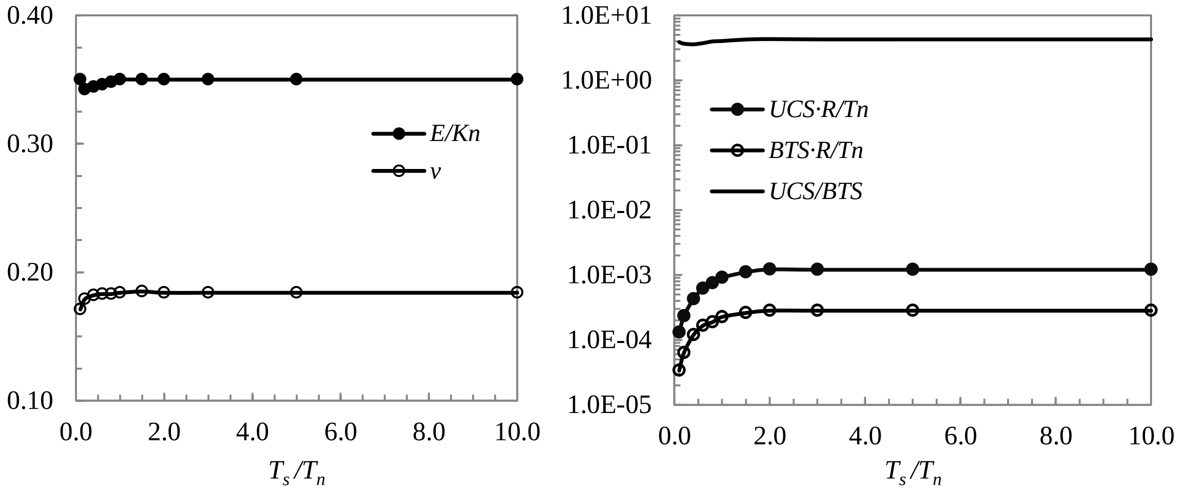

(a) (b)

Fig. 2.5 Dependence of macroscopic properties on T_s/T_n ratio for non-clustered assembly.

As shown in Fig. 2.5b, σ_c and σ_t increase almost at the same rate for non-clustered assembly and therefore the ratio between them keeps approximately constant at 4.0 due to contact bond between particles having the same strengths. On the contrary, the strength difference for contacts within clusters and between clusters for clustered assembly makes σ_c to increase at a greater rate than σ_t, resulting in constantly increasing strength ratio. Therefore, it is expected that the strength ratio can be increased to a more realistic value (e.g., 10) using clustered assemblage so that the characteristics of real rocks can be better represented by the synthetic samples.

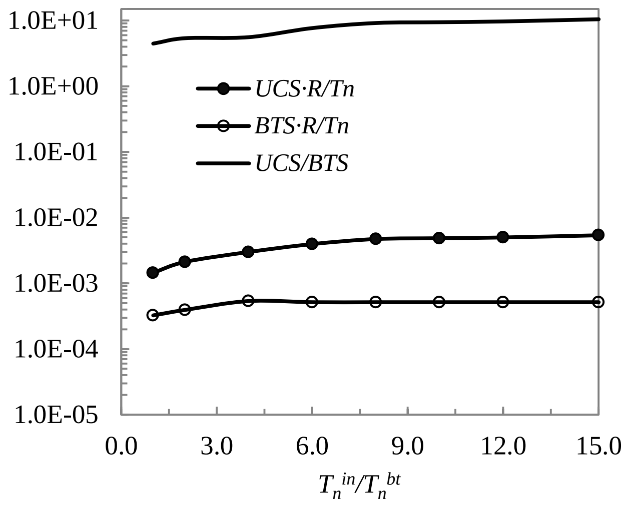

Fig. 2.6 Dependence of UCS and BTS on T_n^{in}/T_n^{bt} ratio for clustered assembly.

2.2.3 Numerical calibration of model parameters for the reference sandstone

Based on the calibration process described above, a numerical calibration was conducted against the reference synthetic sandstone used in Huang et al. (2013). The purpose is to find a set of micro-scale parameters that can produce the macro-properties including the strength ratio as close as possible to those of the real rock. Similar procedures are followed: the micro contact stiffness values are determined first to produce matched elastic constants (E and ν) due to the fact that the macro elastic constants are derived in the elastic deformation phase wherein no bond strength related parameters are involved; after the equivalent macro elastic constants are obtained, choices for micro-bond strength parameters are then made to generate models with σ_c roughly equal to that of the reference rock; finally the clustered assembly is made with the improved strength ratio.

Table 2.4 Calibrated micro-parameters for non-clustered assembly and clustered assembly

Micro parameters	n	S	μ	k_n	k_s/k_n	T_n	T_s/T_n	T_n^{bt}	T_n^{in}/T_n^{bt}	T_s^{bt}/T_n^{bt}	T_s^{in}/T_s^{bt}
Non-clustered assembly	0.17	–	0.839	52	0.48	80	10	–	–	–	–
Clustered assembly	0.17	10	0.839	40	0.50	–	–	20	10	10	10

Table 2.5 Comparison of calculated macro-properties in DEM

Macro properties	E (GPa)	ν	σ_c (MPa)	σ_t (MPa)	σ_c/σ_t
Reference material (Huang et al. 2013)	16.9	0.12	155	43	3.6
Non-clustered assembly	18.2	0.18	153.9	36.0	4.3
Clustered assembly	18.2	0.18	155.4	16.5	9.4

Shown in Table 2.4 are the calibrated micromechanical parameters which give two sets of macro-properties for the DEM samples listed in Table 2.5. Compared with the reference synthetic rock, it can be seen that most macro-properties are comparable with each other except the values of σ_t and the strength ratio. Normally the true strength ratio for sandstone vary in the range of 6~10 while the reference synthetic rock used in Huang et al. (2013) only managed to achieve a ratio of 3.6, which is similar to the ratio achieved in our NCPA model. In contrast to this, using the proposed CPA approach, a more realistic strength ratio of 9.4 is achieved (Table 2.5) using the set of parameters listed in Table 2.4. Obviously, using the cluster approach assures better match of strength ratio between synthetic samples and real rocks, which the non-clustered assembly fails to achieve. Further discussions on the differences are given below.

2.3 2D simulation of rock cutting processes

A system consisting of a cutter and a rock sample of the size 200mm × 80mm is considered in the rock cutting model (Fig. 2.7). The cutter made up of two walls is considered as a rigid body advancing at a velocity of V with a back rake angle α. The tool–rock interaction is modelled by the Coulomb friction model and the rock material ahead of the cutter is removed as the cutter advances.

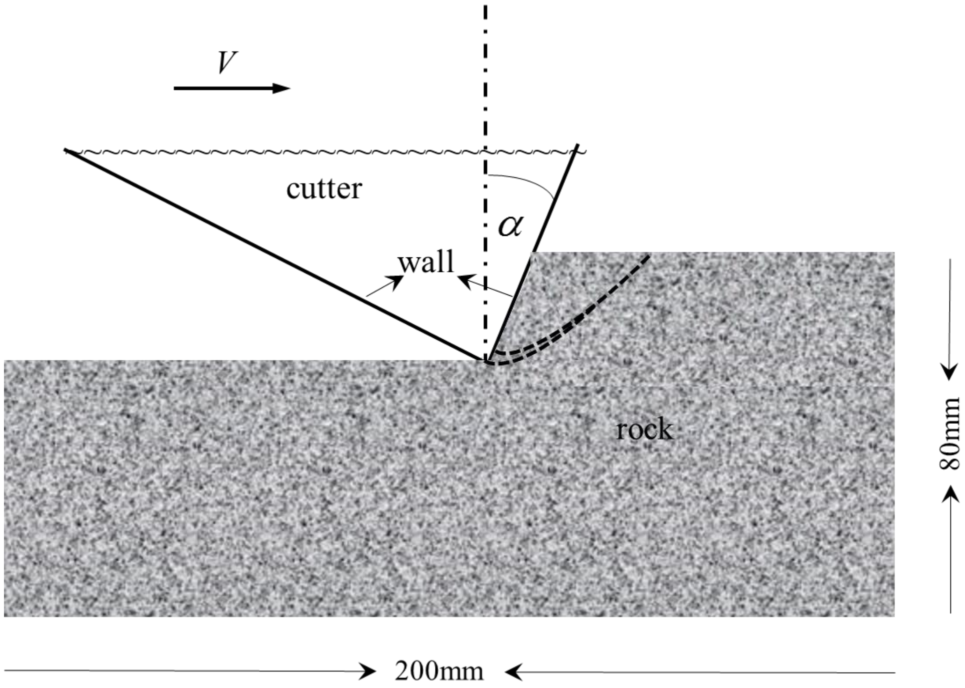

Fig. 2.7 Schematic illustration of cutting geometry and cutter-rock interaction.

2.3.1 Simulations of rock cutting on the two assemblies discussed

After the micro-parameter calibration, the rock cutting simulations were performed on the specimens constructed using two different assemblages discussed above. The cutting starts at the left edge of the specimen and various different cutting depths are simulated (Fig. 2.8). The back rake angle is set at 15º. The cutting process was simulated by moving the cutter horizontally from left to right at a relatively low constant velocity to ensure quasi-static equilibrium state of the assembly. The interaction between the cutter wall segments and particles are described by normal and shear contact stiffeness $k_{nw} = k_n$ and $k_{sw} = 0.1k_s$, and by a contact friction coefficient $\mu_w = \mu$.

As can be seen in Fig. 2.1, the ductile mode cutting produces cuttings that pile up in front of the cutter face while this phenomenon becomes less pronounced during the brittle cutting process. This difference is reproduced reasonably well in the simulation (see Fig. 2.8 and Fig. 2.11). The output images would be clearer to demonstrate this difference if particles already detached completely from the assemblage were removed from the model, which was not implemented in our simulations due to software limitation.

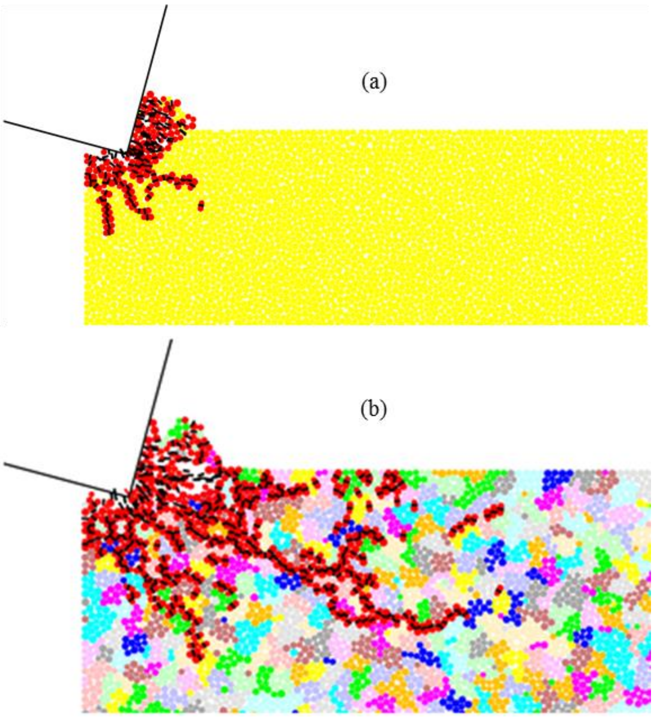

Fig. 2.8 Rock-cutter interaction occurring in (a) NCPA model and (b) CPA model for the case $d/\overline{R} = 4$ captured at the initial cutting stage. Red-dotted particles are those with broken bonds, displayed as black line segments. Both models (only the areas close to the cutter) are shown enlarged 10 times, compared to the original figures in Fig. 2.11.

As the cutter advances, it comes into contact with particles and the interaction begins by micro-crack initiation and propagation in the specimen from the tip of the cutter. When a bond is broken, a micro-crack is produced. Coalescence of micro cracks evolves into macro-fractures, which leads to chip formations if they reach the top surface of rock specimen. During the simulations the following quantities were recorded as a function of the relative position of the cutter, $l/\bar{R}$:

(a) Damage indicated by the intensity, orientation and location of micro-cracks and quantified by the number of broken bonds.

(b) Forces acted on the cutter involving the total tangential component F_t and total normal component F_n .

(c) The number of cracks when the bonds are broken, induced by cutting forces acting on the bonded particles.

Fig. 2.8 shows typical cutting actions for both non-clustered and clustered assemblages. It can be seen clearly that cracks propagating downwards exist for both cases and no chipping results from the vertically propagating cracks. Fig. 2.8a shows that the damage takes place in the vicinity of the cutter tip and almost all particles in this damage region have broken bonds. For the clustered assembly (Fig. 2.8b), fractures develop further away from the cutter than the non-clustered model and thus more damage is resulted with a thicker layer of loose particles. The crack extension in the clustered model can be attributed to the relatively low inter-cluster bond strength between the cluster boundary particles, which is, as shown in Table 2.4, one order of magnitude smaller than the intra-cluster bond strength. Fig. 2.8b also demonstrates features that some fractures propagate horizontally and gradually upwards to the top surface of rock specimen, leading to the formation of small cut chips. In addition, simulations using the clustered model also successfully capture the crushing process of large rock particles into smaller ones, as demonstrated by the change of colour used to plot the particles ahead of the cutter, where red particles represent de-bonded particles resulted from transgranular cracking and particles shown in other colours are clusters not yet damaged (Fig. 2.8b).

Further analysis on the crack development in Fig. 2.8 reveals that the damage depth for both CPA and NCPA models is larger than the depth of cut, spreading over approximately 4 times and 2 times the depth of cut in CPA model and NCPA model, respectively. Though there are no published experimental observations to confirm any of these numbers due to the difficulty in observing the crack propagation within rock, a recent experimental study using fluorescent resin by Entacher et al. (2014) demonstrates that the cracks can even propagate beneath the cutter for more than 5 times the depth of cut, see their observation image reproduced in Fig. 2.9a. However, we have to be aware that their experiment was done with a disc cutter, not a drag pick. The normal force for a disc cutter in general is expected to be greater than that for a drag pick at the same depth of cut and therefore the crack damage zone beneath the disc cutter is expected to be larger. Fig. 2.8 also shows that more significant horizontal cracks are being developed in the CPA model as the cutter advances further to the right. This suggests a higher possibility of chipping formations using the CPA model. It is widely observed in experiments that significant chippings can take place due to horizontal cracks propagating upwards to the top free surface (Lin and Zhou 2013), as illustrated in Fig. 2.9b. Therefore, the CPA is expected to model better the formation of chippings in rock cutting processes.

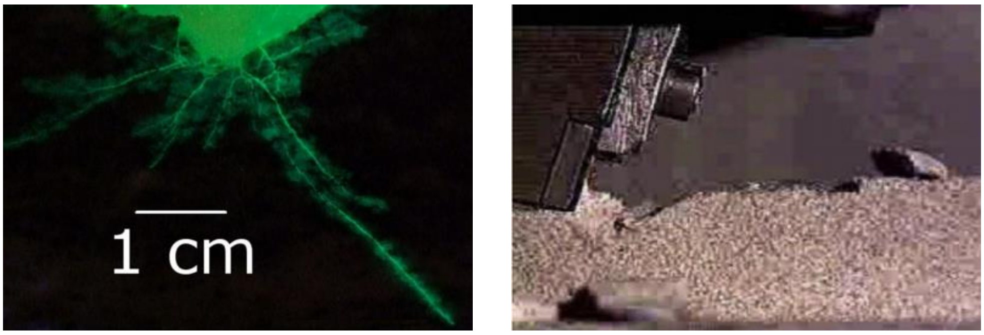

(a) (b)

Fig. 2.9 Crack development during cutting process: (a) cracks development beneath a disc cutter (after Entacher et al. (2014)); (b) crack development in the horizontal direction leading to chippings and complex geometry of fragmentations (after Lin and Zhou (2013)).

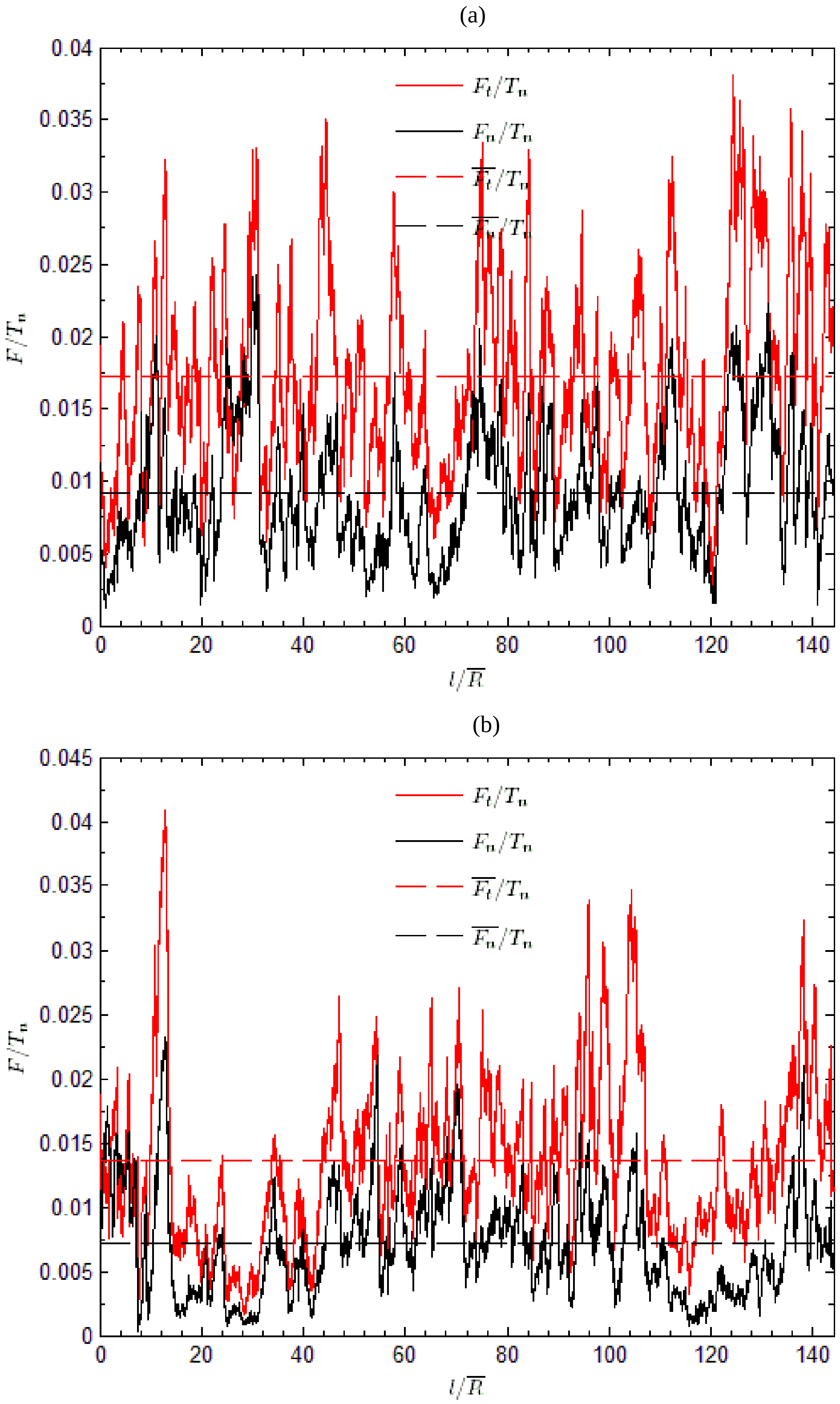

Fig. 2.10 Comparison of histories of forces versus distance between (a) non-clustered model and (b) clustered model for depth of cut $d = 4\overline{R}$.

The corresponding cutting force logs for the two different assemblages are shown in Fig. 2.10. The mean forces, $\bar{F}_n$ and $\bar{F}_t$ (averaged over the cutting distance), for both assemblages are at the same level, although the forces for the non-clustered assemblage are slightly higher compared with those for the clustered assemblage. The force variation for the depth of cut at $d = 4\bar{R}$, shown in Fig. 2.10a, is reasonably uniform and can be viewed as an indication of ductile-regime cutting described in Richard et al. (2012). On the contrary, the forces for the clustered model (Fig. 2.10b) show much greater variability including some peak values followed by an extended period of low values, a typical force profile corresponding to the cutting chip formation, which can be regarded as the occurrence of brittle mode failure. In this case higher peaks correspond to the coalescence of micro cracks and the formation of rock chips, while local small peaks with smaller intervals in between higher peaks correspond to the cracking events between particles within clusters as a result of bond breaking.

The force log, to some degree, can be used to assess the transition point of cutting mode from ductile to brittle as the depth of cut increases. Comparing the force logs for cutting on the two distinct assemblies, we can find that the clustered assembly undergoes brittle mode cutting at a smaller depth of cut than the non-clustered assembly. In other words, the clustered assembly with larger value of σ_c/σ_t displays brittle cutting mode at shallower depth of cut. It is therefore clear that the ratio σ_c/σ_t does play an important role in the failure mode transition for rock cutting.

2.3.2 Failure mode transition

Cutting depth is the key factor influencing the rock cutting failure mode. The study on the failure model transition is conducted based on cutting simulations on the two types of synthetic rocks at $d/\bar{R}$ ranging from 2 to 25. Fig. 2.11

shows the comparison of failure modes for non-clustered and clustered assemblages at the cutting depth of $d/\bar{R}$ =4, 8, 16 and 25.

The rock failure mode for non-clustered model shifts clearly from ductile to brittle with increasing depth of cut, i.e., the transition from only shearing off particles to additional chippings at greater cutting depth (Fig. 2.11a). At small depth of cut ($d/\bar{R} = 4,8$), particles near the cutter are sheared off when either their normal or shear bond strength is exceeded by the forces induced by the cutter face. At greater depth of cut (e.g., $d/\bar{R} = 16$, 25), significant amount of micro-cracks occur and they coalescence to form large fractures. Some of these fractures propagate to the top surface well ahead of the cutter and therefore large cutting chips are formed. This feature is particularly clear when $d/\bar{R} = 25$. Based on our observations, significant horizontal fractures only develop when the depth of cut is greater than $12\bar{R}$. Therefore a preliminary conclusion is that $d = 12\bar{R}$ can be viewed as the depth of cut for the transition of failure mode from ductile to brittle as horizontal fracture development is critical for forming large cutting chips.

For the clustered model (Fig. 2.11b), more horizontal cracking (a sign of brittle mode cutting) is observed compared with the non-clustered model at the same depth of cut when the cutting is dominated by ductile mode in the non-clustered model. Based on the fracture pattern developed, it can be claimed that the failure mode is generally dominated by brittle failure in most cases, though ductile failure also make up certain proportions. The crushing of clusters into separate particles becomes gradually stronger as depth of cut increases, which is manifested by the increasing size of the crushed zone in front of the cutter. It is obvious that chips only form in the brittle mode cutting process and the chip size generally increases with the depth of cut. Furthermore, cutting on the CPA model at $d = 16\bar{R}$ shows the existence of smaller chips above the major horizontal fracture, illustrating the potential complex geometry of rock fragmentations under cutting. This is in accordance with the chipping formations often observed in cutting experiments (see, for example, the image reproduce in Fig. 2.9b) and the CPA model can produce results more closely resembling these observations.

Based on the above analysis and the direct observation of Fig. 2.11, a preliminary conclusion in terms of the critical transition depth can be made: the ductile-brittle transition takes place roughly at $d = 4\bar{R}$ for the CPA model compared with the NCPA model where the critical transition depth is approximately at $d = 16\bar{R}$.

The cutting mode transition with respect to depth of cut can also be examined from the changes of average cutting forces, particularly the normal component. Assuming the cutting action is always dominated by ductile mode, i.e., $F \propto \sigma_c W d$, the mean forces should have a linear relationship with the cutting depth. However, the mean forces deviate from the linear relationship as the cutting depth increases (Fig. 2.12). As shown in Fig. 2.12a for NCPA model, the average cutting forces keep increasing linearly until $d/\bar{R} = 12$. For $d > 12\bar{R}$, a non-linear relationship is shown, indicating the change in failure mechanism. A preliminary conclusion based on force variations is that the failure mode transition for NCPA model occurs at approximately $d = 12\bar{R}$. On the other hand, the mean forces for CPA model are no longer proportional to the normalised depth of cut after $d/\bar{R} = 4$ (Fig. 2.12b) and therefore this can be regarded as the critical transition depth for the CPA model.

However, for the CPA model (Fig. 2.12b), the initial linear relationship between mean forces and cutting depth has greater slopes compared with the NCPA model (Fig. 2.12a). This is because that at a very small cutting depth, such as $d = 2\bar{R}$, micro-cracking events for clustered model (Fig. 2.12b) mainly occur within clusters as the intra-cluster strength is much higher (200 of T_n^{in} compared to 80 of T_n shown in Table 2.4) and therefore much higher forces are needed to break the clusters. The opposite happens when the cutting is in brittle mode at greater depth of cut. The mean forces needed for CPA model in brittle cutting mode are actually lower compared with those for the

NCPA model. This is due to the fact that in this mode the micro-cracks predominantly develop along the cluster boundaries and the boundary particles between clusters have lower bond strength, as discussed earlier.

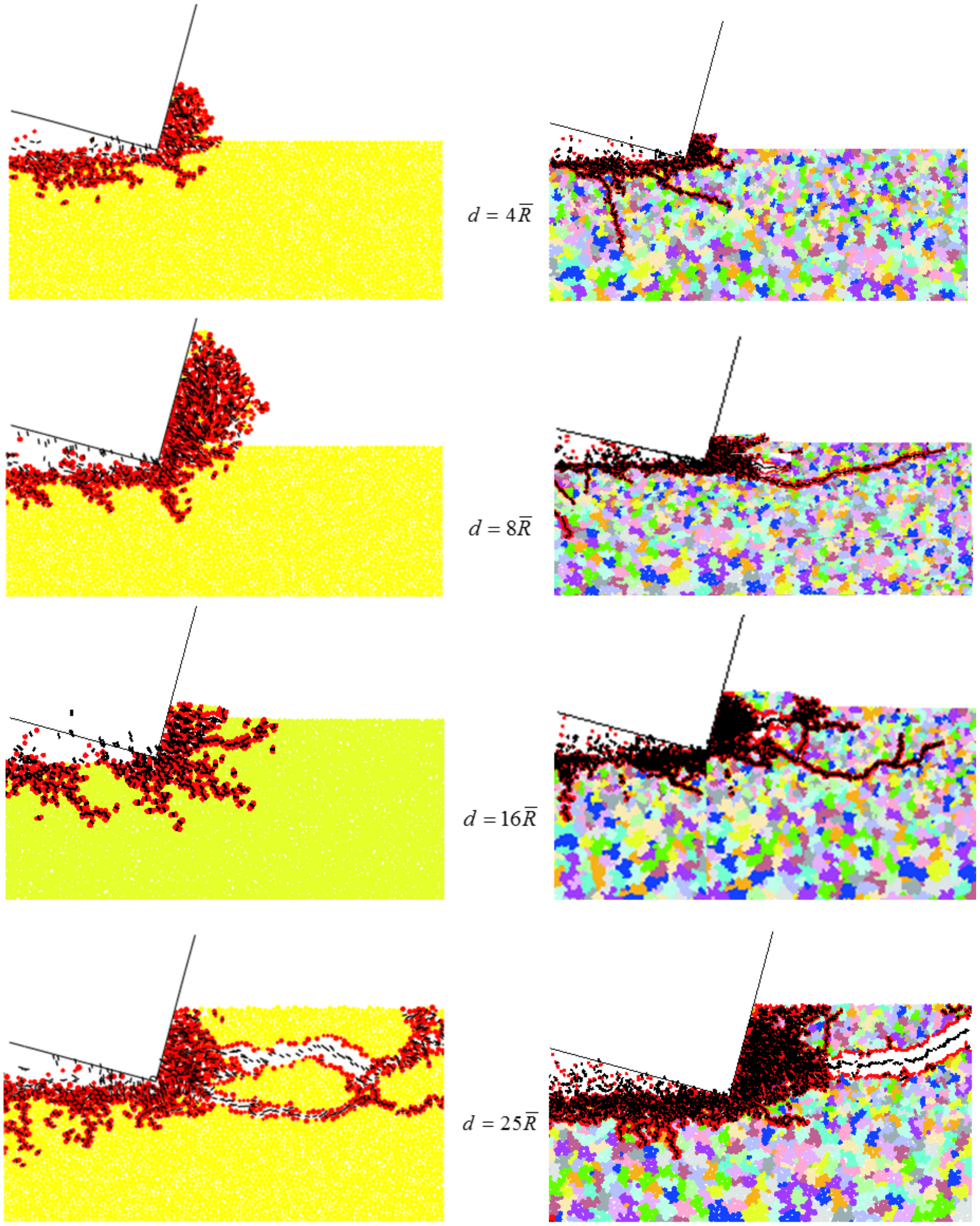

(a) (b)

Fig. 2.11 Comparison of failure mode for (a) NCPA model (b) CPA model under cutting at different depths of cut.

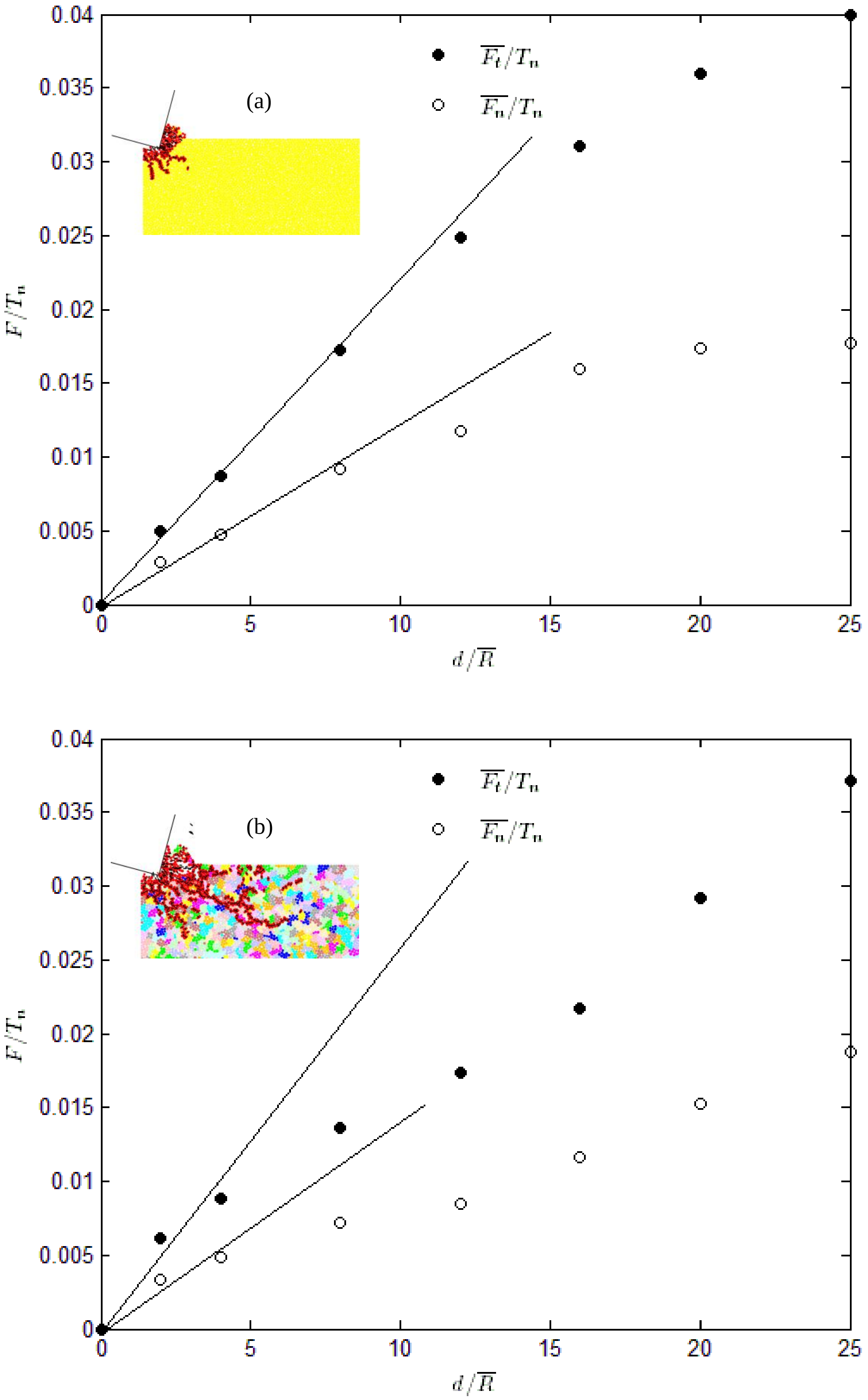

Fig. 2.12 Average cutting forces against the depth of cut d normalised by $\overline{R}$: (a) non-clustered assembly; (b) clustered assembly.

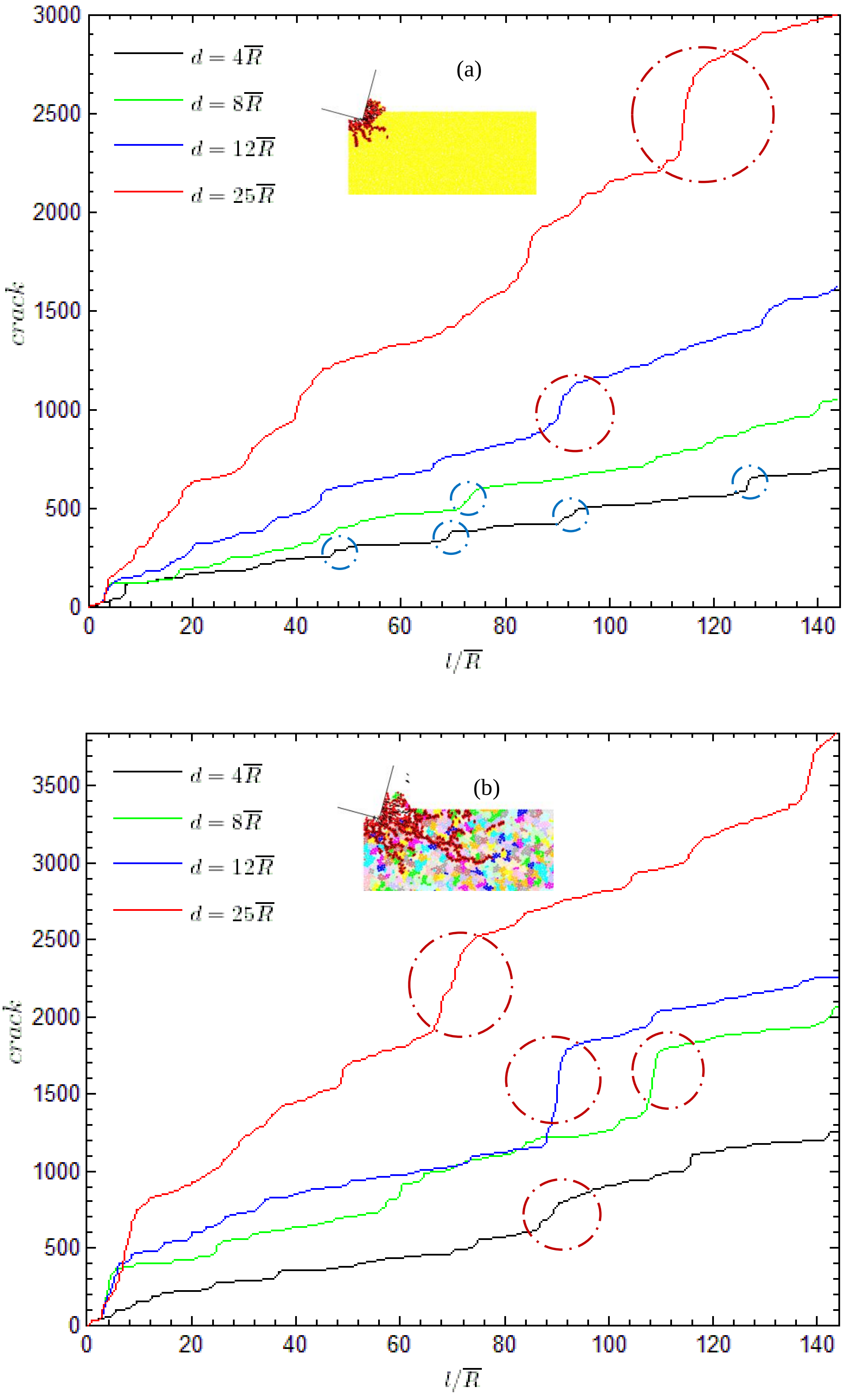

Fig. 2.13 Crack number versus length of cut l normalised by $\overline{R}$: (a) non-clustered assembly; (b) clustered assembly.

In line with our expectations, the magnitude of average cutting forces, calculated over a cutting length of 200 mm, always increase with cutting depth. They increase at a higher constant rate initially and followed by a lower rate once the cutting enters the brittle failure mode. This argument is supported by experimental results presented in Richard (1999). To the contrary, Huang et al. (2013) reported in his work based on a length of cutting of 129.7 mm that smaller forces were required to cut the rock in brittle failure mode than those in ductile mode, which is contradictory to the laboratory test results reported in Richard (1999).

During the cutting simulation, the total micro crack number within the specimen is recorded as a supplementary source to help to identify the rock-cutting cycles, as shown in Fig. 2.13. As expected, for both non-clustered and clustered models, the crack number increases constantly in all cases of cutting depths, but at slightly different rates. More damages are expected at greater cutting depth and therefore the total number of cracks will be higher.

For non-clustered assembly, at a shallow depth of cut, i.e., $d = 4\bar{R}$ or $d = 8\bar{R}$, only less than 100 cracks are generated for each step increases (blue-dotted circles in Fig. 2.13a), indicating the generation of modest local microfractures around the cutter tip. At greater cutting depth, the curves show rapid increase in number of cracks at a few locations as the red-dotted circles marked in Fig. 2.13a, which could be as high as 400. These sudden increases in micro-fractures are indications of cutting chip formations at these locations. Judging by the discrepancy in the number of cracks, it is reasonable to take $d = 12\bar{R}$ as the critical transition depth. This is also in accordance with the results reflected by the variations of cutting forces.

For clustered assembly (Fig. 2.13b), similar trends can be observed. However, the phenomenon of sudden increase in micro-crack numbers is more pronounced, meaning larger cutting chips are formed. The failure mode transition is considered to happen at around $d = 4\bar{R}$ as at less than this cutting depth, the increase in micro-crack numbers is generally gradual which is consistent with ductile failure mode. There are a few locations where there are higher rate of increase in micro-crack numbers, but the increases are less pronounced compared with other cutting depths.

Some general observations based on the discussions above can be summarised below: rock failure mode under cutting is neither purely brittle nor purely ductile, but a mixture of both. However, depending on the depth of cut, one of the failure modes will be dominant. At small depth of cut, ductile failure mode is dominant but some small cut chips can also be formed. At great depth of cut, brittle failure is dominant, illustrated by large cut chips, but ductile failure shown as de-bonded particles ahead of the cutter head also exists. For two different models, the critical cutting depth of transition from ductile dominant failure mode to brittle dominant failure mode is at $d = 12\bar{R}$ for non-clustered model and $d = 4\bar{R}$ for clustered model. In other words, for our numerical specimen, the critical transition depth is $d_c = 7.5\,\text{mm}$ for NCPA model and $d_c = 2.5\,\text{mm}$ for CPA model, i.e., reduced by 3 times. These values are too high compared to Nicodeme's experiment done on Rhune sandstone (Nicodeme 1997; Richard 1999) where the critical transition depth was measured to be $d_c = 0.4$ mm. However, a direct comparison in this case may be misleading as the average grain size in Rhune sandstone is unknown and therefore using $\bar{R} = 0.625$ mm to estimate the d_c value for Rhune sandstone may not be appropriate.

2.4 The relationship between the strength ratio σ_c/σ_t and the critical cutting transition depth

As stated in the introduction section, the critical depth for failure mode transition can be related to rock properties as:

$$d_c \propto \left(K_{IC}/\sigma_c\right)^2 \tag{2.11}$$

Assuming the initial crack size in a particulate assemblage is approximately equal to the average diameter of constituent particles, the mode I fracture toughness in plane strain, within the framework of linear elastic fracture mechanics, can be expressed as follows (Potyondy and Cundall 2004; Stavropoulou 2006),

$$K_{IC} = \sigma_t \sqrt{\pi \bar{R}} \tag{2.12}$$

Combining Eq. (2.11) and Eq. (2.12), the critical depth d_c can be associated with the brittleness of rock as:

$$d_c \propto \bar{R}(1/B)^2 \tag{2.13}$$

Therefore, the critical cutting transition depth, according to Eq. (2.13), is indirectly proportional to the square of B, i.e., the larger the rock's brittleness, the smaller the critical depth will be.

To obtain the scaling coefficient for Eq. (2.13), we used the simulation data from the synthetic rock material with brittleness $B = 9.4$ analysed above. Based on this single data point, the scaling coefficient can be calculated as 353.44 and the critical transition depth can be expressed as:

$$d_c = 353.44\bar{R}(1/B)^2 \tag{2.14}$$

To assess the performance of this relationship for the prediction of the critical depth for rocks with different values of brittleness, four additional cases at the brittleness of 4.5, 7.7, 10.5 and 15 respectively are tested using different CPA model parameters. The results of these cases are listed in Table 2.6 and shown in Fig. 2.14. The data calculated via DEM simulation appears to agree reasonably well with the trend predicted by Eq. (2.14).

Table 2.6 Critical transition depth for synthetic rock samples varying with different values of brittleness.

Rock brittleness B	4.5	7.7	9.4	10.5	15
d_c	6.3	3.0	2.5	2.3	1.9

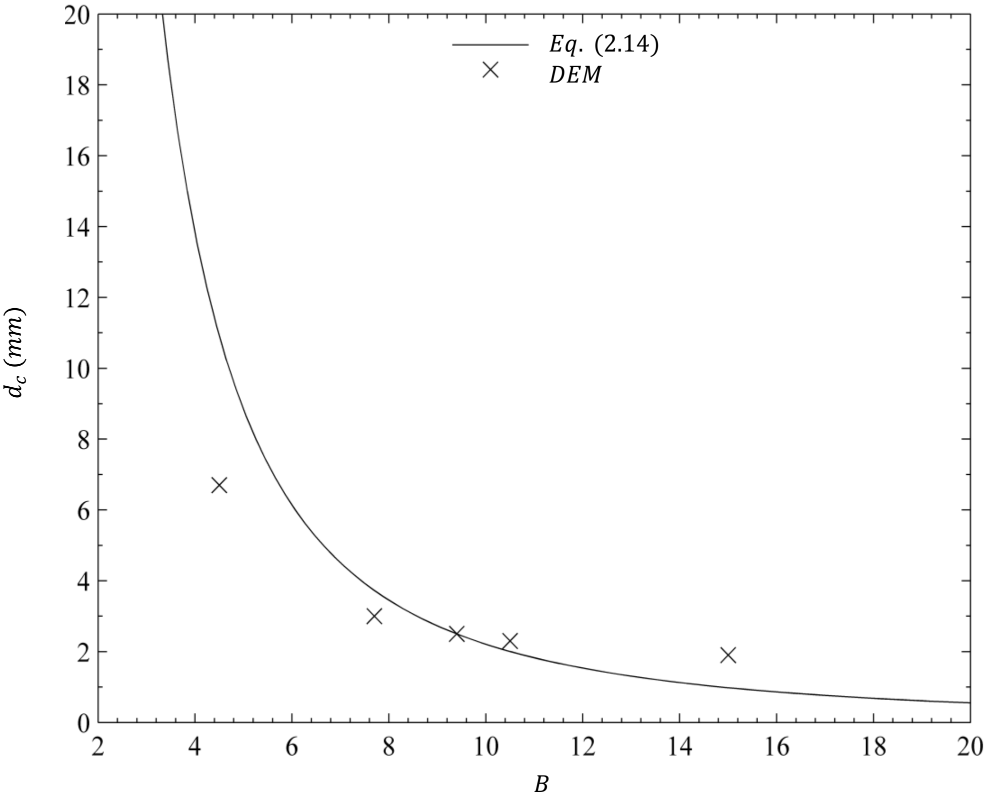

Fig. 2.14 The critical transition depth as a function of brittleness of rock.

2.5 Discussions and conclusions

It is important in the application of discrete element modelling to practical problems to ensure that the mechanical properties of the rock materials are correctly represented in numerical models. These properties include the deformation modulus, strength properties and stress-strain response. In DEM modelling, enforcing all properties are represented correctly in the numerical model may be difficult due to the inherent nature of the DEM algorithm. In this research, we proposed the use of particle clusters to achieve the improvement of the strength ratio representation. The numerical models with properties correctly representing real rocks were generated based on dimensionless relationships between macro properties and micro parameters describing the interaction between particles. Parametric study was carried out, serving as a basis to obtain the calibrated micro parameters for clustered and non-clustered models.

The clustering algorithm used in this study allows the creation of samples with the strength ratios equivalent to that of real rocks, thus overcoming the inherent incapability of conventional DEM models. The cluster itself can break, thereby simulating the case that big rock grains can be crushed into fine particles (or powders) during cutting which is commonly observed in experiments. Although the computation cost is relatively higher than the non-clustered DEM models, particularly for large scale models, the clustering approach potentially opens a new avenue for DEM modelling that can produce results more closely resembling to reality.

In rock cutting, the brittle failure mode is always accompanied by ductile failure mode, and vice versa. The actual failure mode of a cutting at certain depth is defined by the failure mode which is dominating. Apart from the calibration of UCS, the calibration of BTS is also necessary when using DEM to model the fracturing and fragmentation process of rocks subject to mechanical action of cutting tools. The critical transition depth is found to be dependent on not just σ_c and fracture toughness, but rather more on the strength ratio σ_c/σ_t, also termed the brittleness of rock, via the relationship between fracture toughness and tensile strength (cf. Eq. 2.12). This finding clarifies the quantification of the critical cutting depth significantly. For example, rocks of large brittleness would have a small critical transition depth, which is consistent to laboratory observations.

More work is needed to further validate the relationships discussed above. First of all, experimental tests of rock cuttings on different types of rocks need to be conducted. On the modelling side, more comprehensive series of numerical experiments including triaxial compression, indirect tension, fracture toughness measurement as well as direct shear tests are required for more rigorous model calibration. The results of these additional tests will help the selection of more appropriate micro parameters and subsequently the quality of discrete element analysis in rock cutting can be improved. In addition, more realistic particle size distributions and more advanced clustering algorithm should be explored in the construction of the DEM model in order to have a better representation of the real rock matrix. For example, using a fixed number of particles (S=10 in our study) to form clusters is rudimentary and imposing a limit on the possible representation of cluster size distributions. The sensitivity of particle size on the final simulation results, including fracture patterns and crack propagations, and on the relationship $d_c \propto \bar{R}(1/B)^2$ for both CPA and NCPA models should also be investigated.

Acknowledgement

The work has been supported by the Deep Exploration Technologies Cooperative Research Centre whose activities are funded by the Australian Government's Cooperative Research Centre Programme. This is DET CRC Document 2015/619. Valuable discussions about cluster algorithm with Yang Zou at EPFL University are gratefully acknowledged.

References

Atici U, Ersoy A (2009) Correlation of specific energy of cutting saws and drilling bits with rock brittleness and destruction energy. Journal of Materials Processing Technology 209:2602-2612 doi:10.1016/j.jmatprotec.2008.06.004

Bilgin N, Demircin MA, Copur H, Balci C, Tuncdemir H, Akcin N (2006) Dominant rock properties affecting the performance of conical picks and the comparison of some experimental and theoretical results. International Journal of Rock Mechanics and Mining Sciences 43:139-156 doi:10.1016/j.ijrmms.2005.04.009

Che D, Han P, Guo P, Ehmann K (2012) Issues in Polycrystalline Diamond Compact Cutter-Rock Interaction From a Metal Machining Point of View---Part II: Bit Performance and Rock Cutting Mechanics. Journal of Manufacturing Science and Engineering 134:064002-064013

Cho N, Martin CD, Sego DC (2007) A clumped particle model for rock. International Journal of Rock Mechanics and Mining Sciences 44:997-1010 doi:10.1016/j.ijrmms.2007.02.002

Cundall P A computer model for simulating progressive, large-scale movements in blocky rock systems. In: In: Proceedings of the international symposium on rock fracture, Nancy, France, 1971. pp 129-136

Donze FV, Bouchez J, Magnier SA (1997) Modeling fractures in rock blasting. International Journal of Rock Mechanics and Mining Sciences 34:1153-1163

Entacher M, Schuller E, Galler R (2014) Rock Failure and Crack Propagation Beneath Disc Cutters. Rock Mechanics and Rock Engineering:1-14 doi:10.1007/s00603-014-0661-2

Fakhimi A (2004) Application of slightly overlapped circular particles assembly in numerical simulation of rocks with high friction angles. Engineering Geology 74:129-138 doi:10.1016/j.enggeo.2004.03.006

Franca LFP, Lamine E (2010) Cutting Action of Impregnated Diamond Segments: Modelling And Experimental Validation. 27-30 June 2010

Göktan RM (1991) Brittleness and micro-scale rock cutting efficiency. Mining Science and Technology 13:237-241 doi:10.1016/0167-9031(91)90339-e

Huang H (1999) Discrete element modeling of tool-rock interaction. PhD, University of Minnesota

Huang H, Detournay E (2008) Intrinsic length scales in tool-rock interaction. International Journal of Geomechanics 8:39-44

Huang H, Lecampion B, Detournay E (2013) Discrete element modeling of tool-rock interaction I: rock cutting. International Journal for Numerical and Analytical Methods in Geomechanics 37:1913-1929 doi:10.1002/nag.2113

Hucka V, Das B (1974) Brittleness determination of rocks by different methods. International Journal of Rock Mechanics and Mining Sciences & Geomechanics Abstracts 11:389-392 doi:http://dx.doi.org/10.1016/0148-9062(74)91109-7

Kahraman S (2002) Correlation of TBM and drilling machine performances with rock brittleness. Engineering Geology 65:269-283 doi:10.1016/s0013-7952(01)00137-5

Ledgerwood LW (2007) PFC Modeling of Rock Cutting Under High Pressure Conditions. 27-31 May 2007

Lin J-S, Zhou Y (2013) Can scratch tests give fracture toughness? Engineering Fracture Mechanics 109:161-168 doi:http://dx.doi.org/10.1016/j.engfracmech.2013.06.002

Liu HY, Kou SQ, Lindqvist PA (2002) Numerical simulation of the fracture process in cutting heterogeneous brittle material. International Journal for Numerical and Analytical Methods in Geomechanics 26:1253-1278 doi:10.1002/nag.243

Liu HY, Kou SQ, Lindqvist PA (2008) Numerical Studies on Bit-Rock Fragmentation Mechanisms. International Journal of Geomechanics 8:45-67 doi:10.1061/(asce)1532-3641(2008)8:1(45)

Mendoza JA, Gamwo IK, Zhang W, Lin JS (2011) Considerations For Discrete Modeling of Rock Cutting. 26-29 June 2011

Menezes PL, Lovell MR, Avdeev IV, Lin J-S, Higgs CF (2014) Studies on the formation of discontinuous chips during rock cutting using an explicit finite element model. The International Journal of Advanced Manufacturing Technology 70:635-648 doi:10.1007/s00170-013-5309-y

Moon T, Oh J (2012) A Study of Optimal Rock-Cutting Conditions for Hard Rock TBM Using the Discrete Element Method. Rock Mechanics and Rock Engineering 45:837-849 doi:10.1007/s00603-011-0180-3

Nicodeme P (1997) Transition between ductile and brittle mode in rock cutting. Ecole Polytechnique, Paris

Potyondy DO, Cundall PA (2004) A bonded-particle model for rock. International Journal of Rock Mechanics and Mining Sciences 41:1329-1364 doi:10.1016/j.ijrmms.2004.09.011

Richard T (1999) Determination of rock strength from cutting tests. Master thesis, University of Minnesota

Richard T, Dagrain F, Poyol E, Detournay E (2012) Rock strength determination from scratch tests. Engineering Geology 147-148:91-100 doi:10.1016/j.enggeo.2012.07.011

Richard T, Detournay E, Drescher A, Nicodeme P, Fourmaintraux D (1998) The Scratch Test As A Means To Measure Strength of Sedimentary Rocks. Paper presented at the SPE/ISRM Rock Mechanics in Petroleum Engineering, Trondheim, Norway, 8-10 July 1998

Rojek J, Oñate E, Labra C, Kargl H (2011) Discrete element simulation of rock cutting. International Journal of Rock Mechanics and Mining Sciences 48:996-1010 doi:10.1016/j.ijrmms.2011.06.003

Scholtès L, Donzé F-V (2013) A DEM model for soft and hard rocks: Role of grain interlocking on strength. Journal of the Mechanics and Physics of Solids 61:352-369 doi:10.1016/j.jmps.2012.10.005

Stavropoulou M (2006) Modeling of small-diameter rotary drilling tests on marbles. International Journal of Rock Mechanics and Mining Sciences 43:1034-1051 doi:10.1016/j.ijrmms.2006.03.008

Su O, Akcin NA (2011) Numerical simulation of rock cutting using the discrete element method. International Journal of Rock Mechanics and Mining Sciences 48:434-442 doi:10.1016/j.ijrmms.2010.08.012

Tanovic LJ, Bojanic P, Puzovic R, Klimenko S (2009) Experimental Investigation of Microcutting Mechanisms in Marble Grinding. Journal of Manufacturing Science and Engineering-Transactions of the Asme 131 doi:10.1115/1.4000619

Yang B, Jiao Y, Lei S (2006) A study on the effects of microparameters on macroproperties for specimens created by bonded particles. Engineering computations 23:607-631

Yarali O, Kahraman S (2011) The drillability assessment of rocks using the different brittleness values. Tunnelling and Underground Space Technology 26:406-414 doi:10.1016/j.tust.2010.11.013

Yaşar E, Ranjith PG, Viete DR (2011) An experimental investigation into the drilling and physico-mechanical properties of a rock-like brittle material. Journal of Petroleum Science and Engineering 76:185-193 doi:10.1016/j.petrol.2011.01.011

Chapter 3

Specific Energy as an Index to Identify the Critical Failure Mode Transition Depth in Rock Cutting

(Paper 2)

Xianqun He and Chaoshui Xu

Deep Exploration Technologies Cooperative Research Centre, School of Civil, Environmental and Mining Engineering, the University of Adelaide, Australia

Publication:

He X. and Xu C. (2015b) Specific Energy as an Index to Identify the Critical Failure Mode Transition Depth in Rock Cutting. *Rock Mechanics and Rock Engineering*. doi:10.1007/s00603-015-0819-6.

.

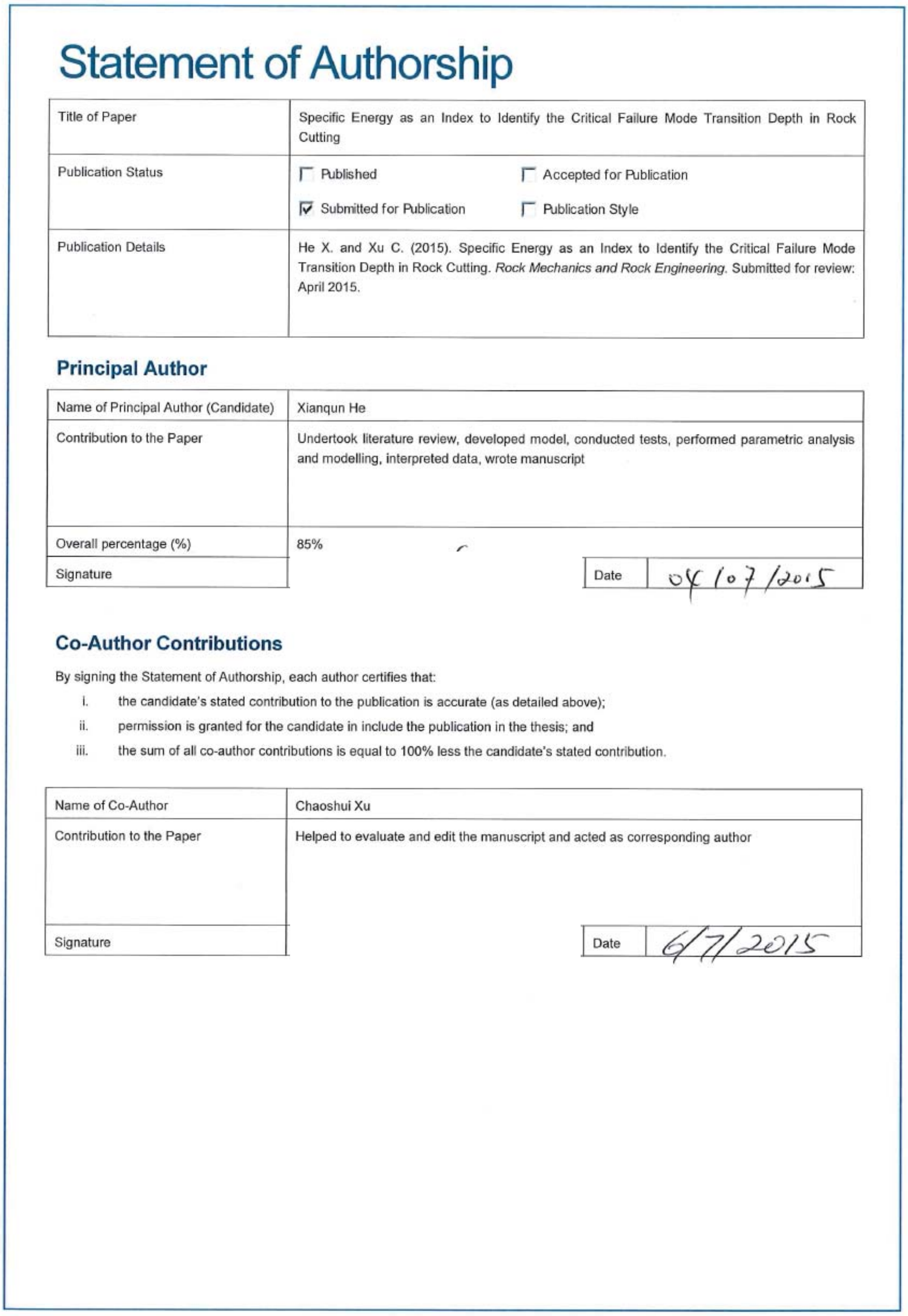

Statement of Authorship

Title of Paper	Specific Energy as an Index to Identify the Critical Failure Mode Transition Depth in Rock Cutting
Publication Status	☐ Published ☐ Accepted for Publication ☑ Submitted for Publication ☐ Publication Style
Publication Details	He X. and Xu C. (2015). Specific Energy as an Index to Identify the Critical Failure Mode Transition Depth in Rock Cutting. *Rock Mechanics and Rock Engineering.* Submitted for review: April 2015.

Principal Author

Name of Principal Author (Candidate)	Xianqun He
Contribution to the Paper	Undertook literature review, developed model, conducted tests, performed parametric analysis and modelling, interpreted data, wrote manuscript
Overall percentage (%)	85%
Signature	Date 04/07/2015

Co-Author Contributions

By signing the Statement of Authorship, each author certifies that:

i. the candidate's stated contribution to the publication is accurate (as detailed above);

ii. permission is granted for the candidate in include the publication in the thesis; and

iii. the sum of all co-author contributions is equal to 100% less the candidate's stated contribution.

Name of Co-Author	Chaoshui Xu
Contribution to the Paper	Helped to evaluate and edit the manuscript and acted as corresponding author
Signature	Date 6/7/2015

Abstract

Rock scratch or cutting typically involves driving a rigid cutter across the rock surface at certain depth of cut and is used to remove rock material in various engineering applications. It has been established that there exist two distinct failure modes in rock cutting, i.e., ductile mode and brittle mode. The ductile mode takes precedence when the cut is shallow and the increase in the depth of cut leads to rock failure gradually shifted to brittle failure dominant mode. The threshold depth, at which rock failure under cutting changes from the ductile to the brittle mode, is associated with not only the rock properties but also the cutting operational parameters and the understanding of this threshold is important to optimise the tool design and operational parameters. This study attempts to identify the critical transition depth using an empirical model to describe the material removal regime from an energy perspective. In the ductile failure cutting mode, the specific cutting energy is found to be independent of the depth of cut; but in the brittle failure cutting mode, the specific cutting energy is found to be dependent on the depth of cut following a power-law relationship. The transition point in terms of the depth of cut is identified as the intersection point between these two relationships. Experimental tests with different combinations of cutting velocity, depth of cut and back rake angle are conducted and the combination of the data and the model developed in this study provides a very effective tool to analyse the cutting mechanism and to identify the critical transition depth.

***Keywords*:** Scratch test; Cutting test; Failure mode; Ductile-brittle transition; Transition depth

3.1 Introduction

Material scratching or cutting is widely used in many fields of science and engineering. The operation typically involves plowing or cutting a material with a scratch device, such as a Polycrystalline Diamond Compact (PDC) cutter, penetrating at a certain depth into the material under the application of a vertical load. Strictly speaking, scratching and cutting, however, are different at least in two aspects. Firstly, the penetration depth for scratching is usually smaller than that for cutting; secondly, in general scratching is performed with either a constant or increasing vertical load while constant vertical load is employed in cutting. As most studies cited in this study use a constant vertical load and the depth of cut falls within a moderately wide range of values, the two terms are used interchangeably in this article. Application examples of scratch tests include the measurement of strength and fracture properties of various materials such as rocks (Akono et al. 2011; Richard et al. 2012), the damage analysis of ceramics (Klecka and Subhash 2008; Tan et al. 2012), the assessment of tool wear (Ersoy et al. 2005; Tönshoff et al. 2002) and the performance measurement of thin films and coatings (Barletta et al. 2008; Randall et al. 2001).

During the scratching or cutting process, there is a critical depth beyond which rock failure shifts from the ductile-dominated to the brittle-dominated regime. When the depth of cut is small, the rock failure is a strength-driven process with energy dissipated within the failed material in the form of a plastic flow (see Fig. 3.1a) and the average cutting force is proportional to the depth of cut (see the black solid line in Fig. 3.1c). In contrast, in deep cutting, in which the rock failure is dominated by the brittle regime with energy dissipated in creating macroscopic discontinuous cracking surfaces ahead of the scratch tool (Fig. 3.1b), the cutting force deviates from the linear trend and exhibits a scaling relationship with the square root of the depth of cut, following the theory of linear elastic fracture mechanics (LEFM), as illustrated by the red solid curve in Fig. 3.1c.

The ductile-to-brittle failure transition of rock subjected to cutting has attracted many researchers' attention and the pioneering work was done by Detournay and his collaborators (Huang et al. 2013; Nicodeme 1997; Richard 1999; Richard et al. 2012; Richard et al. 1998; Zhou and Lin 2014). In the case of rock engineering, such as coring or mechanical excavation, it is often of great significance to ensure high quality coring or to control the extent of rocks being removed. Therefore, ensuring the removal of rock materials via cutting in a particular regime is crucial and it is imperative to identify the threshold value of the depth of cut that separates ductile-regime cutting from brittle-regime cutting. Through extensive cutting tests, Richard et al. (1998), for example, reported that the two different material failure mechanisms are reflected in the variations in cutting forces with regard to the depth of cut, i.e., in ductile-regime cutting, the tangential cutting force (F_t shown in Fig. 3.5b) is proportional to the projected contact area between cutter and rock normal to the direction of cut; while in brittle-regime cutting, the force is expected to be proportional to the square root of the depth of cut. The critical failure mode transition depth is given as $d_c \propto (K_{IC}/\sigma_c)^2$, where K_{IC} and σ_c are fracture toughness and uniaxial compressive strength (UCS) of the rock respectively. This relationship offers mainly a qualitative description between the critical depth and rock mechanical properties and it also requires the determination of K_{IC} and σ_c first which may complicate its application in engineering practice.

Considering the energy dissipation for removing the rock material, ductile mode cutting is accomplished by volumetrically deforming the material ahead of the cutter (see Fig. 3.1a and Fig. 3.2a) while brittle mode cutting, as shown in Fig. 3.1b and Fig. 3.2b, is characterized with chippings formed by macro-scale fracturing. The current study aims to develop a quantitative empirical model to predict the critical transition depth using the evolvement of specific energy for different rocks subjected to various cutting arrangements with different operational parameters such as cutting velocity, depth of cut and back rake angle. Cutting tests were performed on two selected types of rocks following a full factorial experimental design in which cutting velocity, depth of cut and back rake angle have several consideration levels. The quantitative model to determine the critical transition depth from the perspective of energy balance was then established based on the theoretical analyses and the experimental data.

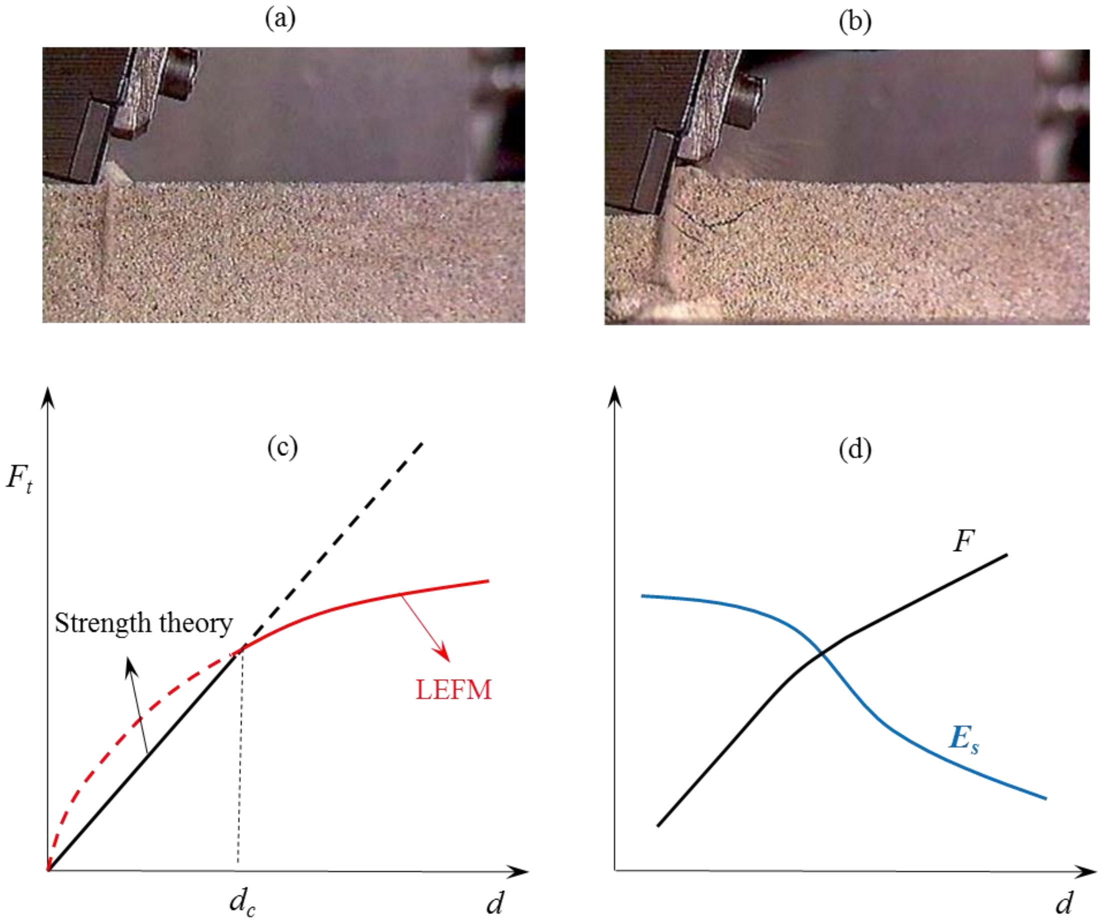

Fig. 3.1 Rock failure in (a) ductile mode (b) brittle mode (after Richard (1999)) and schematic plot for the corresponding variation of (c) tangential cutting force and (d) specific energy with depth of cut.

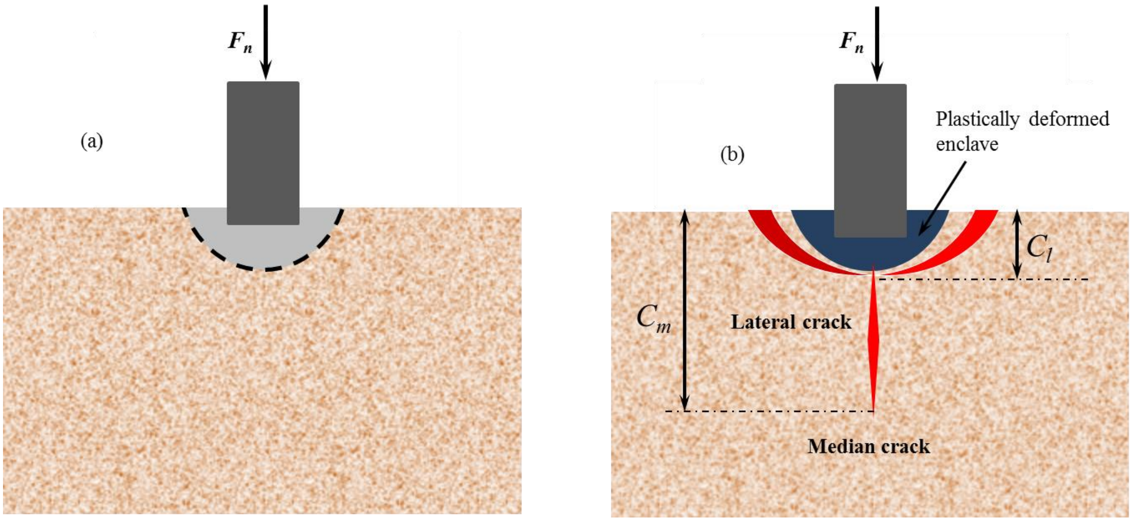

Fig. 3.2 Schematic plot of cutting in (a) ductile mode and (b) brittle mode depicted in the plane normal to the cutting direction and thus the tangential cutting force is not included.

3.2 Model formulation

In rock cutting, the transition from ductile to brittle mode cutting due to the increasing depth of cut is accompanied by a reduction in the specific cutting energy, as sketched in Fig. 3.1d where the specific cutting energy E_s decreases with depth of cut, d , and the cutting force component, either normal or tangential, increases linearly until the critical depth, d_c , above which deviation from this linear relationship becomes evident. Since ductile mode cutting removes the rock material through plastic deformation and brittle mode cutting mainly through brittle fracture, their energy consumptions are expected to be different and therefore it is plausible to use the corresponding specific energy to understand the transition phenomenon. It is therefore potential to characterise the cutting failure transition by means of developing a model to trace specific cutting energy variation.

3.2.1 Ductile-mode energy

The energy consumed in ductile-mode cutting is regarded as the product of tangential component of the resultant cutting force and the moving distance of the cutter. One part of the energy is used to deform the rock material and the other part to overcome the sliding friction at the interface of wear flat of the cutter and the newly-cut rock surface.

Assuming the material in front of rake face is plastically deformed and removed in a continuous fashion (see Fig. 3.1a and Fig. 3.2a), by incorporating the effect of the back rake angle, the tangential component of cutting force for plastic deformation is given as

$$F_{t\_p} = \eta \sigma_c A_c \tag{3.1}$$

where η is a geometric factor characterising the influence of back rake angle α which is defined as the angle between the rake face and the normal to the rock surface (see Fig. 3.5b), σ_c is UCS and $A_c = Wd$ is the cross sectional area normal to the direction of cutting with W and d being width and depth of cut respectively. Eq. (3.1) introduces a geometric factor η to quantify the effect of α on specific cutting energy, which is different from the models developed by Detournay and Defourny (1992) and Richard et al. (2012), who only used $F_{t\_p} = \sigma_c A_c$ with a fixed back rake angle at 15°. As evident from the experimental results from Richard (1999), the specific cutting energy rises with increasing back rake angle.

Therefore, the energy consumed for removing rock material resulting from plastic deformation can be given as

$$E_{d\_p} = F_{t\_p} \Delta l = \eta \sigma_c A_c \Delta l \tag{3.2}$$

where Δl is the cutting distance.

As well as the energy consumed in plastically deforming the rock material, the energy consumed in overcoming the sliding friction is given as

$$E_{d\_s} = \mu_{d\_s} \sigma_f A_f \Delta l \tag{3.3}$$

with μ_{d_s} being the sliding friction coefficient and

$$\sigma_f = kH\sqrt{H/E} \tag{3.4}$$

where k is a constant relating the contact stress σ_f on the wear flat to the rock hardness H and elastic modulus E , and $A_f = WL$ is the contact area between wear flat and rock surface with L being the length of the wear flat (Arcona and Dow 1998).

The total energy for ductile-mode cutting is the sum of energies consumed for the plastic deformation and the friction:

$$E_d = E_{d\_p} + E_{d\_s} \tag{3.5}$$

3.2.2 Brittle-mode energy

When both the depth of cut and the load applied are increased to values large enough to propagate lateral cracks, material is removed by crack propagation and fracturing dominates the cutting process. As a first order approximation, the material removed through lateral cracking is a half cylinder of radius C_l (see Fig. 3.2b) and length Δl (Bifano and Fawcett 1991). Thus the volume of material removal is:

$$V_b = \frac{\pi}{2} C_l^2 \Delta l \tag{3.6}$$

where C_l is the length of the lateral crack and it was found to be roughly related to the subsurface damage (Bifano and Fawcett 1991), i.e., the median crack C_m as shown in Fig. 3.2b by

$$C_l \cong C_m / k_1 \tag{3.7}$$

where k_1 is a scaling constant. As C_m is related to the normal load F_n by a power law $C_m \propto F_n^{2/3}$ and F_n can be further scaled to d by $F_n \propto d^2$ (Bifano and Fawcett 1991; Marshall and Lawn 1986). Combining these results, we can obtain

$$C_l \propto d^{4/3} \tag{3.8}$$

The energy consumption for fracturing is due to the creation of new surfaces associated with lateral and median cracks and is determined by the specific surface energy γ_s of the rock which is the energy required to create a unit of new surface area (Friedman et al. 1972). The fully cracked surface area was given by Bifano and Fawcett (1991) as $A_s = \left(2\pi C_l + 2C_m\right)\Delta l$. Hence the fracture energy associated with the generation of new surfaces considering lateral and median cracks is given by:

$$E_{b\_f} = A_s\gamma_s = \left(2\pi C_l + 2C_m\right)\gamma_s\Delta l \tag{3.9}$$

Apart from the energy required for brittle fracture, there is energy dissipated in the plastically deformed enclave (see Fig. 3.2b) which is related to the yield strength and the volume of deformed material (Bifano and Fawcett 1991) as:

$$E_{b\_p} = \lambda\sigma_y V_p \tag{3.10}$$

where λ is a constant, σ_y is the yield strength and V_p is the volume of the plastically deformed enclave. Assuming the radius of the plastic deformation zone is approximately equal to C_l, then $V_p \approx \pi/4 C_l^2 \Delta l$ and the total energy consumed in brittle-mode cutting amounts to:

$$E_b = E_{b\_f} + E_{b\_p} = \left(2\pi C_l + 2C_m\right)\gamma_s \Delta l + \frac{\pi}{4}\lambda\sigma_y C_l^2 \Delta l \tag{3.11}$$

3.2.3 Specific cutting energy

For cutting length of Δl, the volume of removed material for ductile mode is

$$V_d = A_C \Delta l \tag{3.12}$$

For the brittle mode, much more material is removed due to fracturing and the crack propagation to the free surface of the rock. The cross section of the cutting groove is larger than the projection area of the cutter itself (A_C) due to lateral and median cracking. The total volume of material removed in brittle-mode cutting is given in Eq. (3.6) as $V_b = \pi/2\, C_l^2 \Delta l$.

Defined as the energy required to remove unit volume of material (Teale 1965), the corresponding specific cutting energy for ductile mode is given as:

$$E_{s\_d} = \frac{E_d}{V_d} \tag{3.13}$$

Combined with Eqs. (3.2)-(3.4), Eq. (3.13) can be rewritten as

$$E_{s\_d} = \eta\sigma_c + \mu_{d\_s} k H \sqrt{H/E}\, \frac{L}{d} \tag{3.14}$$

For our experiments, since the PDC cutters used are new ones with sharp cutting edge, it is reasonable to assume that the length of wear flat L is small and the contribution of the second term in the above equation is negligible, i.e.,

$$E_{s\_d} = \eta \sigma_c \tag{3.15}$$

Similarly, we have the specific cutting energy for brittle-mode cutting (Bifano and Fawcett 1991):

$$E_{s\_b} = \frac{E_b}{V_b} = \frac{\left(2\pi C_l + 2C_m\right)\gamma_s \Delta l + \frac{\pi}{4}\lambda \sigma_y C_l^2 \Delta l}{\pi/2\, C_l^2 \Delta l} \tag{3.16}$$

Substituting the scaling relationships (3.7) and (3.8) into Eq. (3.16) yields

$$E_{s\_b} = k_b d^{-4/3} + k_p \tag{3.17}$$

where k_b is combination factor associated with both cutting geometry and material properties K_{IC}, γ_s, H and E and the crack sizes of C_l and C_m depend on these material properties (Lawn and Cook 2012; Lawn 1998); k_p is a constant representing the specific energy to create the plastic deformation zone. Eq. (3.17) indicates that the specific cutting energy will decrease as d increases, asymptotically approaching to a constant value k_p for large values of d.

Eq. (3.15), on the other hand, indicates that the specific cutting energy for ductile-mode cutting retains constant for each back rake angle, suggesting that the specific cutting energy is independent of the depth of cut. Note this energy term depends on the back rake angle since the geometry factor η introduced in this study is mainly determined by the back rake angle.

The differences in the specific energy between ductile mode and brittle mode cuttings are used to facilitate the identification of the critical transition depth discussed above. As implied by Eq. (3.15), the specific energy for ductile-regime cutting is independent of the depth of cut; therefore it can be represented by a horizontal line if we plot it with respect to $d^{-3/4}$ (see the black line segment in Fig. 3.3). By comparison, the specific cutting energy for brittle-regime cutting given in Eq. (3.17) becomes a straight line with a slope k_b and an intercept k_p (see the red line segment in Fig. 3.3). Therefore, Eqs. (3.15) and (3.17) together define a piecewise function characterising the whole cutting process by relating the specific energy to depth of cut as:

$$E_s = \begin{cases} \eta\sigma_c & d < d_c \\ k_b d^{-4/3} + k_p & d > d_c \end{cases} \tag{3.18}$$

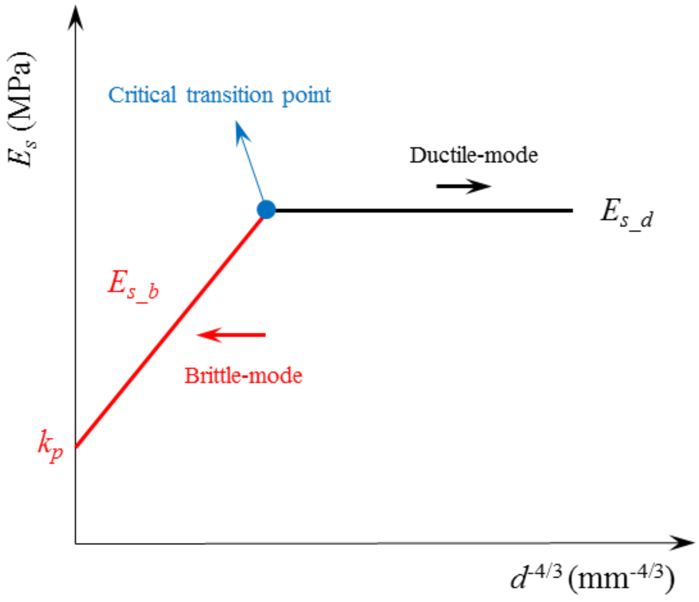

Fig. 3.3 Schematic graph demonstrating the approach to identify the critical transition point where cutting changes from ductile-dominated to brittle-dominated regime.

Subsequently, this specific cutting energy transition model given by the piecewise function is used to fit the experimental data for a particular type of rock under certain operational parameters. The critical transition depth d_c thus can be quantitatively identified as the intersection point of the two line segments representing these two distinct failure regimes. As will be demonstrated later, this approach provides a much better way of defining the value for d_c in terms of both accuracy and clarity, compared with other methods reported in the literature.

3.3 Test methodology

3.3.1 Experimental setup

The scratch tests were carried out using the Rock Strength Device (RSD) in the CSIRO laboratory in Perth, Australia (Detournay and Defourny 1992; Richard et al. 2012). As can be seen in Fig. 3.4a, the main components of RSD include the traverse base with a sample holder (indexed *1* on Fig. 3.4a), a movable cart (*2*) housing the vertical positioning system (*3*), a load cell (*4*) and a cutting unit (*5*). The cart is driven horizontally by a computer-controlled stepper motor (*6*) operating a ball screw (*7*) through a gearbox (*8*). The vertical positioning system (*9*) is tuned to adjust the depth of cut manually with the assistance of a micrometer (*10*). Once the desired depth is reached, the position of cutter is fixed by means of a rigid locking system (*11*) so that a constant depth of cut can be maintained during cutting. Force signal acquisition is achieved by a load sensor and a National Instruments data acquisition (DAQ) system controlled by LabVIEW®. The load measuring system can measure the tangential and normal components of the force acting on the cutter up to 4000 N with a precision of 1 N. For detailed specifications of this testing system, readers are referred to Richard et al. (2012).

The PDC cutter used in the test is clamped to the tool holder, as shown in Fig. 3.4b, which allows a 5-degree incremental change in the back rake angle. The back rake angles in this study are set to 5°, 15°, 30° and 45°. The PDC cutter used in our tests has a width of 10 mm coated with a thin layer of polycrystalline diamond on a tungsten carbide base.

The rocks used in our tests are two types of limestone: Savonnières and Tuffeau (see Fig. 3.4c). The rock samples were selected due to their relatively high homogeneity and low strength. The material homogeneity will help to achieve a low dispersion in terms of the interpretation of the experimental results. Two different types of rocks enable us to investigate the influence of different rock properties on force responses.

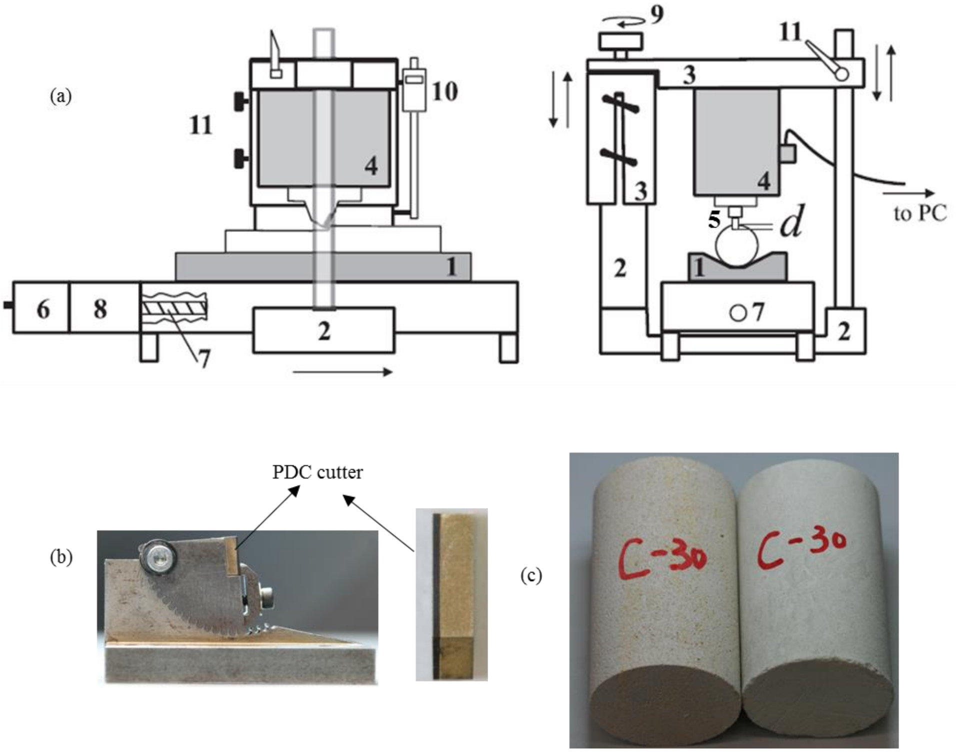

Fig. 3.4 (a) Front and side view of the sketch of the RSD reproduced after Richard et al. (2012); (b) Cutter holder with a PDC cutter held at a 5° back rake angle and (c) Core limestone samples: Savonnières (left) and Tuffeau (right). C-30 represents the third set with a back rake angle of 30°.

3.3.2 Test procedure

The independent variables to be explored in the experiments are the depth of cut, the back rake angle and the cutting velocity to assess the effects of these parameters on rock cutting responses. The depth of cut includes seven consideration levels ranging from 0.1 to 0.7 mm at 0.1 interval; the back rake angle has four levels at 5°, 15°, 30° and 45° and the cutting velocity to be considered has five levels at 4, 8, 13, 17 and 20 mm/s. In other words, there are 4×5×7=140 number of combinations of these parameters for each type of rock. The geometrical representation of the design of experiments is shown in Fig. 3.5a and a typical set of cutting parameters for $\alpha = 5°$ is summarised in Table 3.1. For each rock sample, scratch tests were carried out with a sharp PDC cutter of 10 mm wide with different levels of back rake angle α as shown in Fig. 3.5b, depth of cut d and cutting velocity V. The total 280 tests are grouped into four sets based on four different levels of back rake angles. A typical set of tests consists of measuring forces varying with depth of cut and cutting velocity, i.e., the tangential and normal components F_t and F_n , which are parallel and normal to the cutter advancing direction respectively.

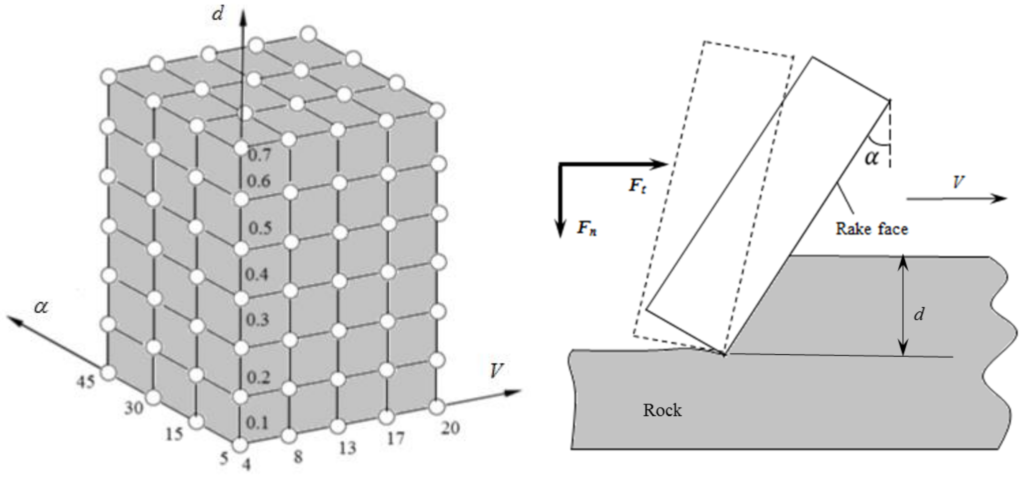

(a) (b)

Fig. 3.5 Geometrical representation of (a) the 4×5×7 full factorial design of experiments and (b) the cutter-rock interaction model.

Before starting the scratch test, samples are visually inspected for potential damage caused by the sample preparation. Then several preliminary cuts were done to give a smooth reference plane. After the reference plane is prepared, the micrometer was reset to zero. The depth of cut was then set to the required value for the desired test. If the failure of rock is in the brittle regime and discontinuous chip formation occurs during the reference plane preparation, a couple of cuts at shallow depths are then applied until a flattened plane is achieved.

Table 3.1 An example of cutting parameters design for $\alpha = 5°$.

	Test no.	α (°)	V (mm/s)	d (mm)
Set 1	1	5	4	0.1
	2	5	4	0.2
	3	5	4	0.3
	4	5	4	0.4
	5	5	4	0.5
	6	5	4	0.6
	7	5	4	0.7
	8	5	8	0.1
	9	5	8	0.2
	10	5	8	0.3
	11	5	8	0.4
	12	5	8	0.5
	13	5	8	0.6
	14	5	8	0.7
	15	5	13	0.1
	16	5	13	0.2
	17	5	13	0.3
	18	5	13	0.4
	19	5	13	0.5
	20	5	13	0.6
	21	5	13	0.7
	22	5	17	0.1
	23	5	17	0.2
	24	5	17	0.3
	25	5	17	0.4
	26	5	17	0.5
	27	5	17	0.6
	28	5	17	0.7
	29	5	20	0.1
	30	5	20	0.2
	31	5	20	0.3
	32	5	20	0.4
	33	5	20	0.5
	34	5	20	0.6
	35	5	20	0.7

Each test with the preset cutting specifications was conducted at least three times along the same groove to minimise the influence of possible inhomogeneity such as fracture, micro defects and bedding plane in the rock specimen. Due to the difficulty in changing the back rake angle through adjusting the cutter holder, tests with different pairs of (*d*, *V*) at one level of the four back rake angles were completed first before moving on to the tests on the next back rake angle.

3.4 Results and discussions

In the following discussions, Section 3.4.1 presents the general descriptions of force logs during the course of cutting. In Section 3.4.2 the effects of operational parameters including cutting velocity, depth of cut and back rake angle on the cutting forces and specific cutting energy are discussed. These discussions lead to the identification of the critical cutting depth. Section 3.4.3 describes the effect of rock properties, using two different types of rocks, on cutting forces and the specific cutting energy, which leads to the discussion of the dependence of the critical transition depth on rock mechanical properties. Finally, comparison between the conceptual mode proposed in Richard et al. (1998) and the empirical model developed in this study in terms of the critical cutting depth prediction is presented.

3.4.1 General characteristics of the force logs

The two force components were measured at a sampling rate of 600 Hz in our tests. Fig. 3.6 gives an example of force traces for the Savonnières and Tuffeau sample, from which we calculate the mean and standard deviation of the forces using the values within the steady-state cutting section. Overall, the force components exhibit a similar trend: an initial peak when the cutter comes into contact with the rock specimen followed by the main steady state cutting section. When the cutter approaches the end of the core specimen, the forces experience a mild drop due to change in boundary conditions.

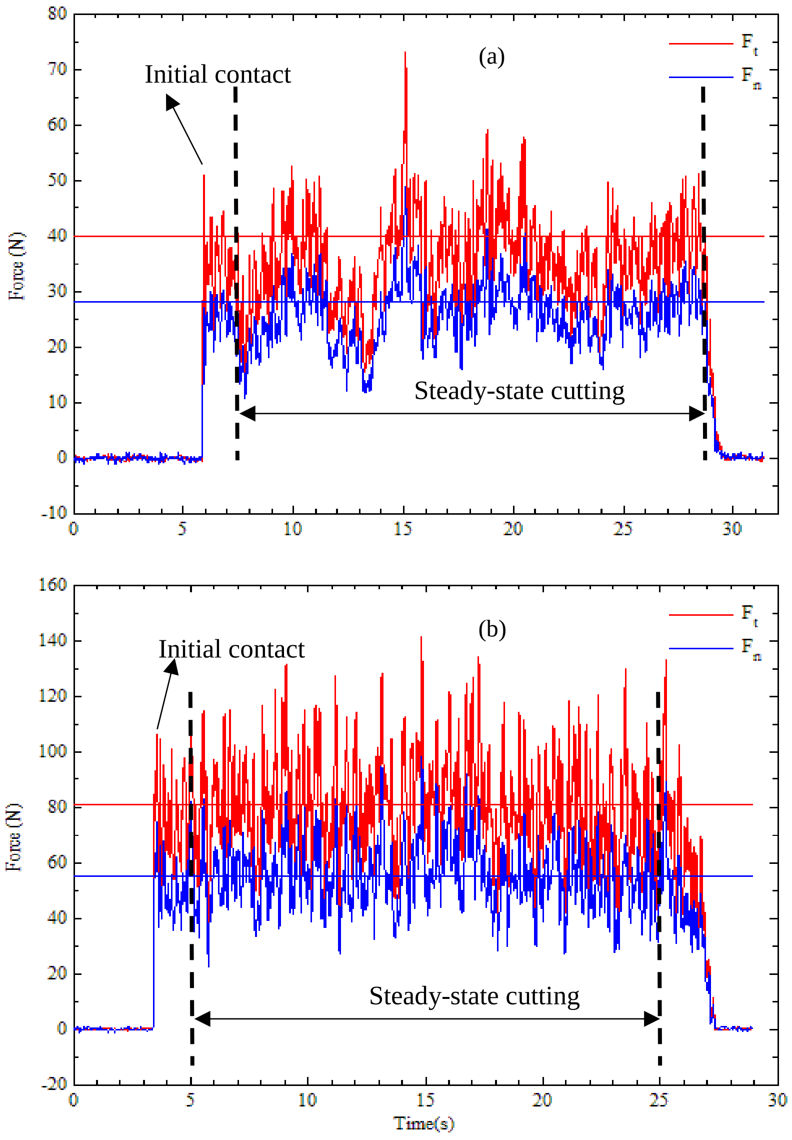

Fig. 3.6 Force traces recorded for a scratch test on (a) Tuffeau and (b) Savonnières showing tangential force F_t and normal force F_n as a function of time (d=0.4 mm, α=15° and v=4 mm/s). Straight lines represent the mean values averaged over the steady-state cutting region.

The force traces can provide a supplementary perspective to examine how rock properties influence the cutting mode. As described by Richard et al. (2012), the force log resembles white noise variation for ductile-regime cutting but it expresses a pattern of saw-tooth fluctuation when cutting enters the brittle mode. Based on this simple judgment, it can be inferred that for the cases shown in Fig. 3.6, under the same operational parameters the brittle-mode cutting occurs on Tuffeau (Fig. 3.6a) but not on Savonnières (Fig. 3.6b). From this observation, we can understand that rock properties play a very important role in charatersing the rock cutting mechanisms.

3.4.2 Effect of operational parameters

3.4.2.1 Effect of cutting velocity

As a preliminary investigation, Fig. 3.7 presents an example of scatter plots and fitted relationships for the tangential cutting force at a back rake angle of 45°. This example shows the variation of forces with different cutting velocity and depth of cut for Tuffeau and Savonnières. The fitted surfaces appear to be parallel with the axis of cutting velocity, suggesting the effect of cutting velocity on force responses is insignificant, which was also reflected in Fig. 3.8-Fig. 3.15 for both Savonnières and Tuffeau (in these figures, red and black markers stand for the tangential and normal cutting force, F_t and F_n, respectively). One might argue that in some cases, especially for the force data of the brittle cutting cases, cutting velocity has some influence on the cutting forces. However no consistent trend can be observed for the range of cutting velocity examined and the differences in cutting forces due to different cutting velocity are likely to be due to the inherent nature of high variability in cutting forces in brittle failure regime (Richard et al. 2012).

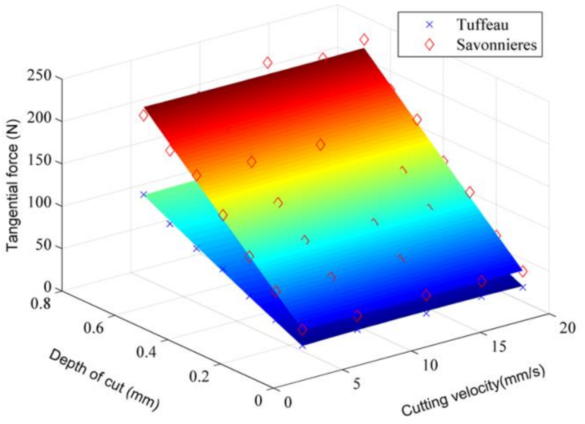

Fig. 3.7 Tangential cutting force for Tuffeau and Savonnières varying with cutting velocity and depth of cut for back rake angle of 45°.

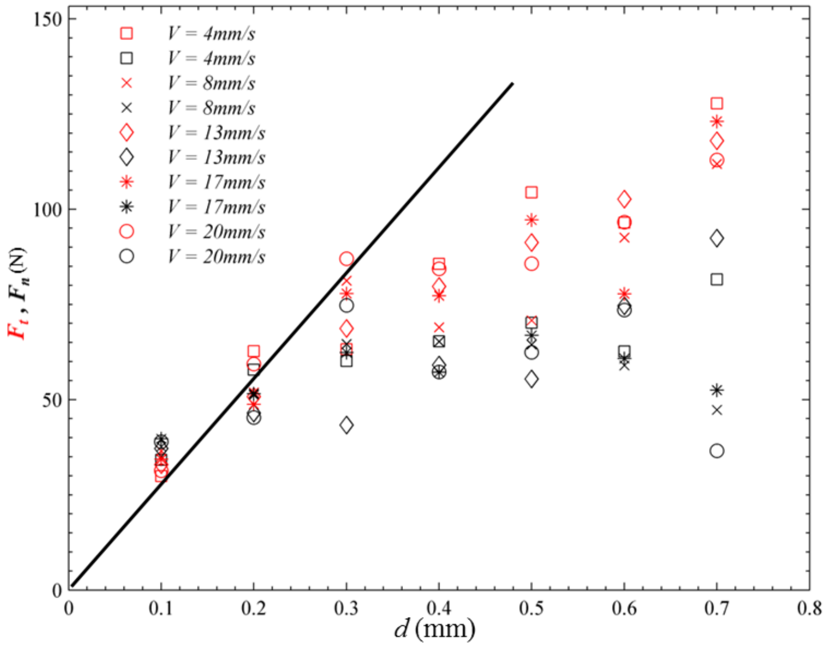

Fig. 3.8 Cutting forces varying with depth of cut for Savonnières at five levels of cutting velocities for back rake angle of 5°.

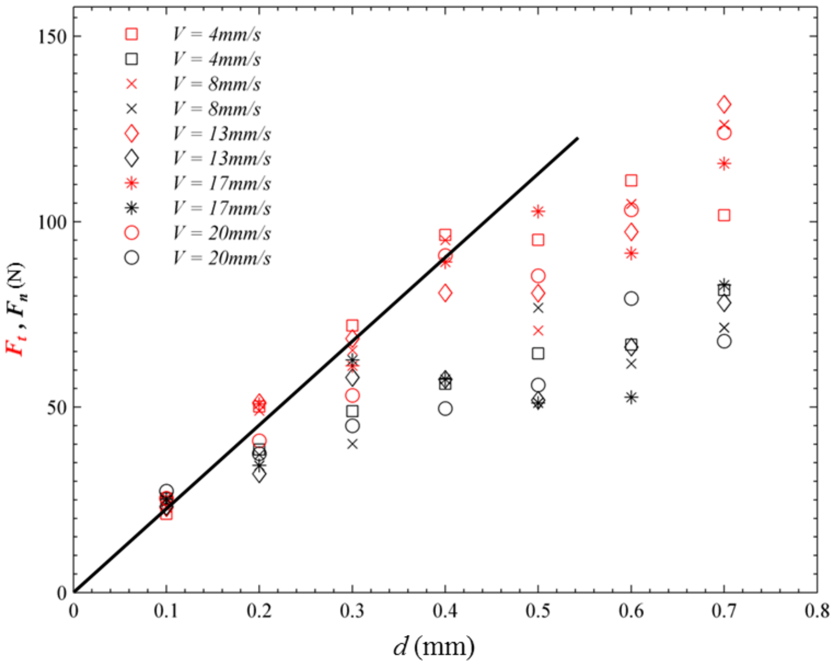

Fig. 3.9 Cutting forces varying with depth of cut for Savonnières at five levels of cutting velocities for back rake angle of 15°.

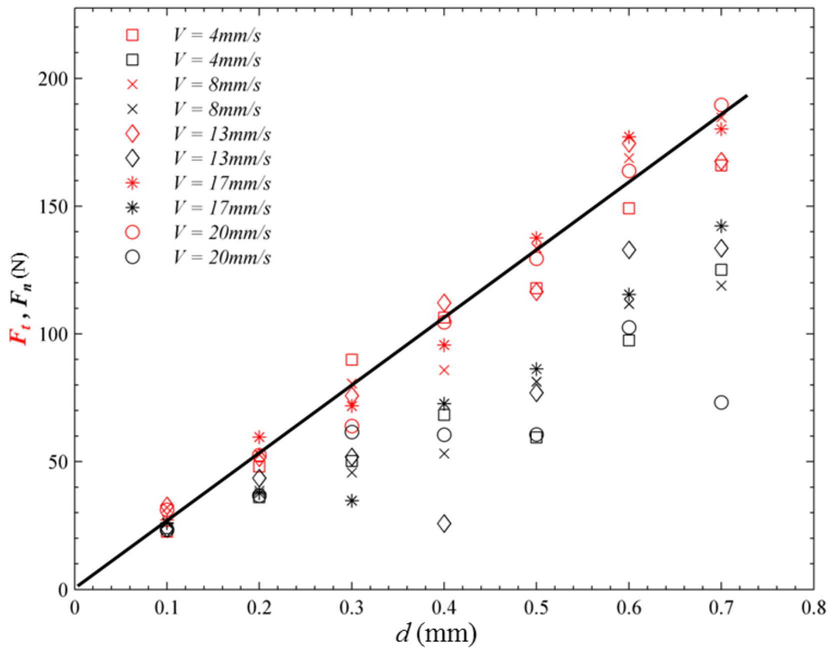

Fig. 3.10 Cutting forces varying with depth of cut for Savonnières at five levels of cutting velocities for back rake angle of 30°.

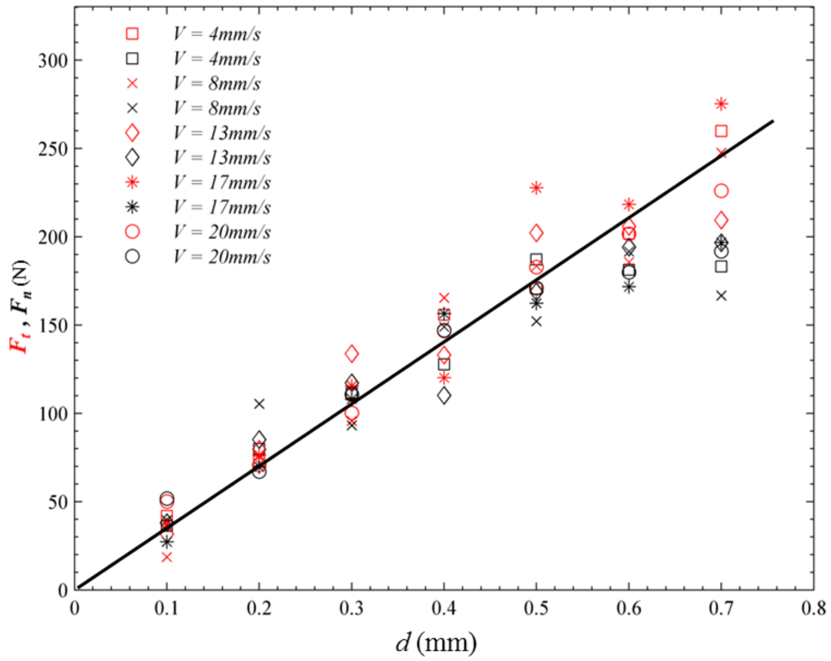

Fig. 3.11 Cutting forces varying with depth of cut for Savonnières at five levels of cutting velocities for back rake angle of 45°.

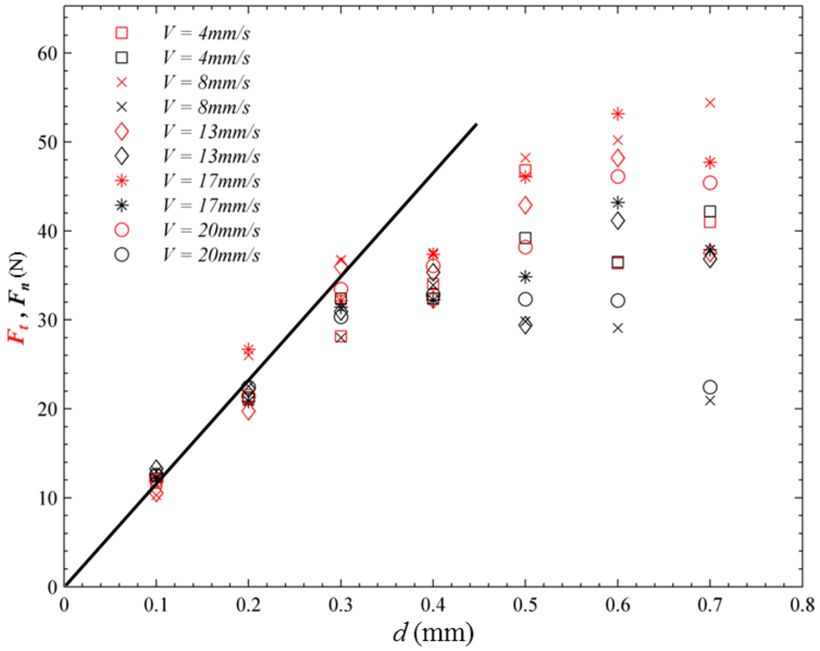

Fig. 3.12 Cutting forces varying with depth of cut for Tuffeau at five levels of cutting velocities for back rake angle of 5°.

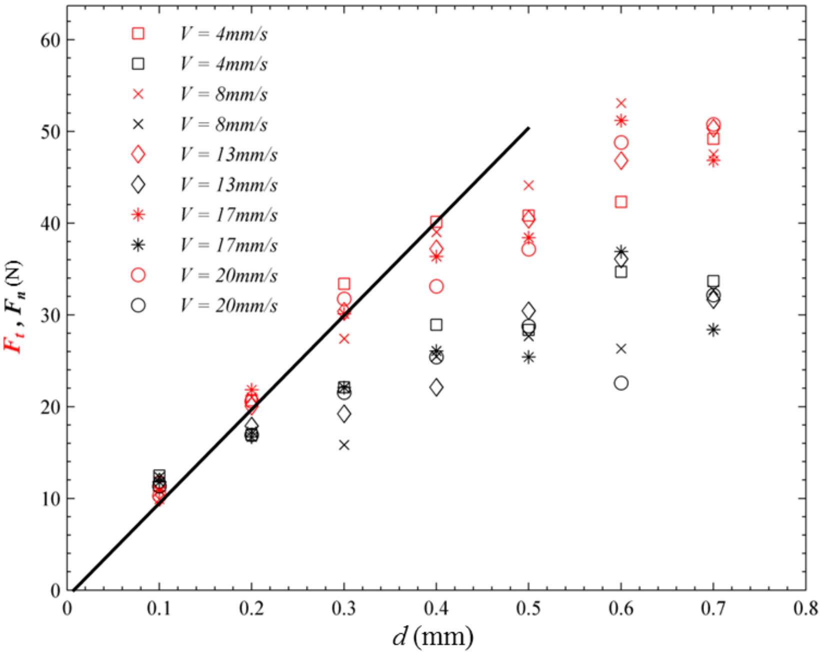

Fig. 3.13 Cutting forces varying with depth of cut for Tuffeau at five levels of cutting velocities for back rake angle of 15°.

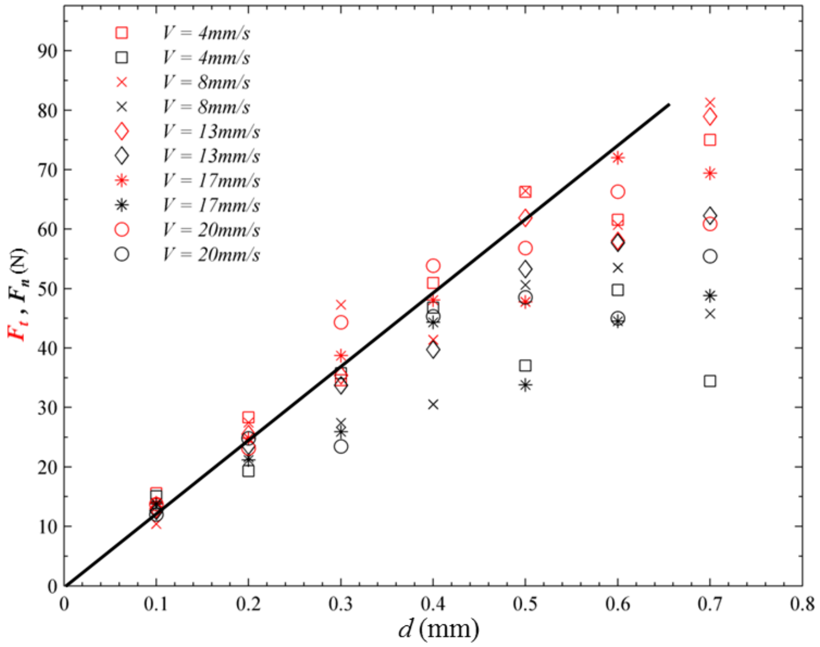

Fig. 3.14 Cutting forces varying with depth of cut for Tuffeau at five levels of cutting velocities for back rake angle of 30°.

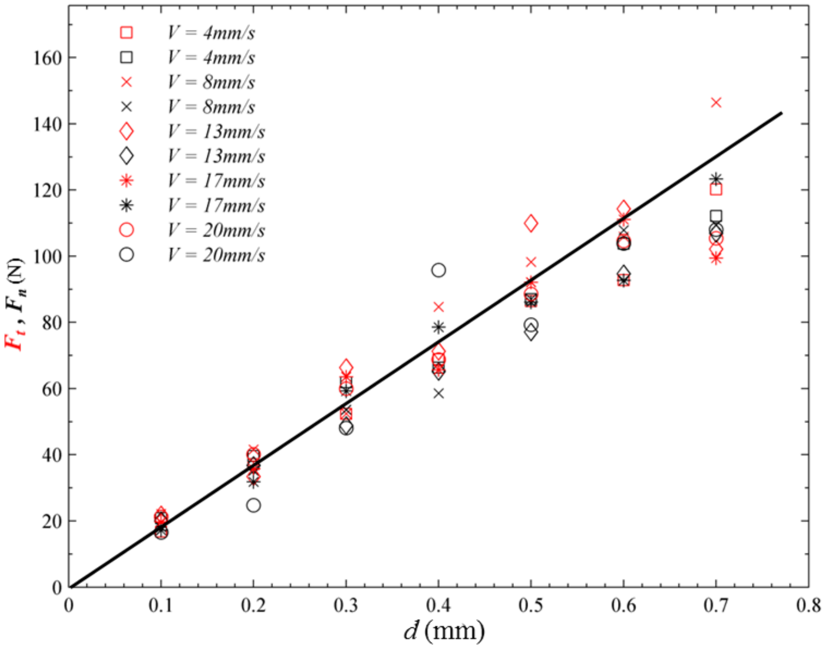

Fig. 3.15 Cutting forces varying with depth of cut for Tuffeau at five levels of cutting velocities for back rake angle of 45°.

Fig. 3.16-Fig. 3.19 and Fig. 3.20-Fig. 3.23 are graphs of the specific cutting energy versus depth of cut d raised to the power of -4/3 for Tuffeau and Savonnières respectively. The specific cutting energy in this case is calculated as $(F_t \Delta l)/(Wd\Delta l)$, where F_t is the measured cutting force and $Wd\Delta l$ is the nominal cutting volume. This nominal cutting volume is an accurate representation of the actual cutting volume in ductile cutting mode but it is only an approximate in brittle cutting mode. This approximation, as demonstrated in our analysis, does not affect the identification of the critical transition point.

Similarly to the trends for cutting forces, the results show that the cutting velocity in the range of 4-20 mm/s hardly influences the specific cutting energy. Based on these results, it is reasonable to conclude that the effect of cutting velocity in the range of 4-20 mm/s on cutting forces or the critical transition depth is insignificant compared with other parameters and therefore they can be neglected in further considerations. However, one should be aware this conclusion may not be valid for high cutting velocity when rock dynamic responses have to be considered (Li et al. 2001; Menezes et al. 2014).

3.4.2.2 Effect of depth of cut

As an important operating parameter, the depth of cut is the dominant factor controlling the transition from ductile-to-brittle failure cutting mode. In this study, tests were performed at depth between 0.1-0.7 mm. The plots in Fig. 3.8-Fig. 3.15 show that the forces, both the tangential and normal components, increase with the depth of cut, as expected. When the back rake angle is small, e.g., when $\alpha = 5°$, the variability of forces becomes greater as the depth of cut increases, which is a sign of the occurrence of brittle fractures where periodical material removal mechanism dominates the cutting process (Guo et al. 1992; Nishimatsu 1972). The dispersion and deviation of the cutting forces provides a qualitative way to determine the critical transition depth. The lines in these graphs show the proportional relationship between the cutting force and the cutting depth ($F_t \propto \sigma_c Wd$) only if the ductile failure mode is considered. As can be seen from these graphs, as the depth of cut gets greater the actual cutting force deviates more and more from the linear relationship, indicating the brittle failure mode becomes more and more dominant. The point where the cutting force starts deviating from the linear relationship can then be used to give an approximate estimate on the critical transition depth, even though the point in most cases is not directly obvious particularly when the test data are limited. For example, cutting on Tuffeau at $\alpha = 15°$, shown in Fig. 3.13, suggests a possible value of d_c between 0.3 mm and 0.4 mm. For other cases of cutting on both Tuffeau and Savonnières, the cutting force graphs do not give a clear indication of the transition point corresponding to d_c. As can be seen, there is significantly higher amount of uncertainty involved in this process compared with the method proposed in this research.

Unlike cutting forces, the degree of variability of specific cutting energy at different depths of cut appears to remain more or less the same (see Fig. 3.16-Fig. 3.23). Despite the increment in cutting forces, the specific energy for both Tuffeau and Savonnières with increasing depth of cut keeps roughly constant for ductile-regime cutting and decreases after the transition from ductile to brittle cutting mode. The volume of removed material increases discontinuously when the cutting mode changes. In other words, the volume of material removed is no longer linearly correlated with the depth of cut in brittle cutting mode, as it is in ductile cutting regime. The volume removed in this case is related to lateral crack dimension that has a power-law relationship with the depth of cut and the lateral cracks contribute greatly to more material being removed by brittle fractures. This is the main reason that the specific cutting energy shows a reduction with regard to the depth of cut even where the cutting forces actually increase. In comparison with Fig. 3.13 where there is no clear indication of the d_c value based on force logs for cutting on Tuffeau at $\alpha = 15°$, Fig. 3.17 constructed using the model proposed in this study offers a simple and clear method to estimate the d_c value which in the case is 0.35 mm.

Regardless of method used (cutting forces or specific energy), no obvious cutting mode transition can be observed for cutting tests on Tuffeau at $\alpha = 45°$

as shown in Fig. 3.15 (forces) and Fig. 3.19 (specific energy) and on Savonnières at $\alpha = 30°$ or $\alpha = 45°$ as shown in Fig. 3.10-Fig. 3.11 (forces) and Fig. 3.22-Fig. 3.23 (specific energy). This is caused by the relatively large back rake angle as discussed below.

3.4.2.3 Effect of back rake angle

Fig. 3.8-Fig. 3.15 display the forces varying with depth of cut for Tuffeau and Savonnières at different back rake angles. Overall the cutting forces increase as the back rake angle increases. In terms of the critical transition depth, smaller back rake angle causes forces to depart from the linear increasing trend at shallower depth, as shown in Fig. 3.8-Fig. 3.15 for both Tuffeau and Savonnières and the departing point can be used to estimate the d_c, as discussed above and also in Richard et al. (1998). For instance, the forces for Savonnières departing from the linear relationship at the depth of cut beyond 0.3 mm for α=5° (Fig. 3.8) and 0.4 mm for α=15° (Fig. 3.9). This is also reflected in the dispersion (or variability) of the measured data. Comparing between Fig. 3.8-Fig. 3.11, it is found that cutting on Savonnières at larger back rake angle, such as α=45°, generates less scattered data, which suggests the dominance of the ductile failure in cutting. This means the increase in α would lead to rock cutting changing from the brittle-dominated to the ductile-dominated failure when cutting at the same depth. Despite the qualitative description of the ductile-brittle transition, in general it is not clear about the specific depth at which the failure mode transition occurs.

To give a better and clearer estimate, the empirical model proposed in this study again can be used. When using the specific cutting energy transition model to fit the experimental data, initial values are given by examining the experimental data. For example, when cutting on Tuffeau at α=5° (Fig. 3.16), an initial value 0.3 mm for d_c seems to be a good choice and data fitting produces a very close d_c of 0.31 mm (Table 3.2).

The transition from ductile to brittle cutting mode can be clearly identified in these graphs. The data points for large α suggest the cutting tends to follow the ductile-regime (horizontal line), while points for small α suggest the cutting tends to follow more closely the brittle-regime (slopped line). The critical transition depth for both Tuffeau and Savonnières increases with the back rake angle until nearly α=45° for Tuffeau and α=30° for Savonnières wherein only ductile-mode cutting is observed. With increasing back rake angle, the intercept k_p also increases, implying more energy is consumed in plastically deforming the rock material (see Fig. 3.16-Fig. 3.18 for Tuffeau and Fig. 3.20-Fig. 3.21 for Savonnières). This is also partially attributed to the changes in cut debris flow from upward to downward as α increases, as demonstrated experimentally in Richard (1999) and Huang et al. (2013).

In comparison with the approximate estimation of d_c derived from the force logs, more accurate predictions can be achieved based on the specific cutting energy model proposed in this study, which give a specific critical depth of 0.33 mm for α=5° (Fig. 3.20) and of 0.42 mm for α=15° (Fig. 3.21) for Savonnières.

3.4.3 Effect of rock properties

We focus on the uniaxial compressive strength σ_c to investigate the influence of rock properties on the cutting responses. Cutting rocks of higher strength obviously requires greater forces to be applied on the cutter. Savonnières used in our tests has a UCS of 25 MPa and Tuffeau 10 MPa (Franca 2010). Both the tangential and the normal forces from the tests on Savonnières are always higher, as expected, than those of Tuffeau under the same operational parameters, i.e., same depth of cut and same back rake angle. However, based on force logs, we cannot make a definite conclusion on the influence of rock properties on the critical transition depth because most of the cutting force logs fail to give specific values of d_c. Instead, force logs can only offer an estimated range of d_c. For example, when cutting at α=5°, the failure mode transition can only be estimated to happen at the depth greater than 0.2 mm for both Savonnières and Tuffeau (Table 3.2). It is not possible in this case to draw any conclusion on the differences in the critical transition depths of these two rocks.

The specific cutting energy also varies with rock properties considerably. For cutting in ductile regime at the same back rake angle, Savonnières with higher UCS requires larger ductile specific cutting energy than Tuffeau, as expected. On the other hand, when the cutting changes into brittle mode, Savonnières exhibits a larger slope k_b than Tuffeau. However we have to be aware that the slope k_b is a factor related to both rock strength and rock fracture properties. Nevertheless a larger k_b indicates that harder rock may tend to have the failure mode transition occurring at greater cutting depth. Using the specific cutting energy as an index to determine the critical transition depth, it is interesting to see, for example, the critical depth d_c is 0.35 mm for Tuffeau when α=15°, compared to 0.41 mm for Savonnières. This may be explained by our previous work (He and Xu 2015) where the critical depth is linked to both the mineral grain size and the brittleness that is defined as the ratio of UCS to Brazilian tension strength. If we presume that the brittleness for the two rocks has the same value, say 10, then d_c depends only on the grain size. As can be seen in Fig. 3.4c, Savonnières is composed of larger grains than Tuffeau and therefore a larger d_c can be expected for Savonnières.

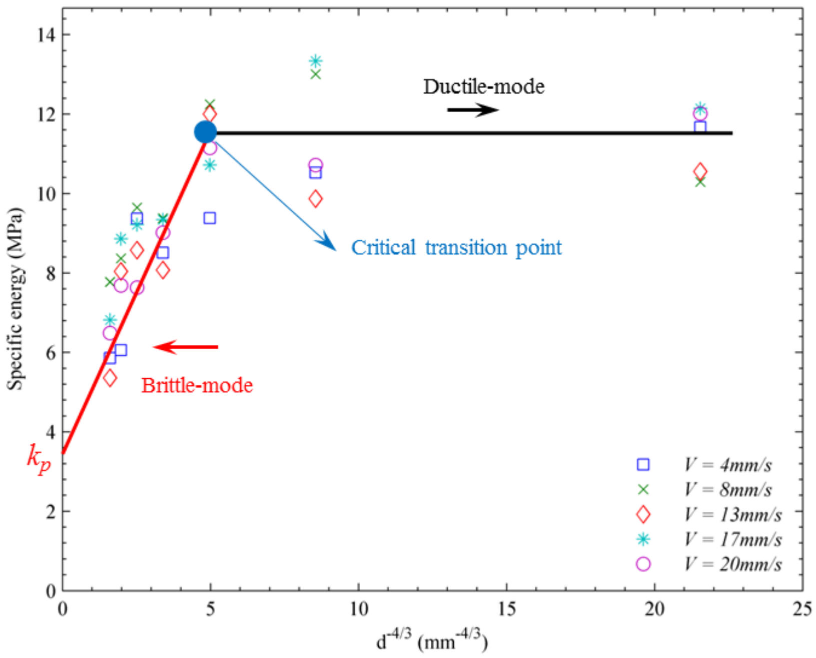

Fig. 3.16 Specific cutting energy versus $d^{-4/3}$ for Tuffeau at various cutting velocities with α=5°.

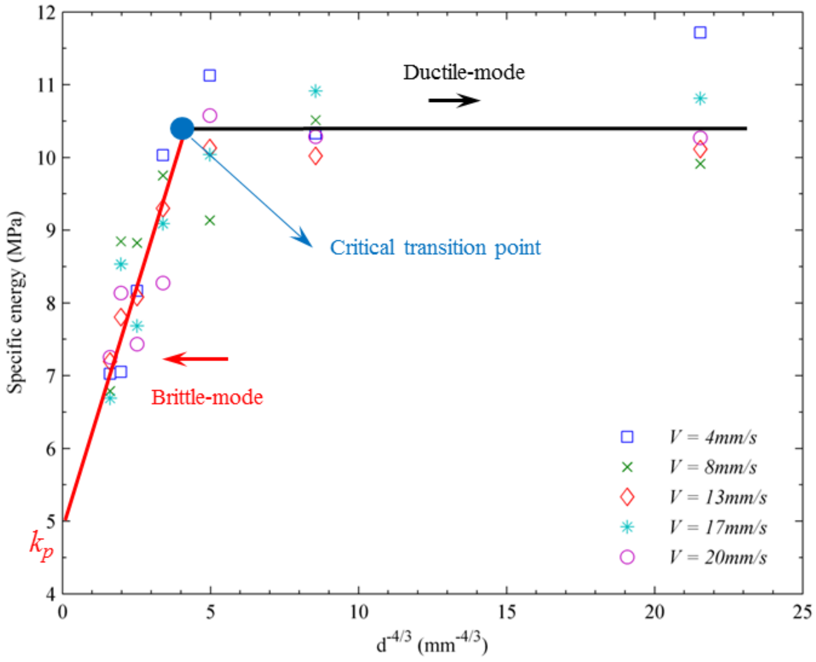

Fig. 3.17 Specific cutting energy versus $d^{-4/3}$ for Tuffeau at various cutting velocities with α=15°.

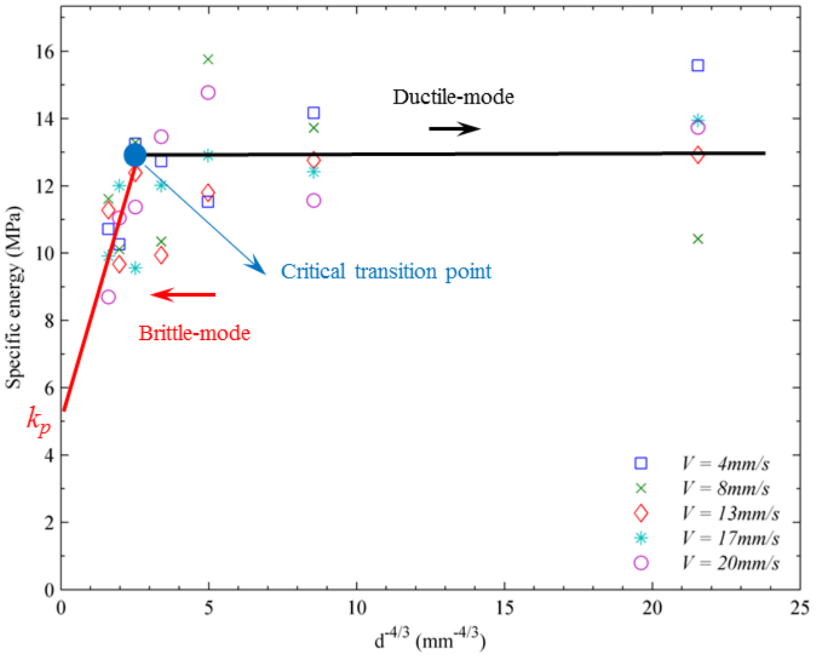

Fig. 3.18 Specific cutting energy versus $d^{-4/3}$ for Tuffeau at various cutting velocities with α=30°.

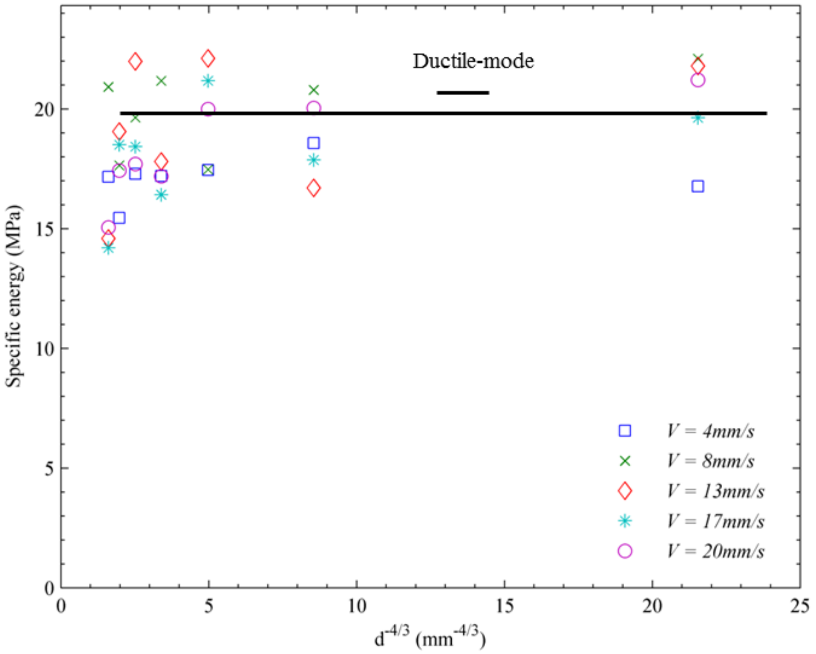

Fig. 3.19 Specific cutting energy versus $d^{-4/3}$ for Tuffeau at various cutting velocities with α=45°.

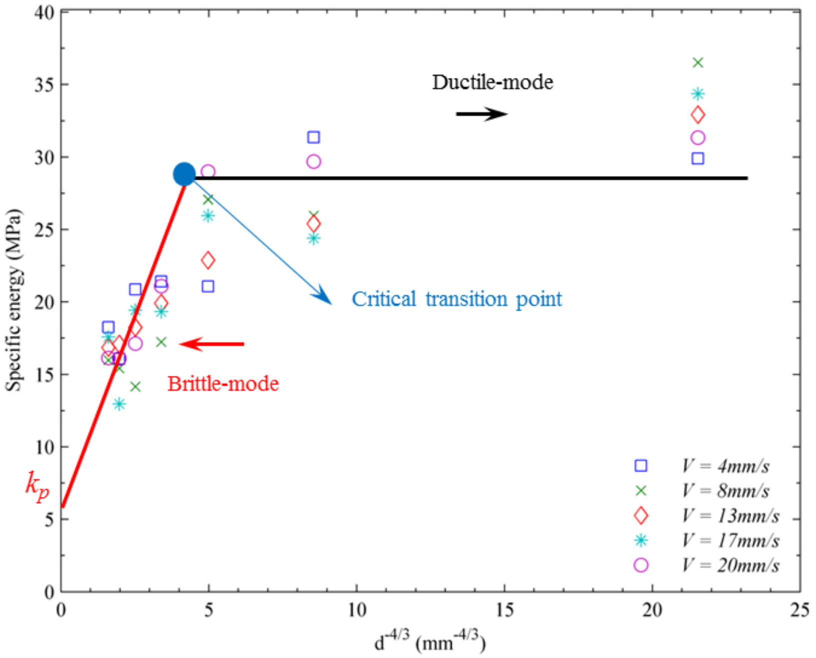

Fig. 3.20 Specific cutting energy versus $d^{-4/3}$ for Savonnières at various cutting velocities with α=5°.

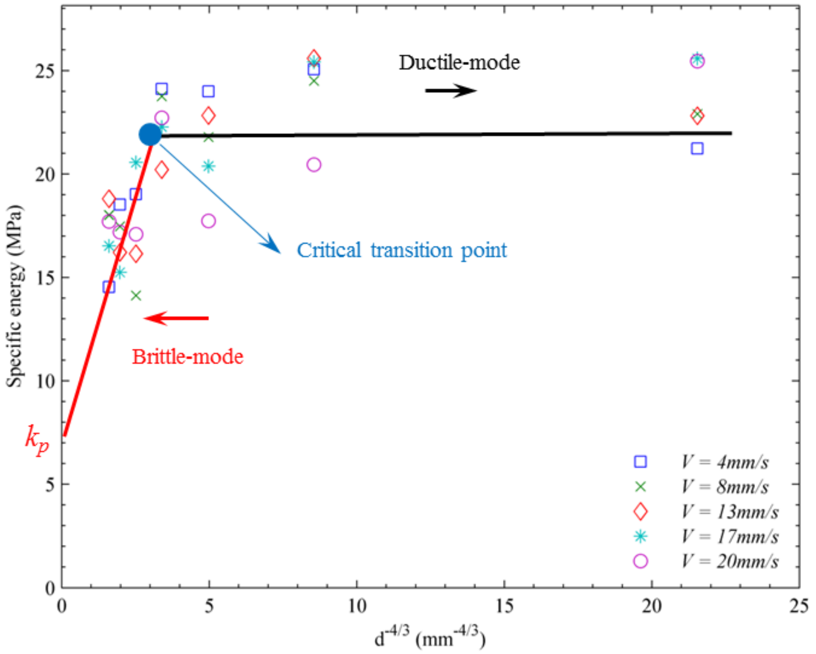

Fig. 3.21 Specific cutting energy versus $d^{-4/3}$ for Savonnières at various cutting velocities with α=15°.

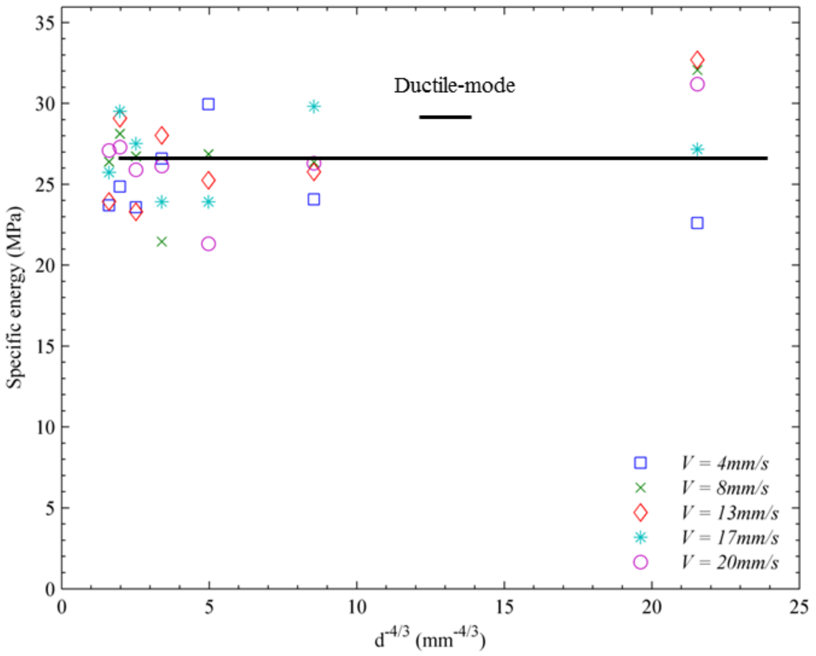

Fig. 3.22 Specific cutting energy versus $d^{-4/3}$ for Savonnières at various cutting velocities with α=30°.

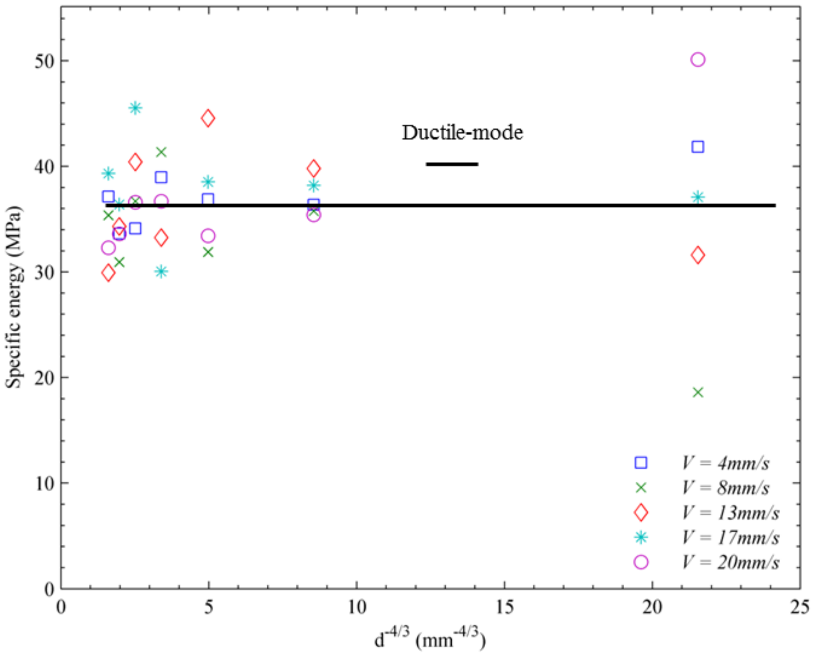

Fig. 3.23 Specific cutting energy versus $d^{-4/3}$ for Savonnières at various cutting velocities with α=45°.

To sum up, Table 3.2 presents the values of d_c determined using cutting force logs as suggested in Richard et al. (1998) and specific cutting energy transition model as proposed in this study. Note in Ricard's model, d_c is related to rock properties using a qualitative relationship $d_c \propto \left(K_{IC}/\sigma_c\right)^2$ and therefore it is difficult to get a specific value for d_c. The results given in the table were estimated approximately based on Fig. 3.8-Fig. 3.15 in combination with the corresponding cutting force logs (not shown, but see Fig. 6 for an example). On the other hand, the specific energy transition model proposed in this study enables the identification of the specific value for d_c. For example, when cutting on Tuffeau at $\alpha = 5°$, as shown in Table 3.2, the best we can say about d_c estimated from the cutting force log is d_c>0.2 mm and no specific value can be identified. However, based on the specific energy transition model, a specific value of 0.31 mm can be obtained for d_c. Clearly the approach proposed is a much better method for the prediction of d_c.

Table 3.2 Critical transition depth determined by the force logs (*F*) and the specific cutting energy transition model (*E*).

α/°	Tuffeau		Savonnières	
	d_c/mm (*F*)	d_c/mm (*E*)	d_c/mm (*E*)	d_c/mm (*E*)
5	>0.2	0.31	>0.2	0.33
15	>0.3	0.35	>0.3	0.42
30	>0.5	0.50	—	—
45	>0.6	—	—	—

3.5 Conclusions

This study introduces a data analysis technique based on rock cutting test results to determine the critical transition depth of cut separating the ductile from brittle cutting mode under different cutting conditions. The back rake angle and rock properties are demonstrated to be the key factors influencing the critical transition cutting depth. Two types of rocks, Tuffeau and Savonnières, are used in our analysis to demonstrate our approach.

A model is proposed in this study to quantify the specific cutting energy for rock cutting. The specific cutting energy transition model proposed in this study can describe effectively the whole evolution of the cutting transition from ductile to brittle mode. This model takes into account both ductile-regime and brittle-regime cuttings while incorporating the effects of different operational parameters and material properties. Ductile cutting can be reflected by a horizontal line segment in the proposed model while brittle cutting is represented by a slopped line segment that describes the specific cutting energy in brittle mode as a linear function of the depth of cut with an exponent of -4/3. The critical transition depth corresponds to the depth where these two line segments intersect.

In our analysis, the ductile-brittle transition was identified directly from the experimental data using our proposed model. The specific cutting energy in general decreases with depth of cut but tends to increase with back rake angle. The experimental data suggest cutting mode leans more toward ductile for large back rake angle, but more toward brittle for small back rake angles, when other operational parameters are the same. As a result, the critical transition depth increases when the back rake angle increases. The critical transition depth appears to be independent of the cutting velocity tested in our experiments.

Using specific cutting energy to determine the critical transition depth has two advantages over the conceptual mode developed by Richard et al. (1998). Firstly, our model can give definitive values for the critical transition depth while the conceptual model only predicts them qualitatively. Secondly, the new specific cutting energy model possesses the ability to predict the critical depth without involving the measurement of rock properties whilst the conceptual model requires the UCS and fracture toughness to be known in prior.

The Savonnières rock with higher UCS has a larger critical transition depth compared with Tuffeau, as expected. However, as demonstrated in He and Xu

(2015), in addition to operational parameters, the critical transition depth depends not only on brittleness, i.e., the ratio of UCS to BTS, but also on other rock properties such as the grain size. However, further experimental studies are needed before definite relationships can be established.

Acknowledgement

The work has been supported by the Deep Exploration Technologies Cooperative Research Centre whose activities are funded by the Australian Government's Cooperative Research Centre Programme. This is DET CRC Document 2015/733. The generous support of CSIRO, Perth for the experimental tests reported in this article is also greatly acknowledged.

References

Akono AT, Reis PM, Ulm FJ (2011) Scratching as a fracture process: From butter to steel. Physical Review Letters 106:204302

Arcona C, Dow TA (1998) An empirical tool force model for precision machining. Journal of Manufacturing Science and Engineering 120:700-707

Barletta M, Gisario A, Lusvarghi L, Bolelli G, Rubino G (2008) On the combined use of scratch tests and CLA profilometry for the characterization of polyester powder coatings: Influence of scratch load and speed. Applied Surface Science 254:7198-7214 doi:10.1016/j.apsusc.2008.05.315

Bifano TG, Fawcett SC (1991) Specific grinding energy as an in-process control variable for ductile-regime grinding. Precision Engineering 13:256-262 doi:10.1016/0141-6359(91)90003-2

Detournay E, Defourny P (1992) A phenomenological model for the drilling action of drag bits. International Journal of Rock Mechanics and Mining Sciences & Geomechanics Abstracts 29:13-23 doi:10.1016/0148-9062(92)91041-3

Ersoy A, Buyuksagic S, Atici U (2005) Wear characteristics of circular diamond saws in the cutting of different hard abrasive rocks. Wear 258:1422-1436 doi:10.1016/j.wear.2004.09.060

Franca LF (2010) Drilling Action of Roller-Cone Bits: Modeling and Experimental Validation. Journal of Energy Resources Technology 132:043101

Friedman M, Handin J, Alani G (1972) Fracture-surface energy of rocks. International Journal of Rock Mechanics and Mining Sciences &

Geomechanics Abstracts 9:757-764 doi:10.1016/0148-9062(72)90034-4

Guo H, Aziz NI, Schmidt LC (1992) Rock cutting study using linear elastic fracture mechanics. Engineering Fracture Mechanics 41:771-778 doi:10.1016/0013-7944(92)90159-c

He X, Xu C (2015) Discrete element modelling of rock cutting: from ductile to brittle transition. International Journal for Numerical and Analytical Methods in Geomechanics doi:10.1002/nag.2362

Huang H, Lecampion B, Detournay E (2013) Discrete element modeling of tool-rock interaction I: rock cutting. International Journal for Numerical and Analytical Methods in Geomechanics 37:1913-1929 doi:10.1002/nag.2113

Klecka M, Subhash G (2008) Grain size dependence of scratch-induced damage in alumina ceramics. Wear 265:612-619 doi:10.1016/j.wear.2007.12.012

Lawn B, Cook R (2012) Probing material properties with sharp indenters: a retrospective. Journal of Materials Science 47:1-22 doi:10.1007/s10853-011-5865-1

Lawn BR (1998) Indentation of ceramics with spheres: A century after Hertz. Journal of the American Ceramic Society 81:1977-1994

Li XB, Summers DA, Rupert G, Santi P (2001) Experimental investigation on the breakage of hard rock by the PDC cutters with combined action modes. Tunnelling and Underground Space Technology 16:107-114 doi:10.1016/s0886-7798(01)00036-0

Marshall DB, Lawn BR (1986) Indentation of brittle materials. Microindentation Techniques in Materials Science and Engineering:26-46

Menezes PL, Lovell MR, Avdeev IV, Lin J-S, Higgs CF (2014) Studies on the formation of discontinuous chips during rock cutting using an explicit finite element model. The International Journal of Advanced Manufacturing Technology 70:635-648 doi:10.1007/s00170-013-5309-y

Nicodeme P (1997) Transition between ductile and brittle mode in rock cutting. Ecole Polytechnique, Paris

Nishimatsu Y (1972) The mechanics of rock cutting. International Journal of Rock Mechanics and Mining Sciences 9:261-270

Randall NX, Favaro G, Frankel CH (2001) The effect of intrinsic parameters on the critical load as measured with the scratch test method. Surface and Coatings Technology 137:146-151 doi:10.1016/s0257-8972(00)01097-5

Richard T (1999) Determination of rock strength from cutting tests. Master thesis, University of Minnesota

Richard T, Dagrain F, Poyol E, Detournay E (2012) Rock strength determination from scratch tests. Engineering Geology 147-148:91-100 doi:10.1016/j.enggeo.2012.07.011

Richard T, Detournay E, Drescher A, Nicodeme P, Fourmaintraux D (1998) The Scratch Test As A Means To Measure Strength of Sedimentary Rocks. Paper presented at the SPE/ISRM Rock Mechanics in Petroleum Engineering, Trondheim, Norway, 8-10 July 1998

Tan Y, Jiang S, Nie S, Yang D, Zhang G, Peng R (2012) Prestress Scratching on SiC Ceramic. International Journal of Applied Ceramic Technology 9:322-328 doi:10.1111/j.1744-7402.2011.0202726.x

Teale R (1965) The concept of specific energy in rock drilling. International Journal of Rock Mechanics and Mining Sciences 2:57-73 doi:10.1016/0148-9062(65)90022-7

Tönshoff HK, Hillmann-Apmann H, Asche J (2002) Diamond tools in stone and civil engineering industry: cutting principles, wear and applications. Diamond and Related Materials 11:736-741 doi:10.1016/s0925-9635(01)00561-1

Zhou Y, Lin J-S (2014) Modeling the ductile–brittle failure mode transition in rock cutting. Engineering Fracture Mechanics 127:135-147 doi:10.1016/j.engfracmech.2014.05.020

Chapter 4

On the critical failure mode transition depth for rock cutting with different back rake angles

(Paper 3)

Xianqun He and Chaoshui Xu

Deep Exploration Technologies Cooperative Research Centre, School of Civil, Environmental and Mining Engineering, the University of Adelaide, Australia

Publication:

He X. and Xu C. (2015) On the critical failure mode transition depth for rock cutting with different back rake angles. *Journal of the Mechanics and Physics of Solids*. Submitted for review: July 2015.

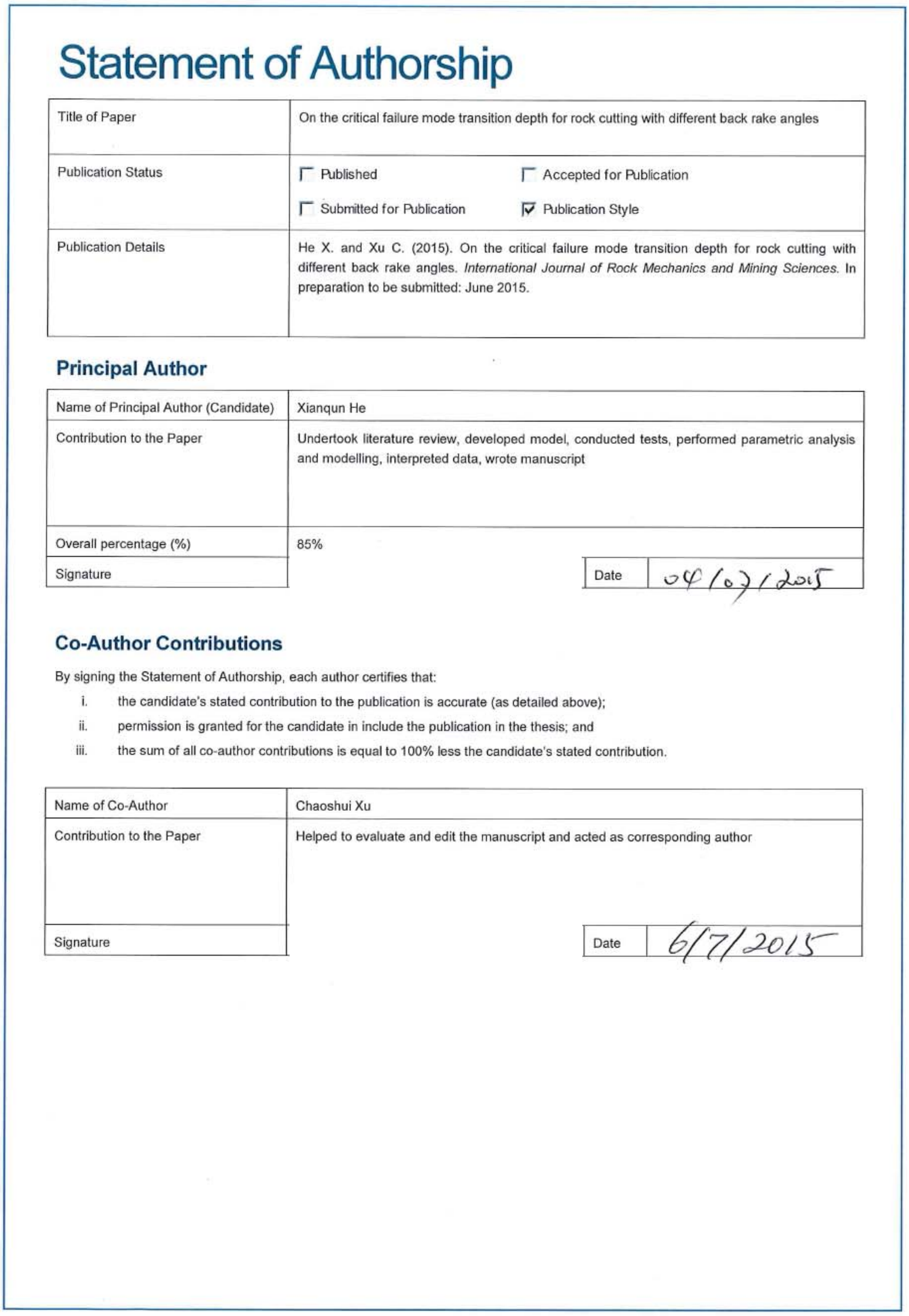

Statement of Authorship

Title of Paper	On the critical failure mode transition depth for rock cutting with different back rake angles
Publication Status	☐ Published ☐ Accepted for Publication ☐ Submitted for Publication ☑ Publication Style
Publication Details	He X. and Xu C. (2015). On the critical failure mode transition depth for rock cutting with different back rake angles. *International Journal of Rock Mechanics and Mining Sciences*. In preparation to be submitted: June 2015.

Principal Author

Name of Principal Author (Candidate)	Xianqun He		
Contribution to the Paper	Undertook literature review, developed model, conducted tests, performed parametric analysis and modelling, interpreted data, wrote manuscript		
Overall percentage (%)	85%		
Signature		Date	04/07/2015

Co-Author Contributions

By signing the Statement of Authorship, each author certifies that:

i. the candidate's stated contribution to the publication is accurate (as detailed above);

ii. permission is granted for the candidate in include the publication in the thesis; and

iii. the sum of all co-author contributions is equal to 100% less the candidate's stated contribution.

Name of Co-Author	Chaoshui Xu		
Contribution to the Paper	Helped to evaluate and edit the manuscript and acted as corresponding author		
Signature		Date	6/7/2015

Abstract

The failure mode of rock under cutting exhibits a ductile-brittle transition as the depth of cut increases. The critical transition depth, beyond which energy consumed in brittle fracturing surpasses the energy consumed in plastic flow, is the key to differentiating between the ductile and brittle cutting modes and therefore is an important parameter to optimise tool design and operational parameter to meet specific application requirements. This critical failure mode transition depth depends not only on the rock properties but also on the cutting operational parameters, in particular, the back rake angle. In this work, a series of rock cutting tests were performed to investigate the influence of back rake angle on the critical failure mode transition depth. Size effect law is employed first to identify the critical transition depth, which is then compared with values derived from the analysis of the specific cutting energy. It is found that the critical failure mode transition depth increases with the back rake angle. This suggests that the brittle fracture failure induced at large depth of cut can be inhibited by increasing the back rake angle. Cutting at small back rake angle, on the other hand, is desirable if minimisation of the cutting energy is required in the application.

***Keywords*:** Rock cutting; Ductile-brittle transition; Critical failure mode transition depth; Size effect law; Specific energy

4.1 Introduction

Understanding the interaction between rock and a mechanical cutter is critically important for many rock engineering applications, including exploration drilling, tunnelling, mining, stone sawing and polishing (Buyuksagis 2007; Che and Ehmann 2014; Franca 2011; Kahraman 2002; Li et al. 2001). The cutting process involves removing a fraction of rock material with a cutter being driven across the surface of rock at a prescribed velocity while penetrating into the rock at certain depth, see illustration in Fig. 4.1. This penetration depth is referred to as depth of cut, *d*.

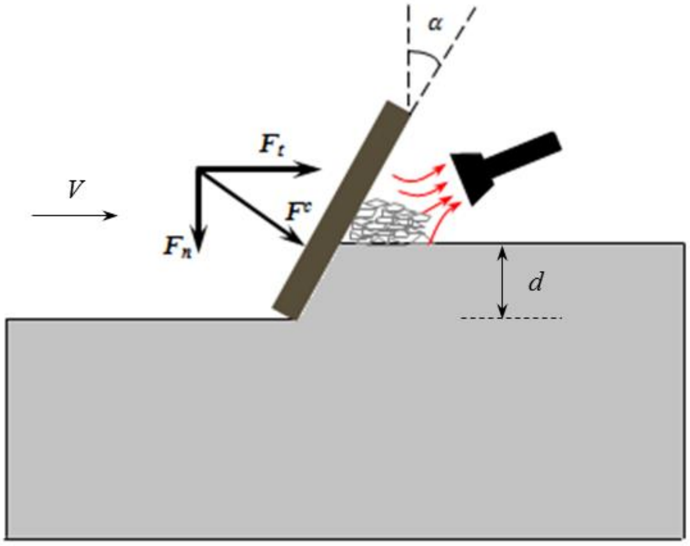

Fig. 4.1 Schematic representation of a cutting test with an inclined cutter. The inclination of cutter with respect to the normal to the top surface of rock is the back rake angle α. F_t and F_n are the tangential and normal component of the resulting cutting force F^c.

It is well known that there exist two different failure modes in rock cutting, namely, ductile and brittle failure modes (Huang et al. 2013; Nicodeme 1997; Richard 1999; Richard et al. 1998; Zhou and Lin 2013) and both failure mechanisms in general coexist in any cutting operation (He and Xu 2015a). In shallow cutting, the ductile failure mode dominates, which is characterised by crushing of particles in the vicinity of the tip of the cutting tool and shearing of rock grains in front of the tool (see Fig. 4.2a and Fig. 4.2b). Brittle failure mode will dominate at greater cutting depths with energy dissipated mainly in creating macroscopic cracking surfaces ahead of the cutting tool (see Fig. 4.2c and Fig. 4.2d). Therefore, a critical transition depth emerges where the failure of rock in cutting changes from ductile-dominated to brittle-dominated failure as the depth of cut increases.

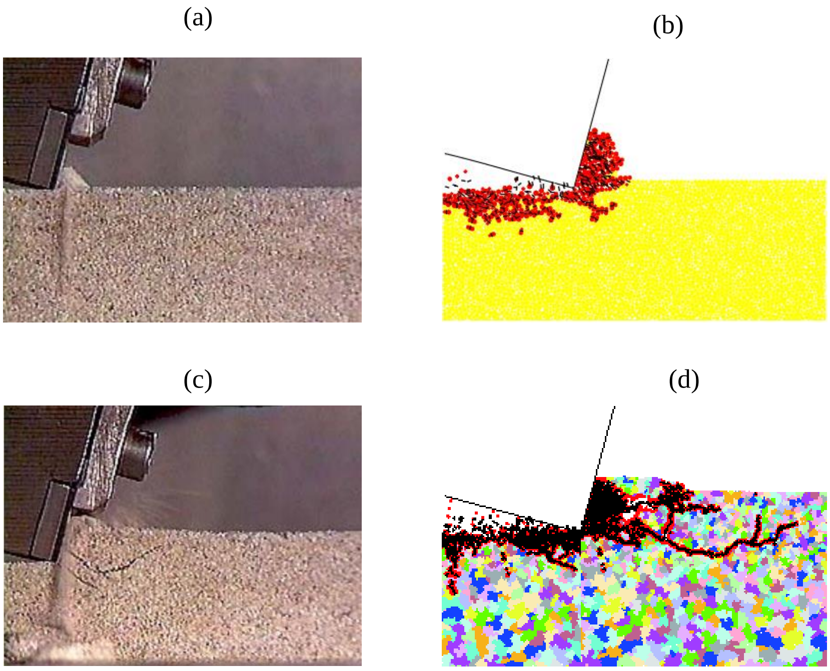

Fig. 4.2 Typical ductile failure mode of cutting in (a) test and (b) simulation and typical brittle failure mode of cutting in (c) test and (d) simulation. Results of experiment (left) and simulation (right) are reproduced after Richard (1999) and He and Xu (2015a), respectively.

The failure mode transition has been an active research topic in rock cutting mechanics, e.g., (He and Xu 2015a; Huang et al. 2013; Nicodeme 1997; Richard 1999; Richard et al. 2012; Richard et al. 1998; Zhou and Lin 2013; Zhou and Lin 2014). Most of these studies focused on linking the critical failure mode transition depth with the mechanical properties of rock such as opening-mode fracture toughness, K_{IC}, uniaxial compressive strength, σ_c, and tensile strength, σ_t. For example, Richard et al. (1998) proposed the relationship between the critical failure mode transition depth, d_c, and rock properties as $d_c \propto (K_{IC}/\sigma_c)^2$. This relationship was later confirmed by discrete element numerical simulations in Huang and Detournay (2008) where d_c is further linked to an intrinsic length scale, $l_i = 1/\pi\ (K_{IC}/\sigma_c)^2$. The effect of the rock grain size on the cutting transition has been analysed in He and Xu (2015a) where they show that the critical transition depth is also proportional to the grain sizes of rock minerals. However, to our best knowledge, the effect of some operational parameters such as the back rake angle on the failure mode transition phenomenon has not been reported yet in available published studies, even it has been demonstrated in experiments (He and Xu 2015c) that back rake angle has significant impact on the failure mode transition.

Experimental observations suggest that the critical failure mode transition depth is dependent not only on rock properties but also on the operational parameters. The study in He and Xu (2015c) presents a confirmation of this claim by analysing the variations of specific cutting energy with regard to operational parameters. It is found in the study that the cutting velocity in the range of 4-20 mm/s has little impact on failure mode transition but the back rake angle plays an important role in the determination of the actual critical transition depth. Specifically, it is demonstrated that cutting on rock with a larger back rake angle tends to make the failure shift from ductile to brittle mode at greater depth of cut.

In this work, cutting tests were conducted on two types of limestone to study the effect of the back rake angle on the transition of cutting failure modes, while incorporating the size effect into the analysis of the cutting mechanisms. The results are then compared with those derived from specific cutting energy analysis He and Xu (2015c).

4.2 Determination of the critical failure mode transition depth

The tool-rock interaction in rock cutting is an extremely complex problem. Rock breakage during rock cutting can occur at different scales, ranging from micron scale for applications such as scratching/polishing to the scale of tens of centimeters in mechanical mining/excavation. The inherent spatial heterogeneity of rock at different scales brings additional complexities in predicting the mechanical responses of rock to the cutting action. Although there are extensive experimental and numerical studies reported on rock cutting processes, few of them deal with the reliable determination of the critical transition depth that quantifies the change of dominant rock failure modes during rock cutting. To deal with this issue, two different approaches are proposed below, with one based on the size effect analysis and the other on specific cutting energy.

4.2.1 Critical transition depth prediction based on size effect analysis

It is well understood, in general, larger structures are more brittle than smaller structures (Van Mier 2012) and there is an decrease in the nominal strength when the structure size exceeds a critical value. To capture the failure transitional behaviour for structures of varying sizes, Bažant proposed a size effect law (SEL) (Bažant 1984; Bažant et al. 1991) to model the blunt fracture behaviour in concrete, rock and metal materials, which, as stated by Van Mier (2012), is in nature a “clever curve-fitting method”. This asymptotic-matching fitting approach, as shown in a log-log representation in Fig. 4.3, connects the horizontal strength asymptote for small sizes and fracture asymptote with a slope of -1/2 based on linear elastic fracture mechanics (LEFM) for large sized structures via a continuous function. The nominal strength of a structure can then be expressed as a simple function of its size, i.e.,

$$\sigma_n = \frac{B_n \sigma_y}{\sqrt{1 + D/D_0}} \tag{4.1}$$

where B_n is a dimensionless geometric factor, σ_y is the yield strength, D is the characteristic structure size under consideration and D_0 stands for the transitional size of the structure. When $D \ll D_0$, the energy release by fracturing is negligible, whereas for $D \gg D_0$, fracture-induced energy release becomes dominant. Both B_n and D_0 depend on rock fracture properties and the structure geometry in question. The nominal strength σ_n is defined as follows (Bažant 1984):

$$\sigma_n = C_n \frac{F}{bD} \tag{4.2}$$

where C_n is a coefficient, F is the peak force applied on the structure, b is the structure width and thus bD is the cross-sectional area of the structure which bears the force.

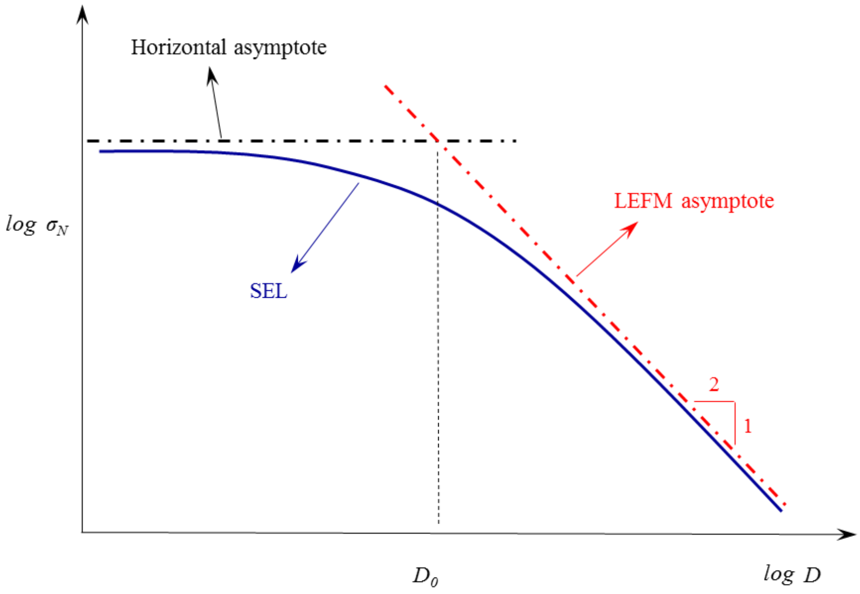

Fig. 4.3 Bažant's size effect law bridging between the strength asymptote and the LEFM asymptote.

In rock cutting, ductile failure dominates at shallow cuts and the specific cutting energy is almost constant, independent of the cutting depth. After the cutting depth is greater than the critical transition depth, brittle failure dominates and the specific energy will decrease against increasing cutting depth. This failure mode transition displays similar characteristics as the size effect law even strictly speaking the underlying mechanisms considered behind these two features are different. The reduction in strength in size effect law is mainly due to the inclusion of more defects in rocks at large scales, while the reduction in specific cutting energy in rock cutting is mainly due to the increment in the proportion of fracturing failure mode as cutting depth increases (He and Xu 2015b). However, there is some equivalence as both are dealing with easier brittle failure at larger scales due to the involvement of fracturing. In this respect, Lin and Zhou tried to promote the understanding of rock cutting mechanics by the application of the size effect law (Lin and Zhou 2013; Zhou and Lin 2013; Zhou and Lin 2014). They show some remarkable results to demonstrate that the size effect law fits and reproduces the cutting test data very well. They choose the depth of cut, $d \equiv D$, as the characteristic structure size, and define the nominal strength σ_n as the ratio of the average peak tangential cutting force to the projected contact area in the cutting direction. Accordingly, Eq. (4.2) is rewritten as

$$\sigma_n = \frac{F_t}{Wd} \tag{4.3}$$

where F_t is the tangential component of the cutting force and W is the width of cut. In addition, in order to be comparable with Eq. (4.1), they replace the yield strength with the uniaxial compressive strength σ_c. Therefore, the size effect equation for rock cutting is expressed in the form of

$$\sigma_n = \frac{B_n \sigma_c}{\sqrt{1 + d/d_c}} \tag{4.4}$$

with d and d_c being the depth of cut and the critical failure mode transition depth, respectively.

In this study, we take the view that the assumption of the tangential cutting force F_t as the sole contributor to the nominal strength might be an oversimplification of the actual loading conditions. The contribution from the normal component of the cutting force F_n cannot be ignored as it maintains the cutter at depth d, and therefore acts as an indentation load (Akono et al. 2012). As vertical indentation and horizontal cutting coexist during the cutting process and these two loading conditions can both induce ductile or brittle failure (Zhou and Lin 2013), depending on cutting conditions. Therefore the effect of the normal cutting force F_n is taken into consideration in this study by a modified nominal strength definition based on Eq. (4.3):

$$\sigma_n = \frac{F^c}{A_b} \tag{4.5}$$

where F^c is the resultant cutting force accounting for both the tangential and normal cutting force components, i.e., $F^c = \sqrt{F_t^2 + F_n^2}$ and A_b is the contacting area between the cutting tool and the rock, i.e., $A_b = W\,d/\cos\alpha$. Eq. (4.4) in combination with Eq. (4.5) is then used to fit the experimental data to derive the critical transition depth, d_c.

4.2.2 Critical transition depth prediction based on Specific cutting energy transition

In view of the difference in the energy dissipation between ductile and brittle cutting modes, the specific cutting energy, an index to measure the cutting efficiency, was utilised to quantitatively determine the critical failure mode transition depth in He and Xu (2015c). Some of the key relationships are summarised below.

For new PDC cutters (as used in this study), it is reasonable to neglect the influence of wear flat of the cutter tip on the cutting force responses. Therefore, when cutting proceeds in ductile failure mode, the specific cutting energy is (He and Xu 2015c):

$$E_{s\_d} = \eta \sigma_c \tag{4.6}$$

where E_{s_d} is the specific energy for ductile cutting and η as a geometric factor characterises the influence of back rake angle α.

On the other hand, when the cutting changes to brittle failure dominating mode, the specific energy is related to the depth of cut as:

$$E_{s\_b} = k_b d^{-4/3} + k_p \tag{4.7}$$

where k_b is a process factor associated with material properties as well as the cutting geometry imposed during the cutting process (Lawn and Cook 2012; Lawn 1998) and k_p is a constant representing the energy to create a unit volume of the plastic deformation zone underneath the cutter.

When the ductile failure mode is dominant in cutting, the energy is dissipated in volumetrically deforming the rock ahead of the cutter and the material is removed via plastic flow. While for brittle failure dominant cutting, the energy is mainly dissipated upon crack propagation and development of fracture surfaces. Eqs. (4.6) and (4.7) present this difference in terms of specific cutting energy. As implied by Eq. (4.6), the specific energy for ductile-regime cutting keeps constant for different cutting depths, but only influenced by the back rake angle and therefore it can be represented by a horizontal line segment on a E_s vs $d^{-4/3}$ diagram (see the black line segment in Fig. 4.4). The specific energy for brittle-regime cutting given in Eq. (4.7), by contrast, is proportional to $d^{-4/3}$, displaying as a straight line with the slope of k_b and the intercept of k_p (see the red line segment in Fig. 4.4).

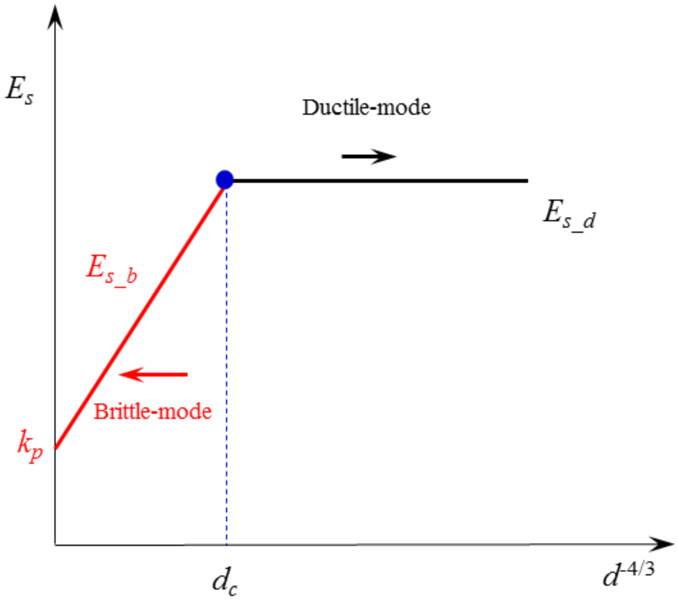

Fig. 4.4 Schematic diagram illustrating the use of the variation of the specific cutting energy to estimate the critical transition depth d_c at which the dominant failure mode changes.

Therefore the complete expression of the specific energy for different cutting conditions is a piecewise function by combining Eqs. (4.6) and (4.7), i.e.,

$$E_s = \begin{cases} \eta\sigma_c & d < d_c \\ k_b d^{-4/3} + k_p & d > d_c \end{cases} \tag{4.8}$$

This specific cutting energy transition model is used to fit the experimental data from cutting such that the critical transition depth d_c can be quantitatively identified as the intersection point of the horizontal ductile-regime cutting line segment and the sloped brittle-regime cutting line segment.

Comparing these two techniques discussed above for the determination of the critical transition depth d_c, one can find that both are based on data fitting method to locate the value for d_c. However, we have to be aware of the difference between them. The specific cutting energy defined in Eq. (4.8) is essentially the ratio of the tangential cutting force to the vertically-projected contact area, i.e., $E_s = F_t / Wd$; whilst the equivalent nominal strength given in Eq. (4.5) based on the size effect law also incorporates the effect of normal component of the cutting force in the evaluation.

4.3 Cutting tests

Linear rock cutting tests were conducted on two selected types of limestone: Savonnières (SL) and Tuffeau (TL) for their homogeneity in order to obtain more reproducible results and minimise the influence of rock heterogeneity on the variability of the experimental data under the same cutting conditions. Rock properties including uniaxial compressive strength σ_c, Brazilian tensile strength σ_t and opening mode fracture toughness K_{IC} are listed in Table 4.1.

Table 4.1 Mechanical properties of SL and TL rock sample.

Uniaxial compressive strength σ_c (MPa)		Brazilian tensile strength σ_t (MPa)		Fracture toughness K_{IC} (MPa·m$^{0.5}$)		Brittleness B	
22.95 (SL)	9.21 (TL)	2.10 (SL)	0.84 (TL)	0.35 (SL)	0.15 (TL)	10.93 (SL)	10.96 (TL)

Note: The brittleness B is defined as the ratio of σ_c to σ_t.

In laboratory rock cutting tests, there are mainly three operational parameters, namely cutting velocity, depth of cut and back rake angle, affecting the cutting responses. It was concluded in He and Xu (2015c) that the cutting velocity in the range of 4-20 mm/s has little influence on the cutting force responses and therefore the cutting velocity is kept constant at 8 mm/s in this study. Three back rake angles at 15°, 30° and 45° respectively are considered in this study. For each back rake angle α, a series of consecutive cuts were performed with different depths of cut increasing from 0.1 up to 1.7 mm in a

0.1 mm increment. During the course of cutting, the tangential and normal components of the cutting force, F_t and F_n, were recorded. Three cutting tests were carried out for each pair of back rake angle and depth of cut.

4.3.1 Insights on failure mode transition from the force profile

Fig. 4.5-Fig. 4.7 display the variations of F_t and F_n with depth of cut for the back rake angle of 15°, 30° and 45° respectively. For all cases, the forces increase as depth of cut increases. It is interesting to see that the force profile exhibits more variability for deeper cuts, indicating the occurrence of brittle-regime failure, as discussed in Richard et al. (2012), that higher dispersion of cutting forces can be expected in the brittle failure cutting regime due to fracturing/chipping.

The increasing rate of the cutting force against cutting depth can be used to estimate the critical transition depth (Richard 1999; Richard et al. 2012; Richard et al. 1998). Fig. 4.5 shows that at α=15°, as depth of cut increases, the measured cutting forces increase linearly initially at small cutting depth, then gradually follow a non-linear increasing pattern. This demonstrates the change in the failure mode from ductile failure dominant to brittle failure dominant as the cutting depth increases. Similarly, the forces for the case of α=30° follow more or less the same pattern (see Fig. 4.6). However, for the case of α=45° (Fig. 4.7), the forces increase linearly until the depth of cut reaches 1.5 mm and then they show an unexpected sharp rise for deeper cuts. As discussed in He and Xu (2015b), this is an artefact due to the inability to timely and properly clear the debris directly ahead of the cutting tool at large back rake angle and therefore the creation of additional resistance to the cutter movement during cutting. In model assessment, these results cannot be used.

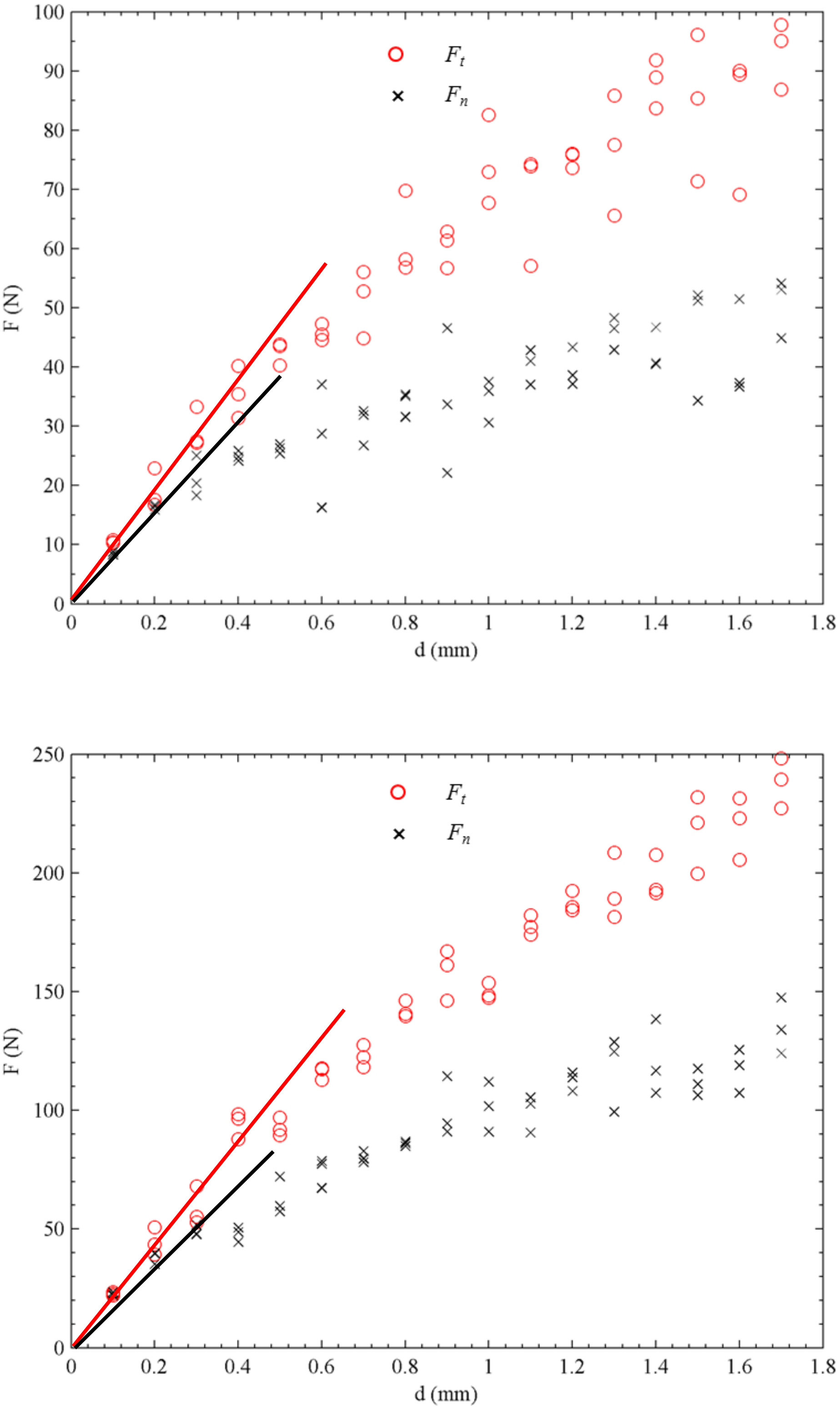

Fig. 4.5 Forces varying with depth of cut for (a) Tuffeau and (b) Savonnières at α=15°.

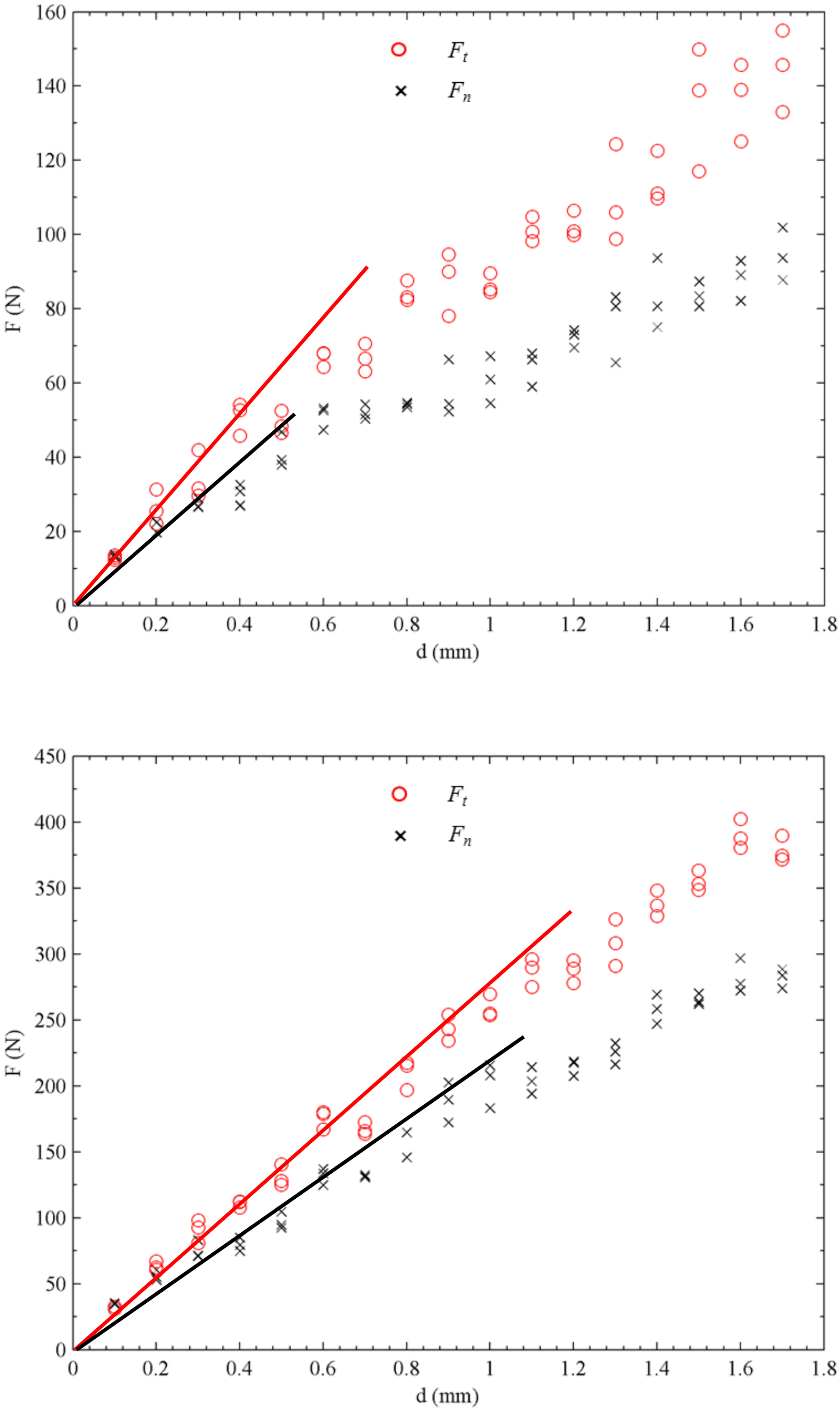

Fig. 4.6 Forces varying with depth of cut for (a) Tuffeau and (b) Savonnières at α=30°.

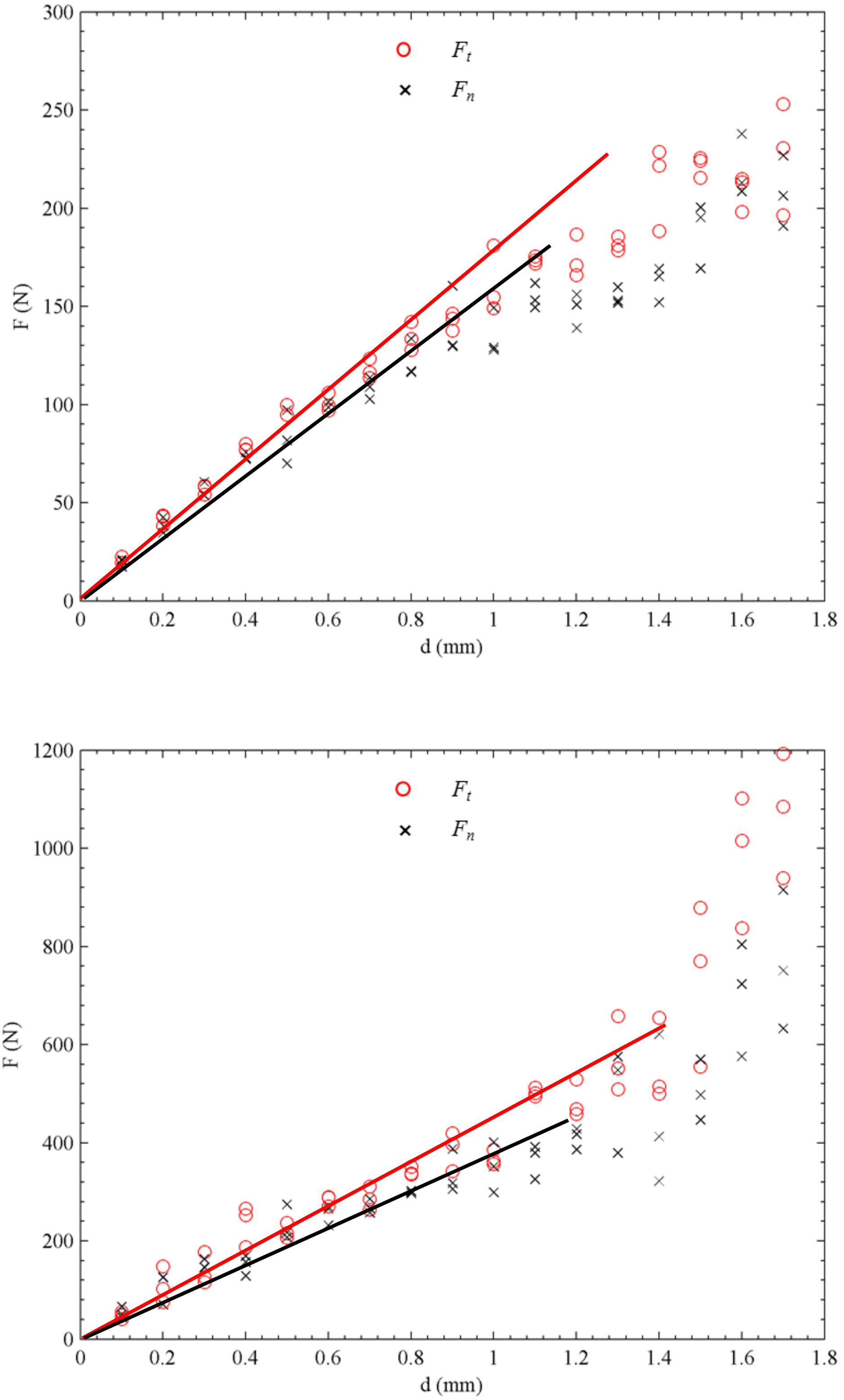

Fig. 4.7 Forces varying with depth of cut for (a) Tuffeau and (b) Savonnières at α=45°.

4.3.2 Quantitative determination of the critical transition depth

The force profiles discussed above only provide a qualitative description of the critical failure mode transition. The quantitative determination of the critical transition depth based on the two data fitting models, i.e., the size effect law and the specific cutting energy transition model, is described below.

4.3.2.1 Critical transition depth for Tuffeau limestone

Fig. 4.8-Fig. 4.10 present the estimation of the critical transition depth for Tuffeau limestone at three different back rake angles based on the two models discussed above. Based on the size effect law model, the estimated critical failure mode transition depth increases from 0.35 mm at α=15°, 0.50 mm at α=30°, to 0.98 mm at α=45° (Fig. 4.8a-Fig. 4.10a and Table 4.2). Based on the specific cutting energy transition model, the corresponding figures are 0.40 mm at α=15°, 0.46 mm at α=30° and 0.79 mm at α=45° (Fig. 4.8b-Fig. 4.10b and Table 4.2). In all cases, the size effect law model fits the cutting data better than the specific energy transition model (Fig. 4.8-Fig. 4.10). For example, the size effect equation, shown as the curve in Fig. 4.9a, fits the experimental data well with R^2 = 0.91, whereas R^2 reduces to 0.78 for the specific energy transition model (Fig. 4.9b).

In addition to fact that the critical failure mode transition depth increases with the back rake angle, it is interesting to note that the specific cutting energy for the ductile failure dominant cutting process, represented by the horizontal line segment in Fig. 4.8b, Fig. 4.9b and Fig. 4.10b, also increase with the back rake angle. For α=15°, it is fitted to be 9.3 MPa based on the specific cutting energy transition model, almost equal to the UCS of Tuffeau of 9.21 MPa, suggesting the geometric factor η in Eq. (4.6) being around 1.0. This is in good agreement with the experimental results in Richard et al. (2012) where the specific cutting energy is proved to be equal to the value of UCS at α=15°. As the back rake angle increases, η increases to approximately 1.3 at α=30°

and 2.0 at α=45°. This indicates an increase in the back rake angle would require more energy to be consumed in ductile cutting. When cutting enters brittle dominant failure regime, k_p in Eq. (4.4), which characterises the energy dissipated in plastically deforming the rock in the direct vicinity of the cutter, also sees some increase as the back rake angle increases. This trend is similar to that reported in He and Xu (2015c) where they found that more energy is consumed in ductile failure of rock at large back rake angles, suggesting the cutting mode transition tends to occur at greater depth of cut.

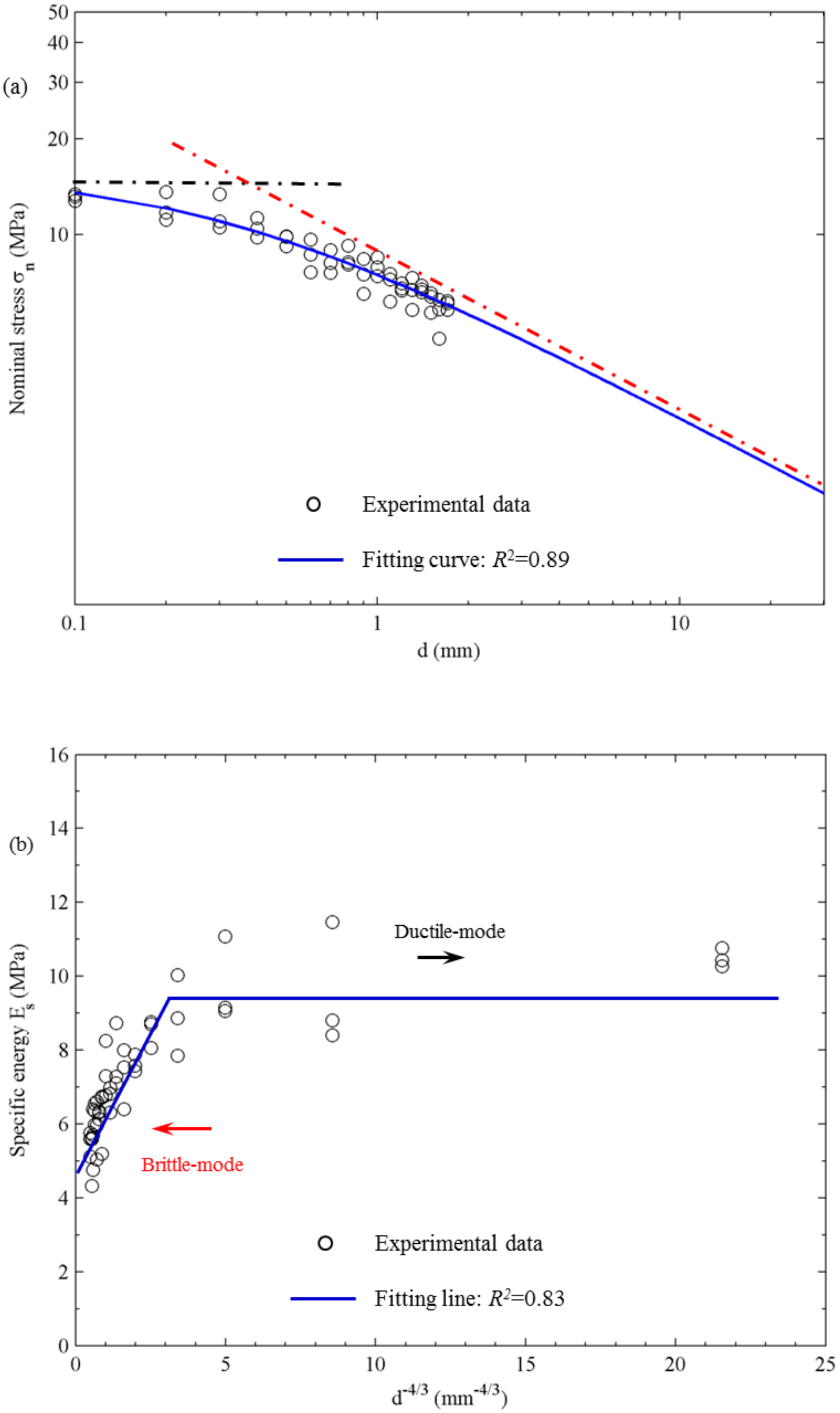

Fig. 4.8 Determination of the critical failure mode transition depth for Tuffeau sample by (a) size effect law and (b) specific energy transition model for α=15°. d is in the range of 0.1-1.7 mm.

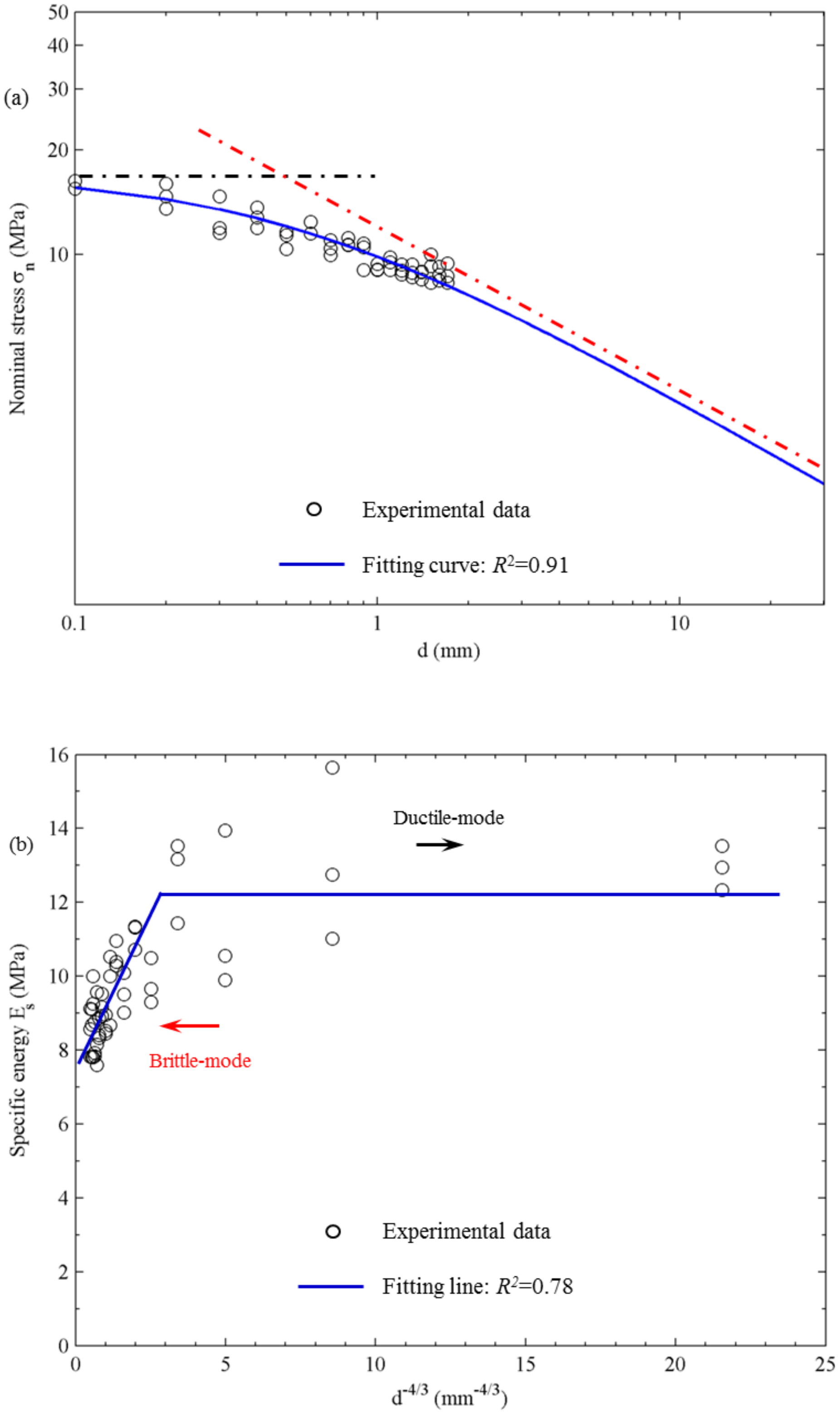

Fig. 4.9 Determination of the critical failure mode transition depth for Tuffeau sample by (a) size effect law and (b) specific energy transition model for α=30°. *d* is in the range of 0.1-1.7 mm.

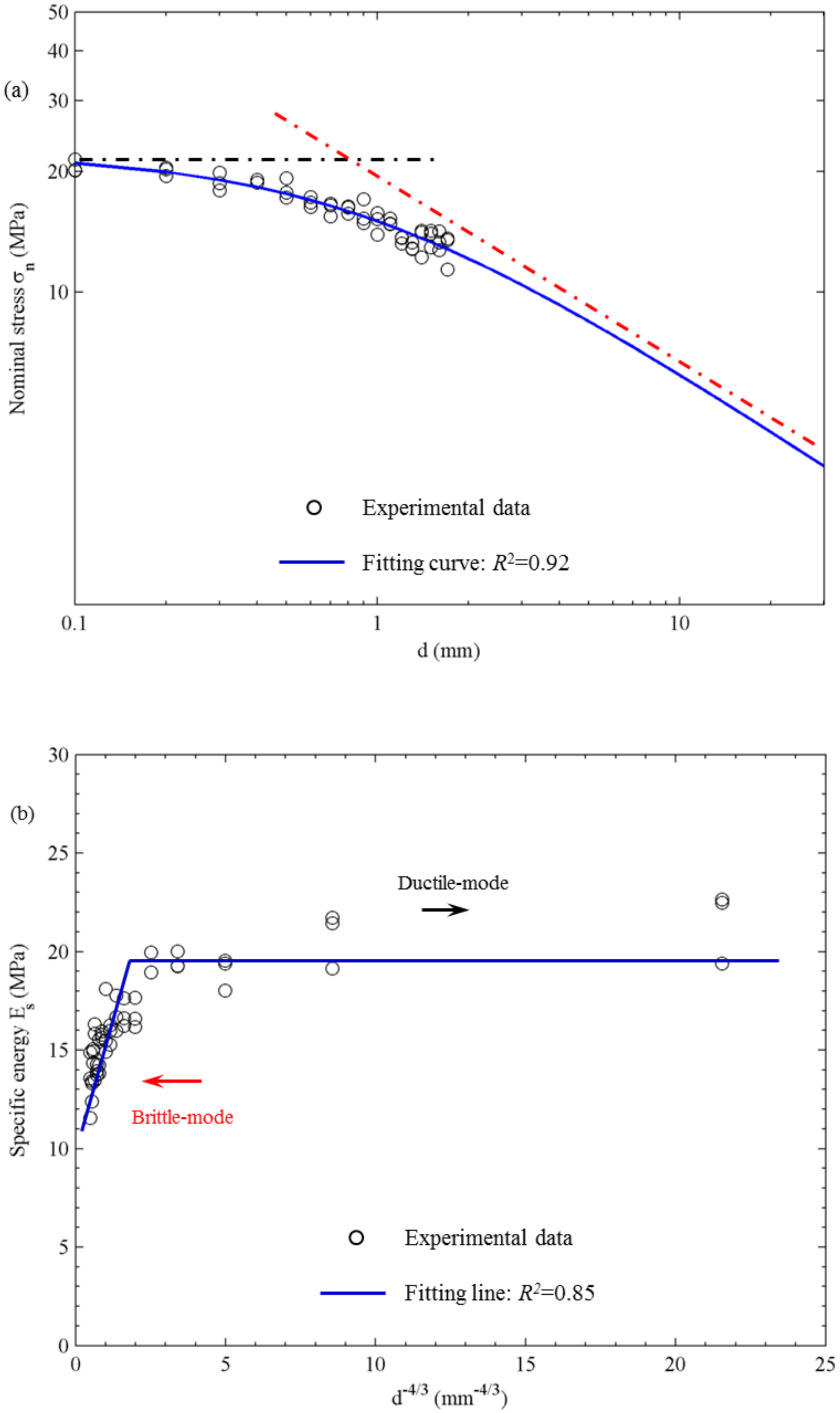

Fig. 4.10 Determination of the critical failure mode transition depth for Tuffeau sample by (a) size effect law and (b) specific energy transition model for α=45°. d is in the range of 0.1-1.7 mm.

4.3.2.2 Critical transition depth for Savonnières limestone

The estimated critical transition depth for Savonnières limestone based on the two models for different back rake angle of 15°, 30° and 45° are displayed in Fig. 4.11-Fig. 4.13. Again the d_c increases as the back rake angle increases. Specifically, based on the size effect law model, d_c is estimated to be 0.41 mm at α=15° (Fig. 4.11a), 0.92 mm at α=30° (Fig. 4.12a) and 2.76 mm at α=45° (Fig. 4.13a), see also Table 4.2. Based on the specific cutting energy transition model, d_c is estimated to be 0.44 mm at α=15° (Fig. 4.11b), 0.61 mm at α=30° (see Fig. 4.12b), but no value can be estimated for 45° at the range of cutting depth used (0.1-1.7 mm), indicating the cutting failure within this range at this back rake angle is dominated by the ductile regime. This might also be attributed to the inability to clear timely and properly the debris directly ahead of the cutter at high back rake angle, hence causing additional obstruction to the cutter movement and additional consumption of energy to re-crush the debris, as discussed above. In fact, the size effect law model for this case gives an unreasonably high d_c value of 2.76 mm since cutting on Savonnières with depth of 1.4 mm at α=45°, as shown in Fig. 4.17, has already shown the occurrence of chipping and therefore a more reasonable d_c value should be less than 1.4 mm. In terms of the goodness-of-fit, R^2 based on the size effect model is again higher than that from the specific cutting energy transition model.

To reduce the undesirable effects of the debris obstruction, the cutting data of Savonnières at α=45° for cutting depth greater than 1.4 mm are disregarded, i.e., only the data for depth ranging from 0.1 mm to 1.4 mm are included in the analysis for these two critical transition depth derivation models. It can be seen from Fig. 4.14a that a new estimated value of d_c = 1.27 mm can be obtained while the data is still fitted by the horizontal ductile cutting regime in the specific energy transition model (see Fig. 4.14b). Therefore, it can be regarded that the specific energy transition model will give an estimate of the critical failure transition depth at a value greater than 1.4 mm. However, by examining the groove trace after cutting, we can find that some severe chippings have already emerged when the depth of cut is set at 1.3 mm (Fig. 4.15). This proves that the size effect law model can give a better estimate (1.27 mm) in this case.

Dividing the fitted result of $\eta\sigma_c$ in Eq. (4.6) by σ_c, the geometric factor η can be determined. As the back rake angle increases, this geometric factor η is nearly doubled from around 1.0 at α=15° (Fig. 4.11b) to about 2.0 at α=45° (Fig. 4.14b). Although for α=30°, η is approximately 1.34 (Fig. 4.12b), slightly larger than 1.30 for Tuffeau, we can claim that the geometric factor η is nearly the same as that for Tuffeau under the same cutting conditions. This implies that η might not depend on rock properties, but rather only on the cutting geometry, e.g.,, the back rake angle in this study. In addition, by comparing Fig. 4.11b with Fig. 4.12b, one can find that the intercept k_p, an indicator of the energy consumption for plastic deformation while in brittle failure dominant cutting regime, also increases with the back rake angle. Similar changes in k_p can also be observed for Tuffeau. However, at large back rake angle (e.g., α = 45°), no intercept can be found (see Fig. 4.14b) due to issues discussed above. It can be seen that for both Tuffeau and Savonnières the increase in d_c as back rake angle increases is accompanied by the increase in η and k_p. Therefore, η and k_p might also serve as a measure to help identify the failure mode transition.

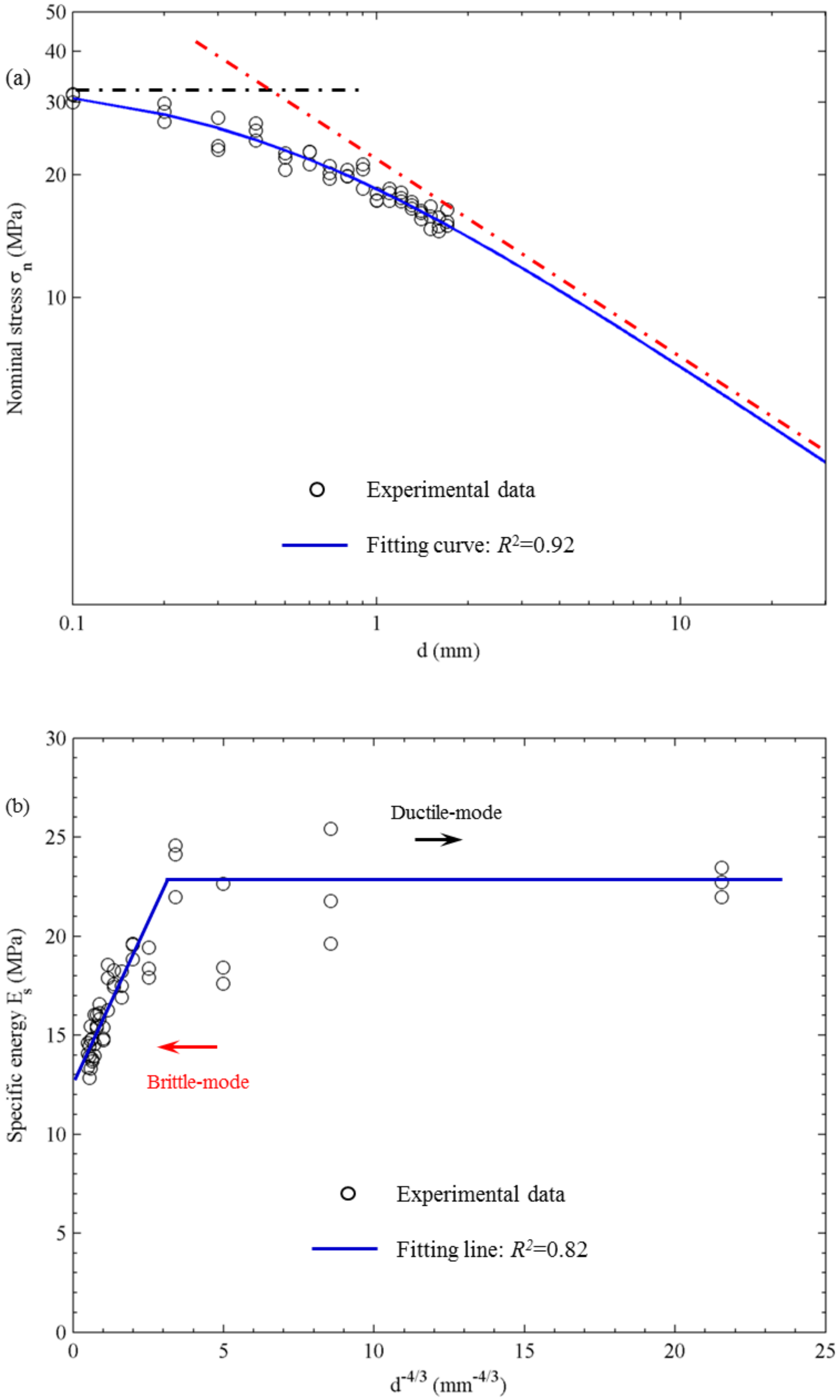

Fig. 4.11 Determination of the critical failure mode transition depth for Savonnières sample by (a) size effect law and (b) specific energy transition model for α=15°. d is in the range of 0.1-1.7 mm.

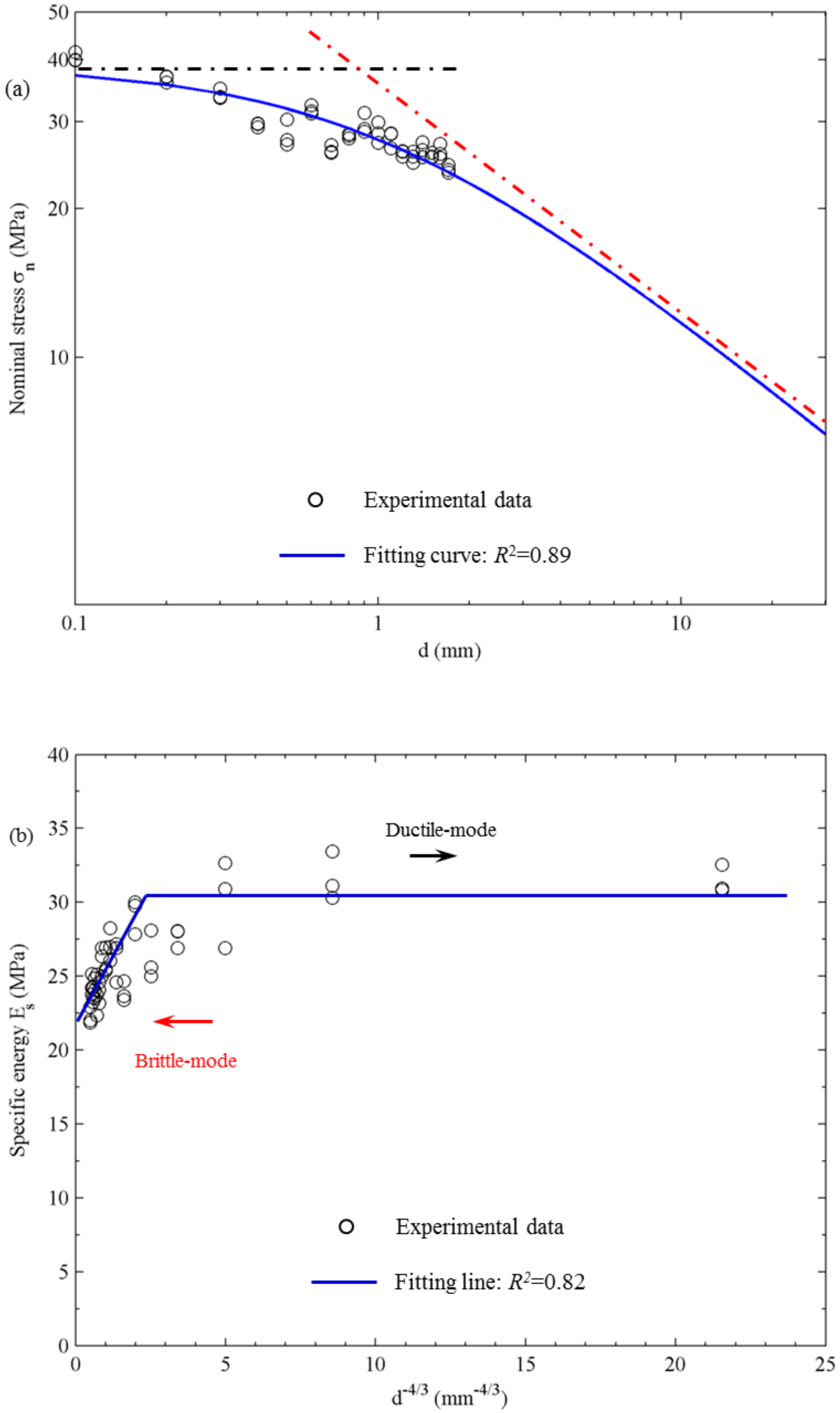

Fig. 4.12 Determination of the critical failure mode transition depth for Savonnières sample by (a) size effect law and (b) specific energy transition model for α=30°. *d* is in the range of 0.1-1.7 mm.

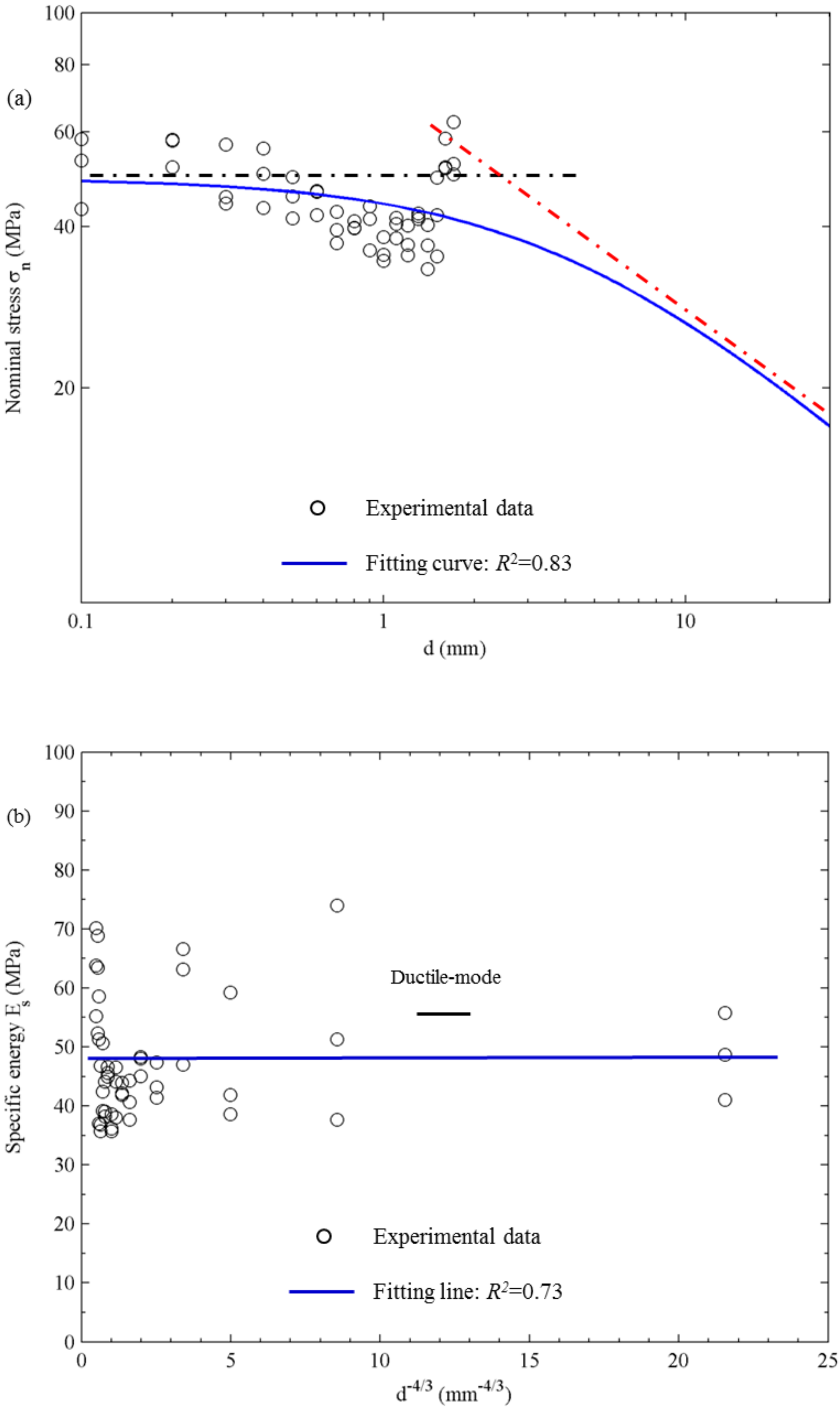

Fig. 4.13 Determination of the critical failure mode transition depth for Savonnières sample by (a) size effect law and (b) specific energy transition model for α=45°. *d* is in the range of 0.1-1.7 mm.

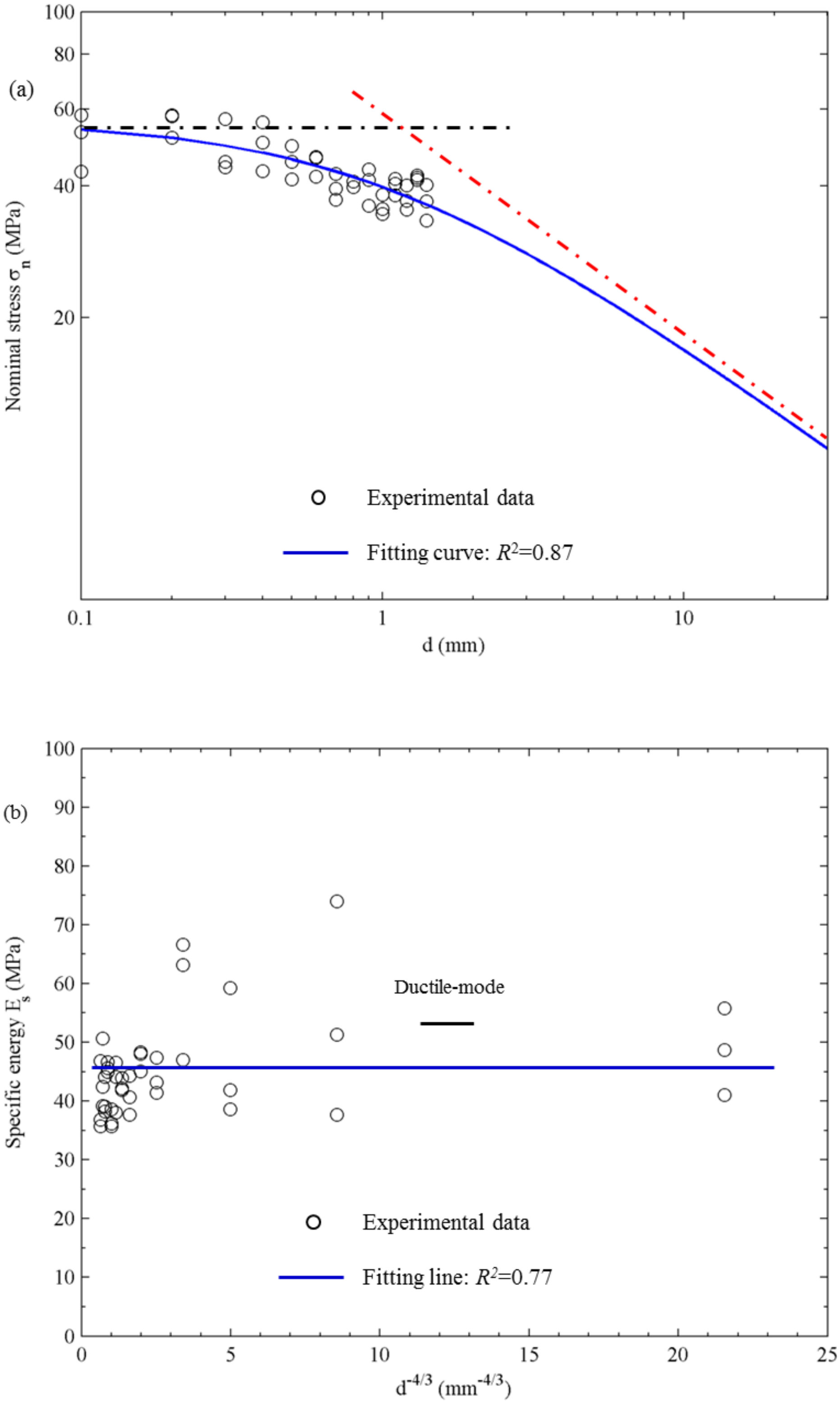

Fig. 4.14 Determination of the critical failure mode transition depth for Savonnières sample by (a) size effect law and (b) specific energy transition model for α=45°. *d* is in the range of 0.1-1.4 mm.

Fig. 4.15 Failure surface profile for Savonnières sample for α=45° and $d = 1.3$ mm.

Table 4.2 Comparison of the critical transition depth determined by the specific cutting energy transition model and the size effect law anslysis.

Back rake angle	d_c (mm) from specific energy varation		d_c (mm) from size effect law	
$\alpha = 15°$	0.40 (TL)	0.44 (SL)	0.35 (TL)	0.41 (SL)
$\alpha = 30°$	0.46 (TL)	0.61 (SL)	0.50 (TL)	0.92 (SL)
$\alpha = 45°$	0.79 (TL)	—	0.98 (TL)	1.27 (SL)*

*: Note this d_c value is derived from the cutting data with cutting depth in the range of 0.1-1.4 mm.

4.4 Discussions

The estimated critical transition depths from the two models discussed are summarised in Table 4.2. As expected, the critical transition depths for both Tuffeau and Savonnières rocks increase as the back rake angle increases. Similar observations are also given in Richard (1999) and Huang et al. (2013). The downward plastic material flow caused by large back rake angles creates large compressive stress within the rock material ahead of the cutting tool. This stress might result in a significant reduction in the opening mode stress intensity factor. As a consequence, the crack propagation within rock directly ahead of the cutting tool is inhibited and therefore ductile failure will be more dominant in the material removal process via cutting.

Obviously the results from the two models are different. To assess the accuracy of these estimates, we can examine carefully the cutting grooves at least to reach a qualitative conclusion. For example, at α=30°, the d_c is estimated to be 0.61 mm by the specific cutting energy transition model and 0.92 mm by the size effect law model (see Table 4.2). Fig. 4.16 shows the cutting grooves at this back rake angle for the cutting depth of 0.4, 0.7 and 1.0 mm respectively for Savonnières rock. As can be observed, chippings occur at the bottom cut surface and walls of the groove at d = 1.0 mm (Fig. 4.16c), but not for d = 0.4 mm (Fig. 4.16a) and d = 0.7 mm (Fig. 4.16b), suggesting that the critical transition depth for this back rake angle should be somewhere between 0.7 and 1.0 mm. Clearly the estimate of 0.92 mm as the critical transition depth from the size effect law model is an acceptable and reasonable estimate but the estimate of 0.61 mm from the specific energy transition model is an underestimated value. Together with the fact that the size effect law model always has higher goodness-of-fit (R^2) compared with the specific cutting energy transition model, it can be concluded that the size effect law can give a better prediction.

Results also show that rock properties play an important part in the determination of the critical transition depth. At the same back rake angle, Savonnières samples have larger values of d_c than Tuffeau (Table 4.2). However, the fact that the two rocks have nearly the same brittleness of about 11 (Table 4.1) implies there must be other rock properties affecting the cutting mechanisms. Previous studies have found that the rock grain size strongly influences the damage, crack initiation and propagation in rocks and ceramics being cut or scratched (Huang and Detournay 2008; Xu and Jahanmir 1995; Xu et al. 1995) and the critical transition depth is proportional to the grain size (He and Xu 2015a). This claim is clearly supported in our experiments as shown in Fig. 4.17 where the cutting grooves at the cutting depth of 1.4 mm with α=45° for both Tuffeau and Savonnières are displayed. As can be observed clearly, severe chippings occur in Tuffeau sample (Fig. 4.17a) but not in Savonnières sample (Fig. 4.17b). Similar patterns are also observed for tests conducted at other back rake angles. As Savonnières has much coarser grains compared with Tuffeau (also visible in Fig. 4.17), it is reasonable to conclude that the critical transition depth is directly proportional to the grain size, as also concluded in He and Xu (2015a).

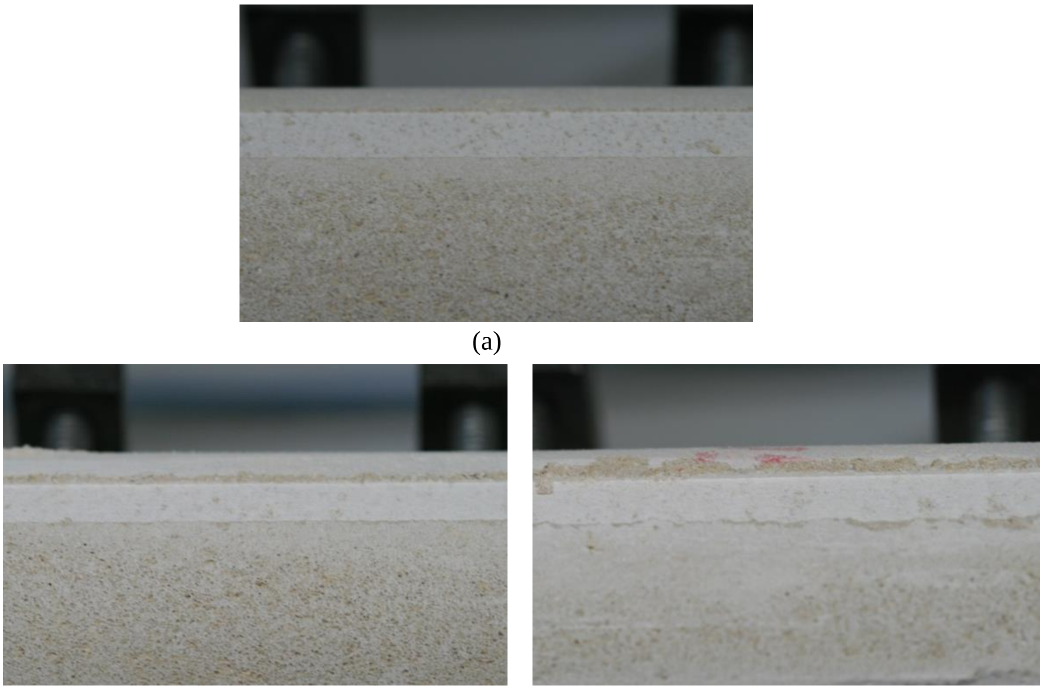

(a)

(b) (c)

Fig. 4.16 Typical failure surface profile on Savonnières sample for d=0.4 mm (a), d=0.7 mm (b) and d=1.0 mm (c) at α=30°.

Fig. 4.17 Failure surface profile for Tuffeau sample (left) and Savonnières sample (right) at α=45° and d = 1.4 mm.

4.5 Conclusions

Rock failure mechanisms can be classified as either a ductile failure regime, which is a rock strength driven process, or a brittle failure regime, which is a rock fracturing driven process. These two mechanisms are fundamentally different and they coexist in rock cuttings and only one of them is dominant depending on rock properties and specific cutting conditions. Understanding how the failure evolves from one regime to the other has important practical implications. For instance, polishing building stone requires the prevention of damage caused by fracturing and thus it is important to ensure the rock material is removed only in the ductile failure mode. On the other hand, mechanical excavation requires the energy consumed to remove unit rock materials to be minimised so it will be necessary to ensure the failure mode during cutting is mainly brittle fracturing dominant. In this work the attempt is made to identify the failure mode transition depth for rock cutting by two different types of data fitting models: the size effect law model and the specific energy transition model.

In the specific cutting energy transition model, the specific energy in the ductile cutting dominant process is considered to be independent of cutting depth while in brittle cutting dominant mode it is related to the cutting depth by a power-law relationship. For the size effect law model, a refinement has been made in this study to include the effect of the normal component of the cutting force, which acts as an indentation load on the cutting force responses. Compared with the more traditional qualitative method of examining the force trace patterns, these two data-fitting models can give definite and more accurate values for the critical transition depth without requiring the rock properties to be known *a priori*. The two models are applicable for different rock materials subjected to various different cutting scenarios with different operational parameters.

The critical failure mode transition depth is found to be dependent on the back rake angle: it increases when the back rake angle increases. The specific cutting energy transition model tends to underestimate the critical failure mode transition depth in comparison with the size effect law model. Cross validation with the failure surface profiles suggests that the size effect law model can give a better estimate for the cases tested.

In addition to the back rake angle, rock properties also affect the critical failure mode transition depth. The Tuffeau limestone used in this work has finer mineral grains compared with the Savonnières limestone. The Savonnières has larger critical failure mode transition depth than Tuffeau has at the same cutting conditions. This provides the experimental support for the claim that the critical failure transition depth is directly proportional to rock grain size, a conclusion based on a discrete element numerical study by He and Xu (2015a).

Acknowledgement

The work has been supported by the Deep Exploration Technologies Cooperative Research Centre whose activities are funded by the Australian Government's Cooperative Research Centre Programme. This is DET CRC Document. The generous support of CSIRO, Perth for the experimental tests reported in this article is also greatly acknowledged.

References

Akono A-T, Randall NX, Ulm F-J (2012) Experimental determination of the fracture toughness via microscratch tests: Application to polymers, ceramics, and metals. Journal of Materials Research 27:485-493 doi:10.1557/jmr.2011.402

Bažant ZP (1984) Size effect in blunt fracture: concrete, rock, metal. Journal of Engineering Mechanics 110:518-535

Bažant ZP, Hasegawa M, Mazars J (1991) Size effect in Brazilian split-cylinder tests: measurements and fracture analysis. ACI Materials Journal 88:325-332

Buyuksagis IS (2007) Effect of cutting mode on the sawability of granites using segmented circular diamond sawblade. Journal of Materials Processing Technology 183:399-406 doi:10.1016/j.jmatprotec.2006.10.034

Che D, Ehmann K (2014) Experimental study of force responses in polycrystalline diamond face turning of rock. International Journal of Rock Mechanics and Mining Sciences 72:80-91 doi:http://dx.doi.org/10.1016/j.ijrmms.2014.08.014

Franca LFP (2011) A bit–rock interaction model for rotary–percussive drilling. International Journal of Rock Mechanics and Mining Sciences 48:827-835 doi:10.1016/j.ijrmms.2011.05.007

He X, Xu C (2015a) Discrete element modelling of rock cutting: from ductile to brittle transition. International Journal for Numerical and Analytical Methods in Geomechanics doi:10.1002/nag.2362

He X, Xu C (2015b) Modelling of rock cutting forces based on the combined effect of ductile and brittle failure mechanisms. International Journal of Rock Mechanics and Mining Sciences (under review)

He X, Xu C (2015c) Specific Energy as an Index to determine the Critical Failure Mode Transition Depth in Rock Cutting. Rock Mechanics and Rock Engineering doi: 10.1007/s00603-015-0819-6

Huang H, Detournay E (2008) Intrinsic length scales in tool-rock interaction. International Journal of Geomechanics 8:39-44

Huang H, Lecampion B, Detournay E (2013) Discrete element modeling of tool-rock interaction I: rock cutting. International Journal for Numerical and Analytical Methods in Geomechanics 37:1913-1929 doi:10.1002/nag.2113

Kahraman S (2002) Correlation of TBM and drilling machine performances with rock brittleness. Engineering Geology 65:269-283 doi:10.1016/s0013-7952(01)00137-5

Lawn B, Cook R (2012) Probing material properties with sharp indenters: a retrospective. Journal of Materials Science 47:1-22 doi:10.1007/s10853-011-5865-1

Lawn BR (1998) Indentation of ceramics with spheres: A century after Hertz. Journal of the American Ceramic Society 81:1977-1994

Li XB, Summers DA, Rupert G, Santi P (2001) Experimental investigation on the breakage of hard rock by the PDC cutters with combined action modes. Tunnelling and Underground Space Technology 16:107-114 doi:10.1016/s0886-7798(01)00036-0

Lin J-S, Zhou Y (2013) Can scratch tests give fracture toughness? Engineering Fracture Mechanics 109:161-168 doi:http://dx.doi.org/10.1016/j.engfracmech.2013.06.002

Nicodeme P (1997) Transition between ductile and brittle mode in rock cutting. Ecole Polytechnique, Paris

Richard T (1999) Determination of rock strength from cutting tests. Master thesis, University of Minnesota

Richard T, Dagrain F, Poyol E, Detournay E (2012) Rock strength determination from scratch tests. Engineering Geology 147-148:91-100 doi:10.1016/j.enggeo.2012.07.011

Richard T, Detournay E, Drescher A, Nicodeme P, Fourmaintraux D (1998) The Scratch Test As A Means To Measure Strength of Sedimentary Rocks. Paper presented at the SPE/ISRM Rock Mechanics in Petroleum Engineering, Trondheim, Norway, 8-10 July 1998

Van Mier JG (2012) Concrete fracture: a multiscale approach. CRC press, Boca Raton, Florida, USA

Xu HHK, Jahanmir S (1995) Effect of grain size on scratch damage and hardness of alumina. Journal of Materials Science Letters 14:736-739 doi:10.1007/bf00253386

Xu HHK, Jahanmir S, Wang Y (1995) Effect of Grain Size on Scratch Interactions and Material Removal in Alumina. Journal of the American Ceramic Society 78:881-891 doi:10.1111/j.1151-2916.1995.tb08409.x

Zhou Y, Lin J-S (2013) On the critical failure mode transition depth for rock cutting. International Journal of Rock Mechanics and Mining Sciences 62:131-137 doi:http://dx.doi.org/10.1016/j.ijrmms.2013.05.004

Zhou Y, Lin J-S (2014) Modeling the ductile–brittle failure mode transition in rock cutting. Engineering Fracture Mechanics 127:135-147 doi:10.1016/j.engfracmech.2014.05.020

Chapter 5

Modelling of rock cutting forces based on the combined effect of ductile and brittle failure mechanisms

(Paper 4)

Xianqun He and Chaoshui Xu

Deep Exploration Technologies Cooperative Research Centre, School of Civil, Environmental and Mining Engineering, the University of Adelaide, Australia

Publication:

He X. and Xu C. (2015) Modelling of rock cutting forces based on the combined effect of ductile and brittle failure mechanisms. *International Journal of Rock Mechanics and Mining Sciences*. Submitted for review: June 2015.

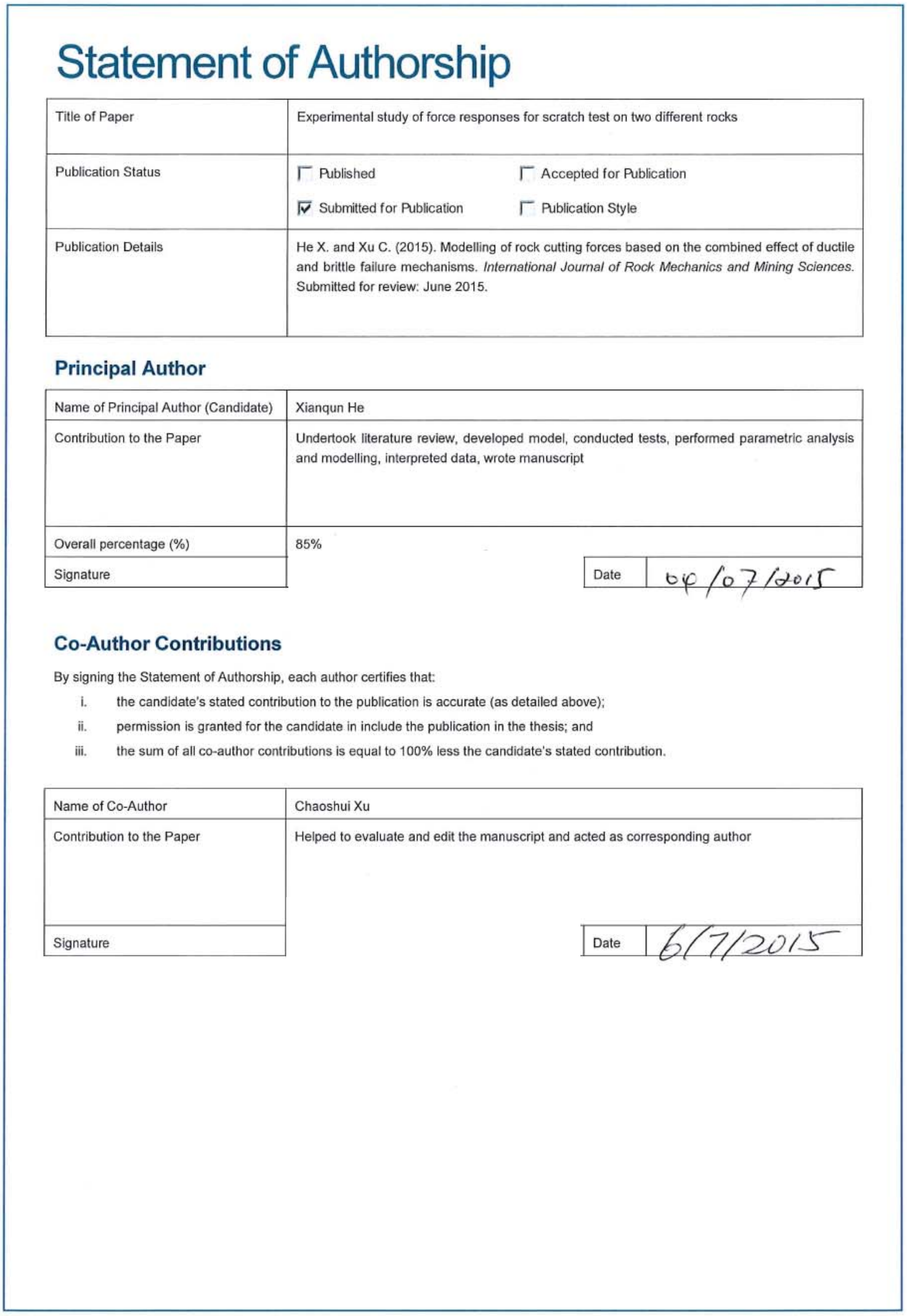

Statement of Authorship

Title of Paper	Experimental study of force responses for scratch test on two different rocks
Publication Status	☐ Published ☐ Accepted for Publication ☑ Submitted for Publication ☐ Publication Style
Publication Details	He X. and Xu C. (2015). Modelling of rock cutting forces based on the combined effect of ductile and brittle failure mechanisms. *International Journal of Rock Mechanics and Mining Sciences.* Submitted for review: June 2015.

Principal Author

Name of Principal Author (Candidate)	Xianqun He		
Contribution to the Paper	Undertook literature review, developed model, conducted tests, performed parametric analysis and modelling, interpreted data, wrote manuscript		
Overall percentage (%)	85%		
Signature		Date	06/07/2015

Co-Author Contributions

By signing the Statement of Authorship, each author certifies that:

i. the candidate's stated contribution to the publication is accurate (as detailed above);

ii. permission is granted for the candidate in include the publication in the thesis; and

iii. the sum of all co-author contributions is equal to 100% less the candidate's stated contribution.

Name of Co-Author	Chaoshui Xu		
Contribution to the Paper	Helped to evaluate and edit the manuscript and acted as corresponding author		
Signature		Date	6/7/2015

Abstract

Rock scratching/cutting using a rigid cutter penetrating the rock at a given depth is commonly used to remove rock material from a rock surface for different purposes. For example, building stones may require a finished rock surface as smooth as possible and therefore the removal of materials is only done at a very small scale under the ductile failure mode. In rock mechanical excavations (e.g., roadheaders), however, it is desired to remove as much rock material as possible using least amount of mechanical energy under the brittle fracture failure. Therefore understanding the interaction between cutter and rock has drawn continuous attention in both the research community and the industry. In order to assess the cutting performance, force responses during the cutting process are usually used to describe the cutter/rock interaction. This paper presents a generalised cutter/rock interaction model based on considerations of rock material removal accomplished by a cutting regime which is a combination of both ductile and brittle failure mechanisms, as commonly existing in rock cutting operations. A failure-mode mixture factor is introduced to quantify the proportions of ductile failure and brittle failure in a cutting operation. It is shown from experiments done on two different rocks that the generalised interaction model provides a significant improvement in the prediction of cutting forces over the commonly used models.

Keywords**:** rock cutting; ductile-brittle transition; fracture toughness; rock cutting force

5.1 Introduction

In rock scratching/cutting, a hard cutting tool, such as a Polycrystalline Diamond Compact (PDC) cutter, is driven across the rock surface at a certain penetrating depth under constant or increasing vertical load, as illustrated in Fig. 5.1 (note scratching or cutting is used interchangeably in this study). The scratching test is widely used in many fields of science and engineering. Examples include the measurement of strength and fracture properties of various materials including rocks (Akono et al. 2011; Richard et al. 2012), damage analysis of ceramics (Klecka and Subhash 2008; Tan et al. 2012), assessment of tool wear (Ersoy et al. 2005; Tönshoff et al. 2002) and performance measurement of thin films and coatings (Barletta et al. 2008; Randall et al. 2001). However, the underlying failure mechanisms in rock cutting are still far from being fully understood. In rock scratching process, the forces arising from the contact are the most important parameters to characterise the interaction between the scratch tool and the rock material. The challenge is in the establishment of a generalized model that can quantify effectively force responses for different rock properties and under complex cutting conditions (Akono et al. 2014; Akono and Ulm 2012).

Over the years, a great number of studies have contributed significantly to the better understanding of tool-rock interaction and better force response predictions based on rock properties and tool operating parameters. The pioneering work on cutting mechanics was done on coal by Evans (1965) who demonstrated theoretically that coal tensile and compressive strengths are dominant properties affecting rock cutting forces. Nishimatsu (1972) developed a model for cases when cutting is dominated by shear failure and the established relationship for the prediction of cutting forces is therefore based on the shear strength of rock. Studies on the effect of basic tool operating parameters such as cutting depth, back rake angle and cutting velocity were also widely published. For example, the influences of back rake angle were studied by Rajabov et al. (2012), Göktan (1990), Kaitkay and Lei (2005) and Che and Ehmann (2014) with the conclusion that an increase in back rake angle will cause the forces to increase. In terms of cutting velocity, several researchers (Germay et al. 2009; Verhoef 1997) reported that it has little influence on the force responses at lower velocities (below one meter per second). More importantly extensive efforts have been made to investigate the dependence of force responses on cutting depth (Bilgin et al. 2006; Detournay and Defourny 1992; Kuru and Wojtanowicz 1992; Richard et al. 2012; Roxborough 1985) wherein it was found that the forces generally increase linearly with depth of cut when it is small but non-linearly for deeper cutting. The linearly increasing trend of forces indicates the cutting mechanism is dominated by ductile failures of rock and the non-linear increase in forces at greater depth of cut, on the other hand, suggests the mechanism of brittle failures (He and Xu 2015a; Richard et al. 1998). As suggested in He and Xu (2015a), rock cutting in general involves the combination of both ductile and brittle failures in the process but one of them is always dominant depending on the depth of cut. Given a rock and a set of cutting parameters, there is a fixed critical transition depth when the dominant failure mode changes from one to the other.

A rich set of experimental results have been used to develop a number of empirical formulations to predict cutting force responses (e.g., (Evans 1965), (Nishimatsu 1972) and (Detournay and Defourny 1992)), with different focuses: some of them put more emphasis on rock properties while others consider more operational parameters. However, none of the published studies has taken the ductile-to-brittle failure transition phenomenon into account when establishing the force prediction model. Therefore these developed models are only valid for some prescribed conditions within a limited range of parameters (Su and Akcin 2011). It is in general difficult to generalise these models for a wide range of cutting conditions.

This investigation aims to develop a generalised model for more accurate cutting force prediction based on rock properties and operational parameters, such as uniaxial compressive strength (UCS), fracture toughness, depth of cut and back rake angle, while incorporating the effect of the ductile-brittle failure transition. Cutting tests were performed on two selected types of rocks with different depths of cut and back rake angles to provide data for model validation. It has been demonstrated that considering the combination effect of ductile and brittle failure modes is necessary for more accurate prediction of forces in rock cutting.

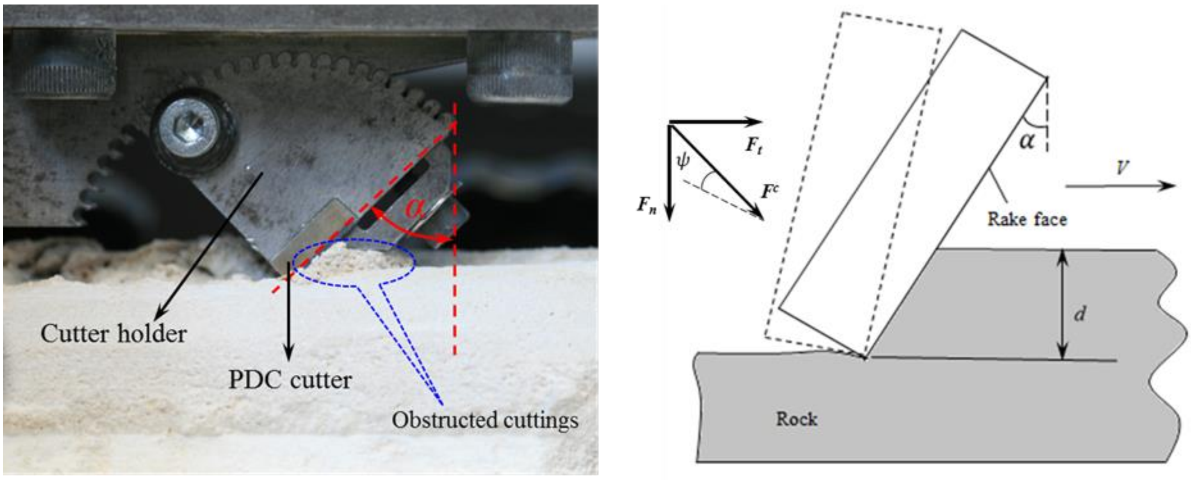

(a) (b)

Fig. 5.1. Description of scratch tests. (a) Scratch tests on Savonnières with back rake angle α of 45°. (b) Idealised 2-D geometry of scratch test: the rectangular PDC cutter is pushed horizontally with cutting velocity V, at depth of cut d by applying resultant cutting force F^c which can be decomposed into a normal cutting force component F_n and a tangential cutting force component F_t. The back rake angle α is defined as the angle between the rake face and the normal to rock surface. ψ is the angle characterising the friction between rake face and rock.

5.2 Mechanics of rock cutting

Rock cutting is normally conducted by means of kinematic controlling the depth of cut d, the inclination of the cutter (i.e., the back rake angle α) and the cutting velocity V with prescribed values, as shown in Fig. 5.1. It was well established two failure modes exist in rock cutting: ductile and brittle (He and Xu 2015a; Nicodeme 1997; Richard et al. 1998). The dominant failure mode is ductile when the cutting depth is small, but as the depth increases to the critical transition depth, the dominant failure mode changes to brittle (He and

Xu 2015a; Huang et al. 2013; Richard et al. 1998) with some ductile failures occurring directly ahead of the cutter. The cutting forces in ductile failure regime are dependent on the uniaxial compressive strength σ_c; while for brittle-mode cutting the forces are dependent on the fracture toughness K_{IC} (Richard et al. 2012). Two representative force prediction models are discussed below, followed by our new proposed model with the consideration of both ductile and brittle failure modes incorporated.

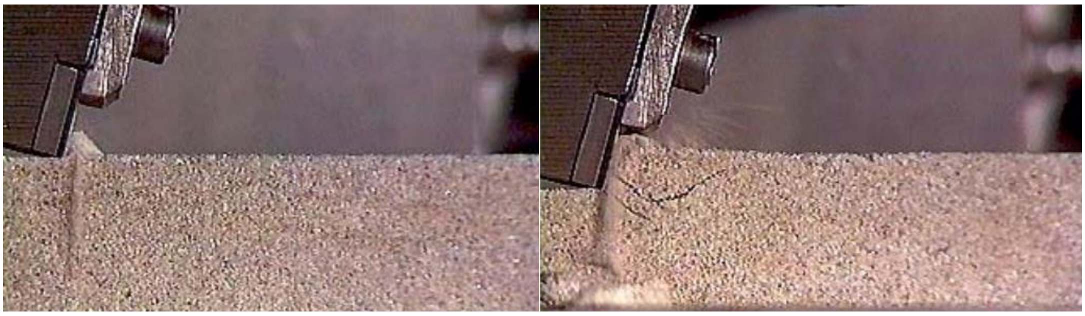

(a) (b)

Fig. 5.2 Material removal in (a) ductile mode at depth of cut d=0.3 mm and (b) brittle mode at depth of cut d =3 mm during cutting tests on slab sample of Vosges sandstone (after Richard (1999)).

5.2.1 Ductile failure mode cutting force prediction (DCFP)

In ductile failure mode rock cutting, the cutting energy is mainly consumed in volumetrically failing the rock material, with broken rock grains in powder form accumulated in front of the cutter (Fig. 5.2a). In this mode, a phenomenological model was proposed by Detournay and Defourny (1992) who suggest that the average tangential cutting force for a sharp cutter, where the force acting on the wear flat is negligible, is proportional to the depth of cut, i.e.,

$$F_{t\_d} = \varepsilon W d \tag{5.1}$$

where W is the cutting width; ε is the intrinsic specific energy that represents the energy strictly used for cutting. ε is defined in the unit of MPa as it is assumed to be directly related to the rock strength properties, i.e., the UCS, σ_c.

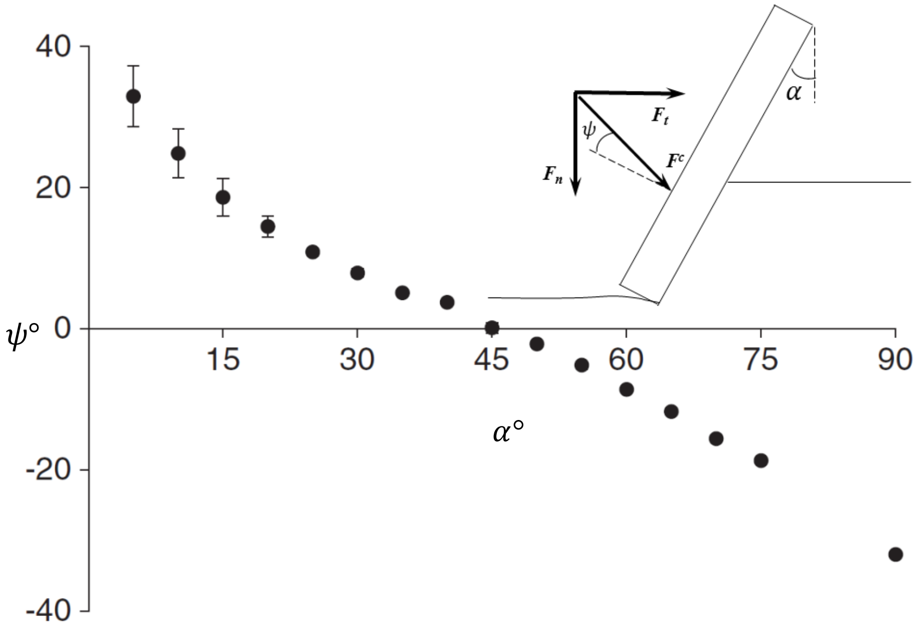

Fig. 5.3 The inclination of the total cutting force F^c with respect to the normal to the cutter, termed the friction angle ψ between cutting face and rock, as a function of the back rake angle α (experimental results from (Richard 1999), reproduced after Huang et al. (2013))

In addition, the normal component of the cutting force is given as:

$$F_{n\_d} = \zeta \varepsilon W d \tag{5.2}$$

where the factor ζ can be expressed as $\tan(\alpha+\psi)$ with ψ being the inclination angle of the resultant cutting force normal to the rake face which characterises the friction between rake face and the rock in direct contact (see Fig. 5.1b). The angle ψ is found to be independent of depth of cut but depends on the back rake angle. As shown in Fig. 5.3, the friction angle ψ

decreases approximately linearly with the increasing back rake angle α (Richard 1999).

5.2.2 Brittle failure mode cutting force prediction (BCFP)

As the depth of cut d reaches the critical transition depth, cutting enters the brittle failure dominant regime with energy dissipation mainly in creating macroscopic cracks that propagates towards the rock surface to form cut chips, as shown in Fig. 5.2b. The cutting forces are no longer linearly related to the depth of cut, but rather, related linearly to the square root of cutting depth (Richard et al. 2012).

A more recent analytical solution was given by Akono and Ulm (2011) who used a cutting mechanics model dependent on both the tool geometry and the rock fracture toughness derived from the linear elastic fracture mechanics (LEFM) approach. The key framework of this model is reviewed below.

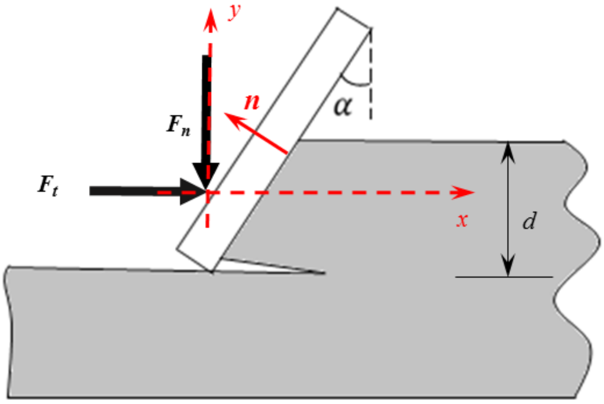

Fig. 5.4 A simplified scratch test geometry considered with existing horizontal crack for deriving the analytical solution that links the force responses to scratch tool geometry and fracture toughness in Akono and Ulm (2011).

Considering a crack emanating horizontally from the tip of the scratch tool, as shown in Fig. 5.4, a stress field due to the loading applied by the cutter inclined with the back rake angle α can be given in the form of

$$\underline{\underline{\sigma}} = \sigma_{xx} e_x \otimes e_x + \sigma_{xy}(e_x \otimes e_y + e_y \otimes e_x) + \sigma_{yy} e_y \otimes e_y + \sigma_{zz} e_z \otimes e_z \tag{5.3}$$

Under plane conditions (i.e., $\sigma_{zz} = 0$ for plane stress; $\sigma_{zz} = \nu(\sigma_{xx} + \sigma_{yy})$ for plane strain), using Airy-stress function, $\varphi(x, y) = -bx\left(y^3 - 3y\left(d/2\right)^2\right) + cy^2$, yields the following stress components:

$$\sigma_{xx} = \frac{\partial^2 \varphi}{\partial y^2} = -6bxy + c \tag{5.4}$$

$$\sigma_{xy} = -\frac{\partial^2 \varphi}{\partial x \partial y} = b\left(3y^2 - \frac{3}{4}d^2\right) \tag{5.5}$$

$$\sigma_{yy} = \frac{\partial^2 \varphi}{\partial x^2} = 0 \tag{5.6}$$

where the constants, *b* and *c*, are determined such that the stress boundary conditions at the cutter-rock interface (*S*) are satisfied:

$$\int_{(S)} \underline{\underline{\sigma}} \cdot n dS = F_{t\_b} e_x - F_{n\_b} e_y \tag{5.7}$$

where the outward unit normal vector at the interface $n = -\cos\alpha e_x + \sin\alpha e_y$ with e_x being the unit vector for x axis and e_y for y axis (Fig. 5.4); F_{t_b} and F_{n_b} stand for tangential and normal cutting forces in brittle failure mode cutting, respectively.

Assuming the only contribution to the cutting force is from the interface between the cutter face and the rock, the contour-independent *J*-integral (Rice 1968) commonly used to estimate the strain energy release rate or the energy dissipated in cracking a unit surface yields:

$$G = \frac{\kappa}{EW^2 d} \frac{F_{eq}^2}{2} \tag{5.8}$$

where G is the strain energy release rate; E is the Young's modulus; $\kappa = 1$ in plane stress conditions and $\kappa = 1 - \nu^2$ in plane strain conditions with ν being the Poisson's ratio; and

$$F_{eq} = \begin{cases} F_{t\_b} & \text{if } \alpha = 0 \\ F_{t\_b}^2 + \frac{3}{5} F_{n\_b}^2 & \text{if } \alpha > 0 \end{cases} \tag{5.9}$$

At the onset of fracture propagation, the energy release rate reaches the critical fracture energy, i.e.,

$$G = G_f = \kappa \frac{K_{IC}^2}{E} \tag{5.10}$$

Combining Eqs. (5.8)-(5.10), the cutting forces for $\alpha > 0$ are linked to the cutting geometry and fracture toughness as:

$$\sqrt{\frac{1}{2} F_{t\_b}^2 + \frac{3}{10} F_{n\_b}^2} = K_{IC} W \sqrt{d} \tag{5.11}$$

5.2.3 Generalised cutting force prediction model (GCFP)

Models such as those discussed above are either based on the consideration of strength-driven process (DCFP) or fracture-driven process (BCFP). However, the findings in He and Xu (2015a) suggest that rock failure mode under cutting is neither purely brittle nor purely ductile, but a mixture of both. Depending on the depth of cut, one of the failure modes will be dominant. In shallow cutting, ductile failure mode is dominant with the possibility of formation of very small cut chips (e.g., agglomerate of rock grains). At greater depth of cut, brittle failure dominates, which generates large cut chips while part of the material directly ahead of the cutter is heavily crushed, indicating the failed material in this region is undergoing ductile failure with plastic flow. The critical transition depth d_c at which rock failure changes from ductile dominant to brittle dominant mode is found to be dependent on rock properties and the back rake angle and the results are summarised in Table 5.1 (He and Xu 2015b; He and Xu 2015c) for the two types of rocks, Savonnières (SL) and Tuffeau (TL) samples used in this study. Note: the values for η and d_c are taken from the derived results using specific energy transition model and the size effect law respectively (see He and Xu (2015b)). ψ is extracted from Fig. 5.3.

Table 5.1 The values of the parameters used for predicting the cutting forces in this study.

Parameters	η	d_c (mm)		ψ (°)
$\alpha = 15°$	1.0	0.35 (TL)	0.41 (SL)	18
$\alpha = 30°$	1.3	0.50 (TL)	0.92 (SL)	8
$\alpha = 45°$	2.0	0.98 (TL)	1.27 (SL)	0

A cutting force prediction model considering the failure mechanism as a combination of these two failure modes is proposed below. The following assumptions are used in our proposed model: (1) the energy consumed during the cutting process can be evaluated as the product of the tangential component of the cutting force and cutting distance and, (2) the total consumed energy can be decomposed into two components: one dedicated for ductile cutting and the other for brittle cutting. A transition of failure mode from ductile dominant to brittle dominant means that more energy would be dissipated in brittle failure with macroscopic crack formation and less energy consumed for the ductile failure. This transition is expected to be gradual and therefore we propose a factor m_f to represent the proportion the contribution to the force response from ductile failure in the cutting process. m_f based on its definition will be close to 1 when the cutting depth d is small and as d increases it is expected to decrease rapidly initially and then gently at large cutting depth, as illustrated in the schematic diagram in Fig. 5.5. To capture this trend, the following relationship is proposed for m_f:

$$m_f = \frac{2}{\pi} arc\cot\left(\frac{d}{d_c}\right) \tag{5.12}$$

where the constant (2/π) is needed so that at the critical transition depth when $d = d_c$, $m_f = 0.5$, i.e., the total energy is dissipated equally for ductile and brittle failures.

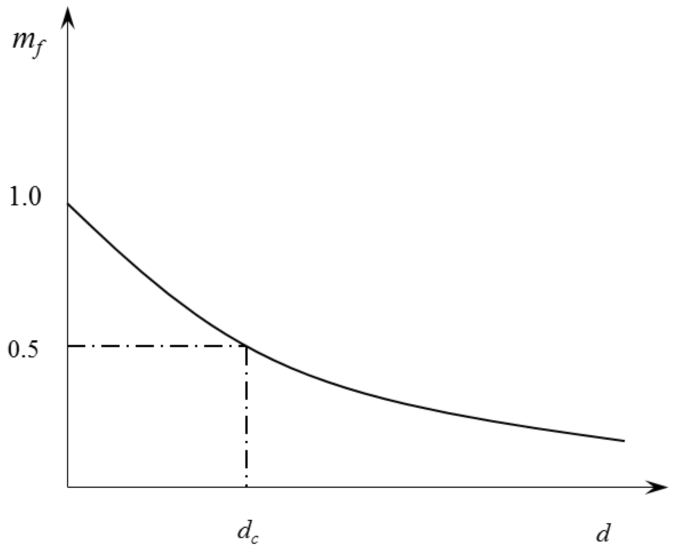

Fig. 5.5 Schematic plot showing the failure mode mixture factor varying with depth of cut.

It is worthwhile to mention that Eq. (5.12) is not a derived relationship, rather a proposed one to capture the trend shown in Fig. 5.5, which by itself is a qualitative perceived variation based on experimental observation. In this sense, the proposed relationship can be regarded as the first attempt to quantify m_f. Even the force prediction model constructed based on Eq. (5.12) shows a significant improvement over existing ones, as demonstrated below, further studies are needed to further validate and improve the proposed relationship (Eq. (5.12) and Fig. 5.5). Other variable that can affect m_f should also be incorporated. For example, as discussed below, back rake angle also affect the rock cutting failure mode but its influence is only considered indirectly by the parameter d_c at this stage in Eq. (5.12).

Based on the definition of m_f, the tangential cutting force taking into account of the two failure modes can then be written as:

$$F_t = m_f F_{t\_d} + \left(1 - m_f\right) F_{t\_b} \tag{5.13}$$

Since the normal cutting force can be related by a ratio of $\tan\left(\alpha + \psi\right)$ to the tangential cutting force (Lin and Zhou 2013), Eq. (5.11) can be rewritten using only the tangential cutting force and material properties and cutting geometry as

$$F_{t\_b} = \frac{\sqrt{2} K_{IC} W \sqrt{d}}{\sqrt{1 + \frac{3}{5}\left(\tan(\alpha + \psi)\right)^2}} \tag{5.14}$$

The tangential cutting force due to ductile failure can be written as (He and Xu 2015b; He and Xu 2015c):

$$F_{t\_d} = \eta \sigma_c W d \tag{5.15}$$

where η is a factor influenced by the back rake angle α and its values are listed in Table 5.1. This expression is identical to Eq. (5.1) if $\eta\sigma_c$ is replaced by ε. As $\varepsilon = \sigma_c$ for α=15° based on experiments (Richard et al. 2012), and therefore η = 1 for $\alpha = 15°$. η is expected to increase with the back rake angle α, indicating the increased difficulty in cutting for larger back rake angles (cf. Table 5.1).

Combined with Eqs. (5.12), (5.14) and (5.15), we can rewrite the tangential cutting force in Eq. (5.13) as:

$$F_t = \frac{2}{\pi} arc\cot\left(\frac{d}{d_c}\right)\eta\sigma_c Wd + \left(1 - \frac{2}{\pi} arc\cot\left(\frac{d}{d_c}\right)\right)\frac{\sqrt{2}K_{IC}W\sqrt{d}}{\sqrt{1+\frac{3}{5}\left(\tan(\alpha+\psi)\right)^2}} \tag{5.16}$$

and the normal component of the cutting force thus can be given as:

$$F_n = \tan(\alpha+\psi)\left(\begin{array}{l}\frac{2}{\pi} arc\cot\left(\frac{d}{d_c}\right)\eta\sigma_c Wd + \\ \left(1 - \frac{2}{\pi} arc\cot\left(\frac{d}{d_c}\right)\right)\frac{\sqrt{2}K_{IC}W\sqrt{d}}{\sqrt{1+\frac{3}{5}\left(\tan(\alpha+\psi)\right)^2}}\end{array}\right) \tag{5.17}$$

As can be seen, the cutting forces, as expected, are dependent on the rock properties such as UCS (σ_c) and fracture toughness (K_{IC}) as well as the cutting operational parameters characterised by the depth of cut *d* and the back rake angle α.

5.3 Experimental validation

5.3.1 Experimental setup

The scratch tests were carried out using the Rock Strength Device. For the detailed specification description of the experimental devices, readers are referred to He and Xu (2015c). The PDC cutter used in the test is mounted to the cutter holder, as shown in Fig. 5.1a, which allows a 5-degree incremental change in the back rake angle.

The rocks used are two types of limestone: Savonnières (SL) and Tuffeau (TL). Each set of rock samples are cored from the same rock block to ensure consistent rock properties. The uniaxial compression tests, Brazilian tensile tests and fracture toughness measurements were conducted following the ISRM suggested methods (Bieniawski and Bernede 1979; Bieniawski and Hawkes 1978; Kuruppu et al. 2014). The mechanical properties of the two rock samples are summarised in Table 5.2.

Table 5.2 Mechanical properties of SL and TL rock sample.

Uniaxial compressive strength		Brazilian tensile strength		Fracture toughness			
σ_c (MPa)		σ_t (MPa)		K_{IC} (MPa·m$^{0.5}$)		K_{eff} (MPa·m$^{0.5}$)	
22.95 (SL)	9.21 (TL)	2.10 (SL)	0.84 (TL)	0.35 (SL)	0.15 (TL)	0.52 (SL)	0.22 (TL)

Note: the values for the effective fracture toughness K_{eff} are derived according to Ayatollahi and Aliha (2008).

5.3.2 Testing design and procedure

Previous study in He and Xu (2015c) has demonstrated the effect of the cutting velocity within the range of 4-20 mm/s on cutting forces is negligible. Thus in this experimental study, the cutting velocity is set at a constant value of 8 mm/s and therefore the operational variables to be explored in the study are the back rake angle α and the depth of cut d. There are 17 different cutting depths ranging from 0.1 to 1.7 mm with a 0.1 mm interval; and three different back rake angles α at 15°, 30° and 45°. Therefore there are 3×17=51 number of combinations of these parameters for each type of rock. The procedure for a typical cutting test is:

(1) Install the PDC cutter with a desired back rake angle, put and secure the rock sample on the cutting station.

(2) Perform several preliminary cuts to generate a smooth and flat reference surface.

(3) Replace the trimming PDC cutter and reset the micrometer to zero, then set the depth of cut to a specified value.

(4) Start the motor to drive the cutter to start cutting. During cutting, record continuously the cutting forces and use vacuum machine to clear cuttings ahead of the cutter.

(5) Prior to performing the next cutting, remove the two side walls of the groove left by the previous cut to eliminate the additional frictional effect. Then repeat step (1)-(4) for the next cutting.

Each test with a set of preset cutting specifications was conducted three times. Due to the difficulty in changing the back rake angle in the testing facility, all tests with the same back rake angles were completed first before moving on to the tests on a different angle. The test configurations and their measured forces are summarized in Table 5.3.

Table 5.3 Test arrangement and force responses for TL and SL rock samples.

				Tuffeau						Savonnières					
	Test no.	α (°)	d (mm)	F_t			F_n			F_t			F_n		
				#1	#2	#3	#1	#2	#3	#1	#2	#3	#1	#2	#3
Set 1	1	15	0.1	10.3	10.8	10.4	8.3	8.8	8.8	23.5	22.0	22.7	22.3	22.0	23.3
	2	15	0.2	17.6	22.9	16.8	16.7	16.4	15.9	50.8	39.2	43.6	35.2	39.6	39.8
	3	15	0.3	27.5	27.2	33.2	20.4	18.3	25.0	52.8	68.0	55.2	48.1	51.7	47.7
	4	15	0.4	40.2	35.5	31.4	24.1	24.8	25.9	96.5	98.3	87.9	44.5	50.6	48.7
	5	15	0.5	40.3	43.8	43.5	25.4	26.3	27.0	91.9	89.6	97.1	72.1	57.4	59.6
	6	15	0.6	44.6	45.5	47.3	16.3	28.8	37.0	117.4	117.7	113.0	78.7	77.5	67.3
	7	15	0.7	44.8	56.0	52.8	31.9	32.6	26.7	127.6	122.5	118.3	82.9	79.7	78.3
	8	15	0.8	56.9	69.8	58.3	35.4	31.6	35.0	139.6	146.3	140.6	86.2	86.9	85.0
	9	15	0.9	61.4	62.8	56.8	33.7	46.5	22.1	146.2	161.1	167.0	91.0	114.4	94.4
	10	15	1.0	82.6	67.7	72.9	30.6	36.0	37.5	153.8	147.4	148.4	90.9	101.7	112.1
	11	15	1.1	73.9	57.1	74.3	37.0	41.0	42.8	174.1	177.3	182.2	90.6	102.7	105.4
	12	15	1.2	73.6	76.1	75.8	38.6	43.3	37.1	192.5	184.4	185.6	115.9	108.1	113.9
	13	15	1.3	65.6	85.9	77.5	42.9	48.3	46.5	189.1	181.5	208.6	124.7	128.8	99.4
	14	15	1.4	83.7	91.8	88.9	46.7	40.5	40.7	193.0	191.5	207.5	116.7	138.3	107.3
	15	15	1.5	96.1	71.4	85.4	34.3	52.1	51.2	199.6	221.1	231.9	111.0	106.3	117.5
	16	15	1.6	90.0	89.4	69.1	51.5	37.3	36.7	205.6	223.0	231.5	125.5	107.4	119.0
	17	15	1.7	95.1	86.9	97.8	53.1	54.1	44.9	227.2	248.3	239.3	133.8	147.5	124.0
Set 2	18	30	0.1	13.5	12.3	12.9	13.1	12.9	13.7	30.8	31.0	32.5	34.3	34.2	35.2
	19	30	0.2	31.3	22.0	25.5	19.7	22.4	22.5	60.6	62.3	66.9	60.3	55.1	52.9
	20	30	0.3	29.7	41.8	31.7	26.8	29.0	26.6	98.0	80.8	92.8	71.2	83.2	70.6
	21	30	0.4	52.6	54.1	45.7	26.9	32.5	30.7	107.7	112.2	112.2	84.7	79.4	74.6
	22	30	0.5	48.3	46.5	52.5	46.8	38.0	39.3	140.5	125.1	127.9	104.4	92.5	94.4
	23	30	0.6	67.9	68.1	64.3	53.2	52.6	47.3	178.7	167.0	180.0	124.6	137.0	133.5
	24	30	0.7	70.6	66.5	63.2	54.2	51.5	50.3	172.6	165.7	163.8	132.3	130.6	130.9
	25	30	0.8	82.3	87.7	83.1	54.2	54.7	53.4	215.2	196.7	217.5	145.7	164.5	145.9
	26	30	0.9	78.1	90.0	94.7	52.3	66.3	54.3	242.9	254.2	234.5	172.2	202.4	189.4
	27	30	1.0	89.6	84.5	85.3	54.5	61.0	67.2	253.7	269.6	254.7	207.9	215.5	182.9
	28	30	1.1	98.2	100.8	104.7	59.0	66.3	67.9	289.7	296.1	275.0	214.2	203.4	194.0
	29	30	1.2	106.4	99.9	100.9	74.2	69.5	73.0	277.9	289.1	295.3	217.4	218.5	207.4
	30	30	1.3	106.0	98.8	124.3	80.7	83.1	65.5	326.4	290.8	308.3	216.1	232.3	225.8
	31	30	1.4	111.0	109.8	122.6	80.7	93.6	75.0	328.9	348.2	336.7	246.8	269.1	258.2
	32	30	1.5	117.1	138.9	150.0	83.4	80.6	87.3	353.1	363.3	348.6	261.9	263.6	270.0
	33	30	1.6	125.1	138.9	145.8	92.9	82.1	89.1	387.7	402.4	380.5	277.3	296.7	272.2
	34	30	1.7	133.1	155.1	145.7	93.7	101.9	87.7	371.6	389.6	374.6	288.3	283.4	273.8
Set 3	35	45	0.1	19.4	22.5	22.6	20.9	20.3	17.3	55.8	41.0	48.7	50.0	45.1	66.2
	36	45	0.2	43.4	38.3	42.9	38.2	42.6	34.6	148.0	75.4	102.7	70.5	124.9	127.0
	37	45	0.3	58.2	58.6	54.1	53.7	60.5	53.5	115.7	177.8	125.7	147.2	163.1	145.8
	38	45	0.4	77.0	80.0	77.1	75.7	72.2	72.9	252.8	266.6	188.1	128.9	169.5	156.8
	39	45	0.5	94.8	99.7	94.8	97.3	69.9	81.7	216.0	207.0	236.9	274.6	206.8	217.3
	40	45	0.6	106.0	99.6	97.0	101.4	101.3	98.6	288.4	289.7	270.0	270.0	265.8	232.0
	41	45	0.7	123.3	113.6	116.5	109.0	102.7	113.8	310.4	284.9	263.9	285.9	266.0	257.1
	42	45	0.8	142.2	127.8	133.5	116.6	133.6	117.1	335.1	351.1	337.5	300.0	301.9	296.7
	43	45	0.9	143.9	137.5	146.2	130.3	129.7	160.4	342.7	397.3	419.1	305.8	387.0	317.6
	44	45	1.0	149.1	154.7	181.2	128.1	149.2	129.0	386.1	357.4	362.0	298.8	351.1	400.8
	45	45	1.1	175.5	172.0	173.6	149.4	153.1	161.9	494.3	501.8	513.0	325.8	379.5	391.4
	46	45	1.2	166.0	170.9	186.7	151.0	156.1	139.0	529.2	458.4	468.9	428.2	386.5	417.3
	47	45	1.3	178.7	185.5	181.1	152.9	159.8	151.7	551.4	509.7	658.2	548.1	575.3	379.1
	48	45	1.4	221.8	188.5	228.6	169.1	152.0	165.2	515.4	500.6	655.4	412.4	621.0	321.7
	49	45	1.5	224.3	225.7	215.4	195.3	200.4	169.3	555.7	770.0	878.6	497.7	446.7	569.5
	50	45	1.6	213.3	198.2	214.9	213.0	208.6	237.9	837.7	1015.2	1102.2	804.3	576.1	723.3
	51	45	1.7	230.8	196.5	253.2	226.7	190.9	206.4	939.3	1193.1	1085.3	751.0	915.0	632.5

5.4 Results and discussions

The analysis of the experimental results is presented below in four sections. Section 5.4.1 describes the general characteristics of the force signals recorded during the whole cutting process. In Section 5.4.2 and 5.4.3 the effects of back rake angle and depth of cut on force responses are reported based on a comparison study of the DCFP, BCFP and GCFP models. The similarity and difference in terms of cutting forces for the two different rocks are discussed in Section 5.4.4.

5.4.1 General description of force traces along cutting distance

In our experiments, the force components are measured at the sampling rate of 600 Hz. As the example shown in Fig. 5.6, the cutting process generally involves three stages:

(1) Initial contact stage (stage I): when the cutter comes into contact with the rock, the forces increase sharply until the cutter is in full contact with the rock.

(2) Stable cutting stage (stage II): the force components reach a relatively stable state, corresponding to the main cutting section. The forces measured in this stage are the cutting forces used in rock cutting mechanics studies.

(3) Unstable cutting stage (stage III): when the cutter approaches the end of the specimen, the forces gradually reduce to zero due to the change in boundary conditions.

In our analysis, the raw data during the stable cutting stage are filtered by a low pass filter with a cut-off frequency of 10 Hz. The filtered data are averaged to obtain the mean tangential and normal cutting forces, F_t and F_n, which are then taken as the representative force responses with respect to different combinations of (d, α), as summarised in Table 5.3.

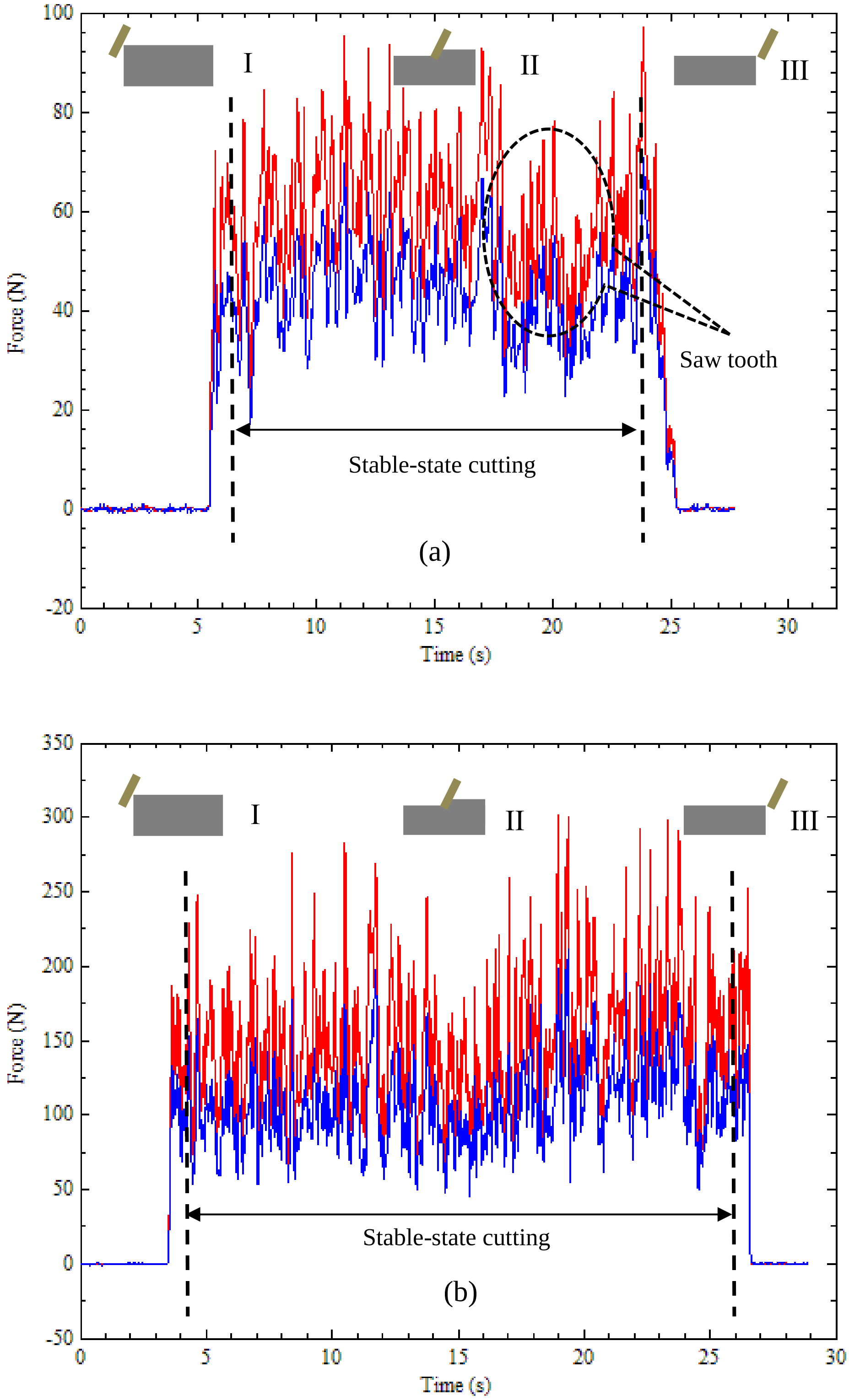

Fig. 5.6 Examples of raw force signals for (a) Tuffeau and (b) Savonnières, showing tangential force (in red) and normal force (in blue) as a function of time (d=0.6 mm, α=30° and V=8 mm/s).

5.4.2 Test results for Tuffeau sample

Fig. 5.7-Fig. 5.9 show the evolution of the cutting forces for the Tuffeau rock with respect to the depth of cut for different back rake angles. The depth of cut, as an important operating parameter, has significant influence over the performance of the cutting tool. As can be seen from Fig. 5.7-Fig. 5.9, both the tangential and normal components of the cutting forces keep increasing with the depth of cut in all cases. However, the increase trend slows down as the depth of cut increases, indicating a non-linear relationship. For example, at α=15°, the tangential cutting force for d = 0.1 mm is 10 N which gives an initial increasing rate of 100 N/mm (Eqs. (5.1) and (5.15)). At d = 1.7 mm, the tangential cutting force is 90 N, which is only nine times (not 17 times) that for d = 0.1 mm (Fig. 5.7). This suggests the force increasing rate has consistently decreased as the cutting depth increases and therefore a non-linear relationship between cutting forces and the depth of cut. In other words, the non-linear increasing cutting force is due to that the cutting enters brittle failure dominating mode after passing the critical transition depth d_c, which in this case is 0.35 mm for α=15° (see Table 5.1).

Fig. 5.7-Fig. 5.9 also demonstrate the effect of back rake angles on the cutting forces. Both the tangential and normal cutting forces increase with α as it becomes more “difficult” to cut at higher back rake angles. More specifically, by comparing Fig. 5.7 with Fig. 5.9 (or the corresponding data in Table 5.3), one can see that an increase in the back rake angle from 15° to 45° doubles the tangential cutting force F_t for d = 0.1 and 0.2 mm. The normal component F_n also increases with the back rake angle, but with a higher increasing rate, leading to F_n almost equal to F_t when α is at 45°. In addition, for larger back rake angles the measured forces are closer to the forces predicted based on the ductile-mode cutting.

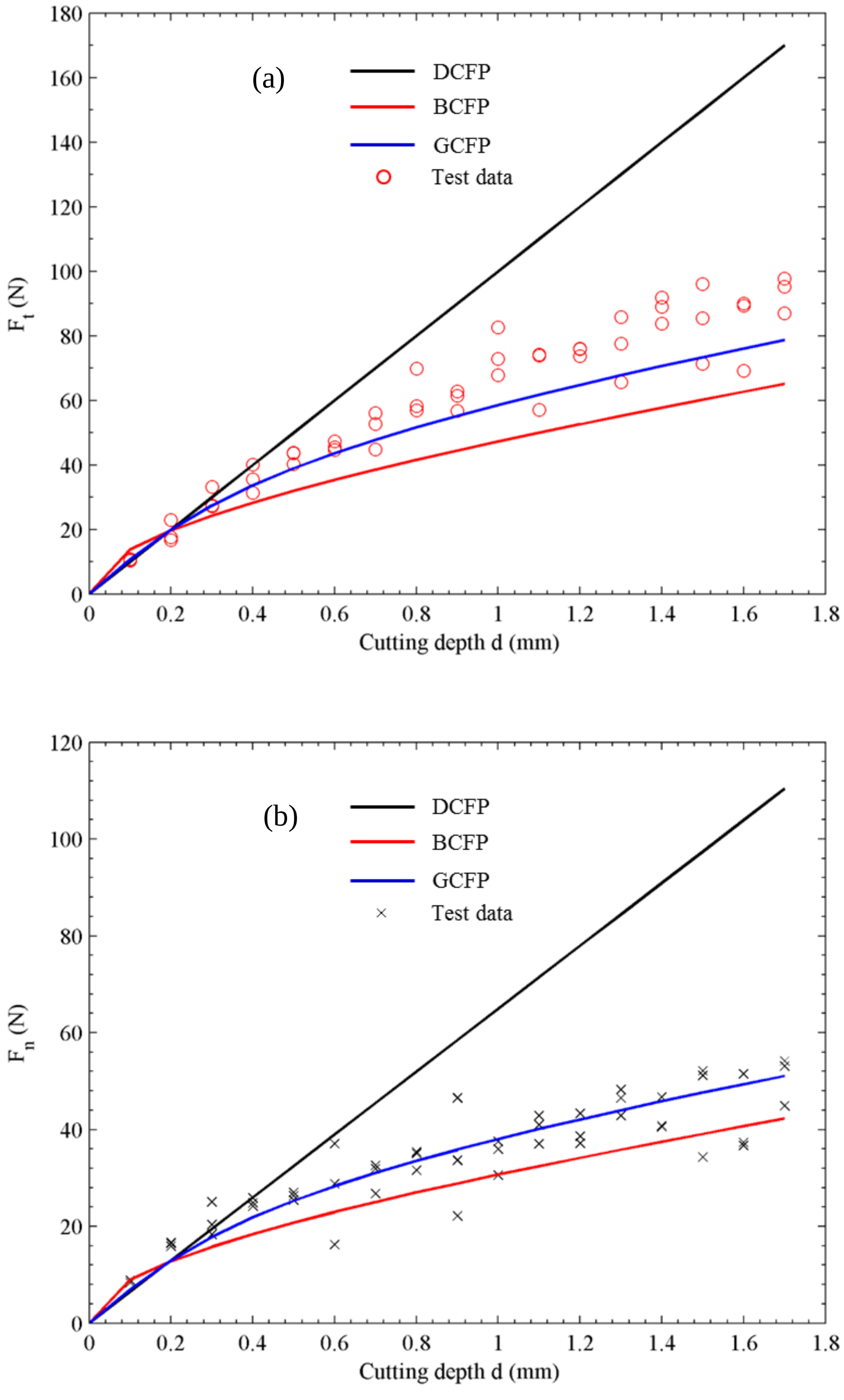

Fig. 5.7 Comparison of DCFP, BCFP and GCFP models for (a) tangential cutting force F_t and (b) normal cutting force F_n on TL sample with α=15°.

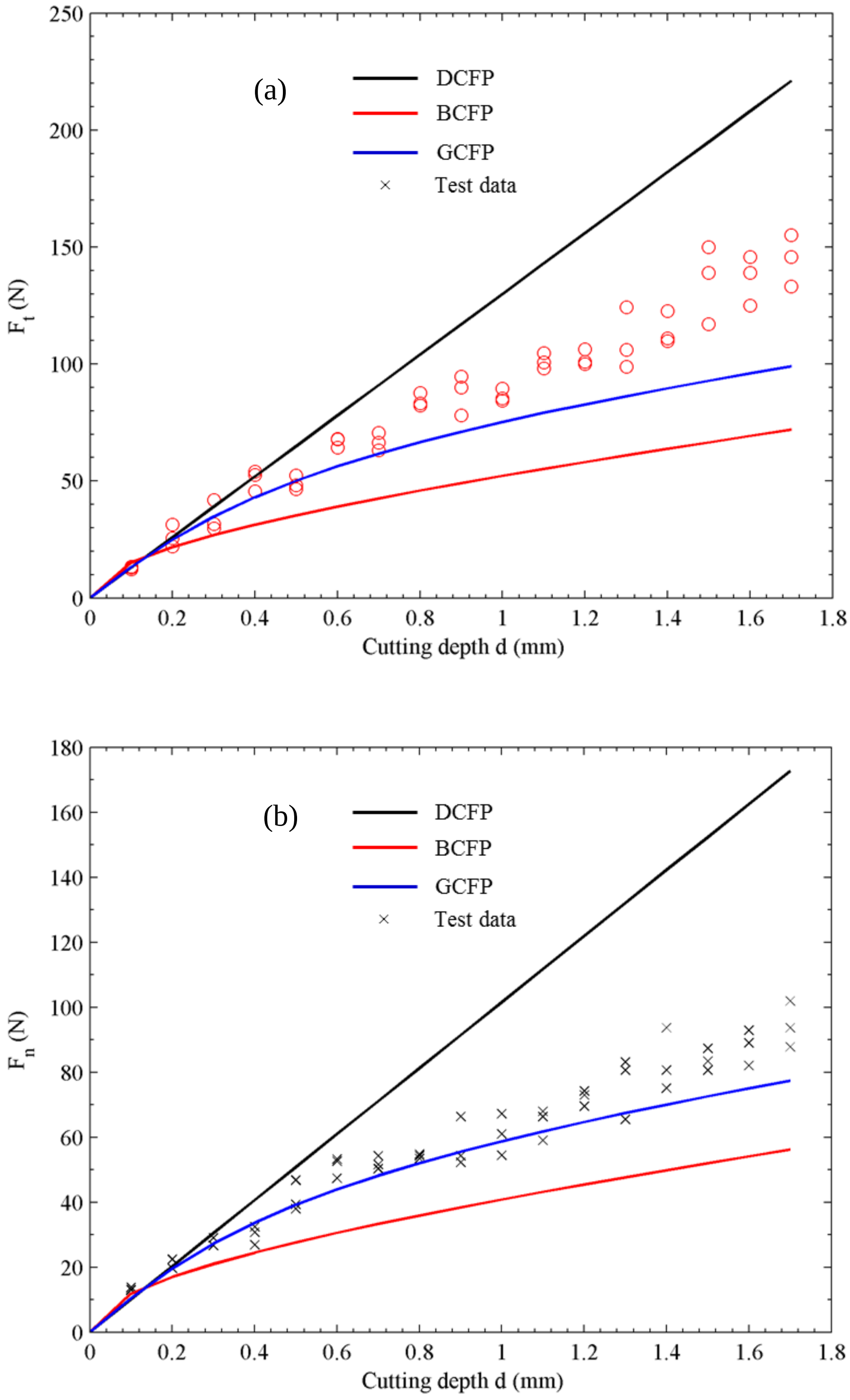

Fig. 5.8 Comparison of DCFP, BCFP and GCFP models for (a) tangential cutting force F_t and (b) normal cutting force F_n on TL sample with α=30°.

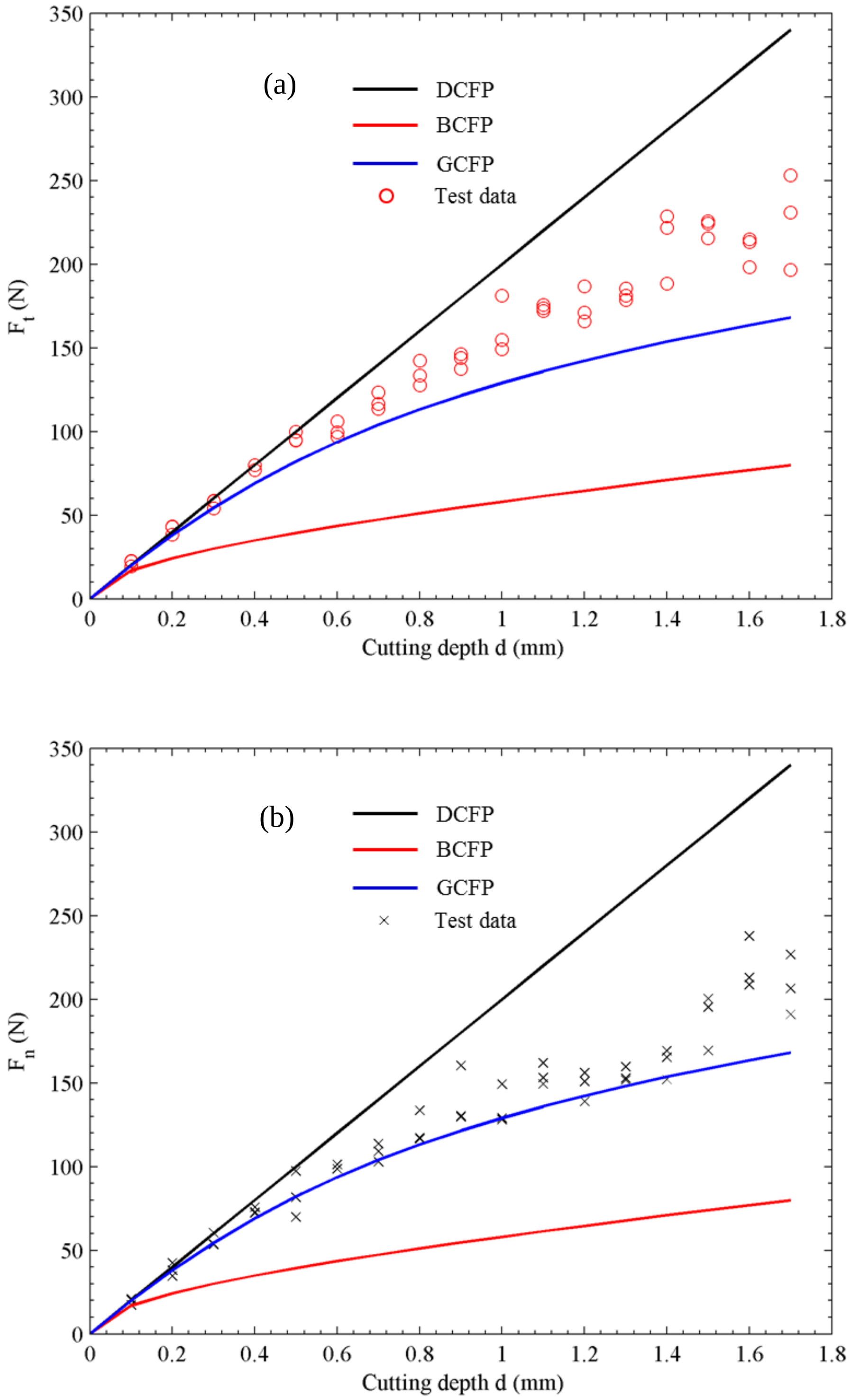

Fig. 5.9 Comparison of DCFP, BCFP and GCFP models for (a) tangential cutting force F_t and (b) normal cutting force F_n on TL sample with α=45°.

In terms of the validity of DCFP, BCFP and GCFP models in predicting the cutting forces, the DCFP model tends to overestimate the cutting forces, F_t and F_n, for all sets of α while the BCFP model underestimates them especially at large depth of cut (see Fig. 5.7-Fig. 5.9). The GCFP model proposed in this study, on the other hand, fits the experimental results well for α=15° (Fig. 5.7). It, however, underestimates values for the tangential cutting force for α=30°, 45° when the depth of cut is greater than 0.8 mm even it still gives a much better prediction of the normal cutting forces compared with the other two models (Fig. 5.8 and Fig. 5.9).

5.4.3 Test results for Savonnières sample

The force variations for the Savonnières rock with different depths of cut and different back rake angles are presented in Fig. 5.10-Fig. 5.12. They follow the same trends as observed on the Tuffeau rock, i.e., the increase in depth of cut results in the increase in cutting forces. The increasing trend also departs from linearity between forces and depth of cut when the depth is greater than the critical transition depth, which in this case is d_c=0.8 mm for α=30° as seen in Fig. 5.11.

A comparison between the tangential cutting force and the normal cutting force reveals that their rates of increment for Savonnières rock in general are greater with larger back rake angles. The rate of increment for the normal cutting force is higher than that of the tangential one, as shown in Fig. 5.10 and Fig. 5.11. Specifically, the normal component of the cutting force for d=1.8 mm is increased from around 130 N for α=15° to 280 N for α=30°, an increment of more than 100%; the tangential counterpart, by contrast, increases from 240 N to 380 N, approximately an increment of 60%. This is in good agreement with the experimental results obtained by Kaitkay and Lei (2005) who found that the ratio of tangential cutting force to normal cutting force reduces when the back rake angle increases. Cutting on Savonnières rock at α=45° displays an unanticipated behaviour: when the depth of cut is greater than 1.4 mm, the cutting forces experience a very sharp increase. Based on close observation during the test, this is likely to be caused by the accumulation of rock cuttings directly ahead of the cutter (difficult to remove immediately at this angle using a vacuum machine) that may obstruct the movement of the cutter (see Fig. 5.1), leading to additional resistance that the cutter has to overcome.

The prediction performances of the DCFP, BCFP and GCFP models can also be assessed by comparing the results shown in Fig. 5.10-Fig. 5.12. For the normal cutting force, GCFP model provides an acceptable estimate for all back rake angles tested whilst the DCFP model overestimates the true values and BCFP model significantly underestimates the true values (Fig. 5.10b, Fig. 5.11b and Fig. 5.12b). The predictions based on the GCFP model for the tangential cutting force at α=15° are slightly lower than the experimental results, but still performs better compared with the DCFP and BCFP models. As the back rake angle increases further (e.g., α=30°), the GCFP model tends to produce underestimated cutting forces. This trend is similar to that observed in cutting on the Tuffeau limestone. DCFP model appears to give a closer prediction on the tangential cutting force but the prediction from the BCFP model does not agree well at all with the experimental results. For α=45°, it appears the DCFP model has a better performance than the other two models, especially for the tangential cutting force. However we have to be aware that the measured cutting forces for $d \geq 1.4$ mm at this back rake angle may offer misleading information due to the accumulated rock debris as discussed above. Therefore, this set of data should be treated with caution. If we only examine the data for cutting depths less than 1.4 mm, the GCFP model still gives a much better cutting force prediction.

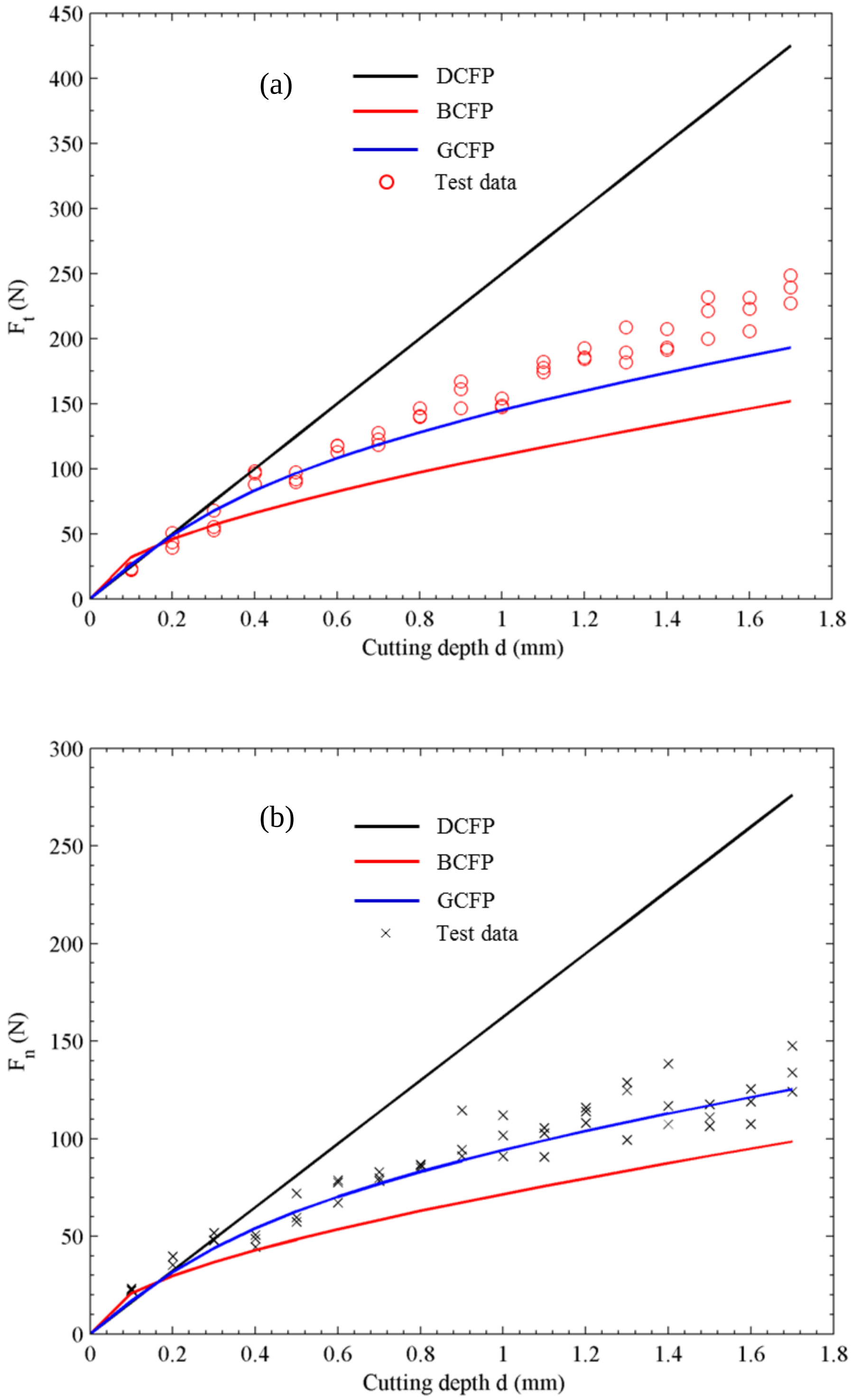

Fig. 5.10 Comparison of DCFP, BCFP and GCFP models for (a) tangential cutting force F_t and (b) normal cutting force F_n on SL sample with α=15°.

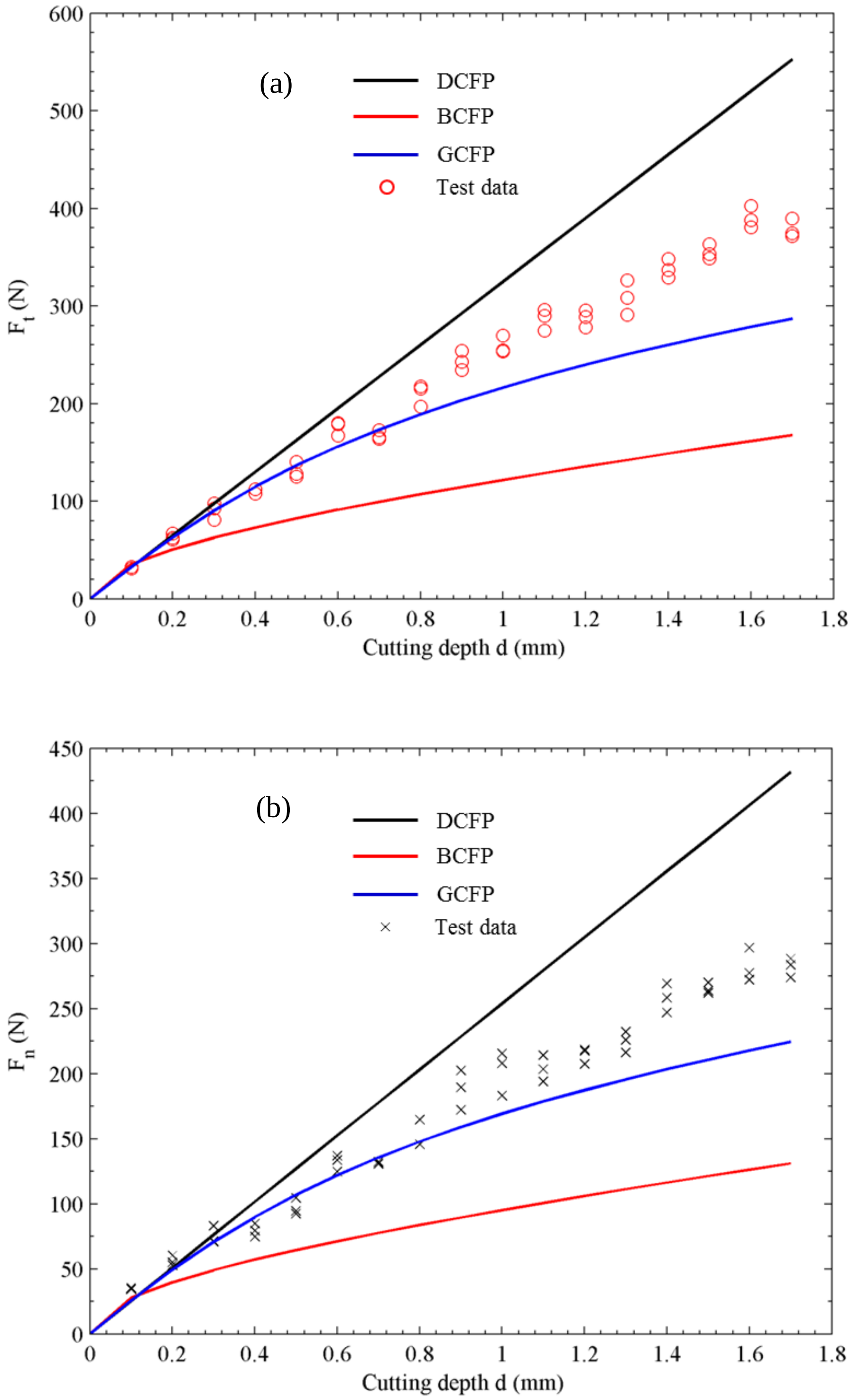

Fig. 5.11 Comparison of DCFP, BCFP and GCFP models for (a) tangential cutting force F_t and (b) normal cutting force F_n on SL sample with α=30°.

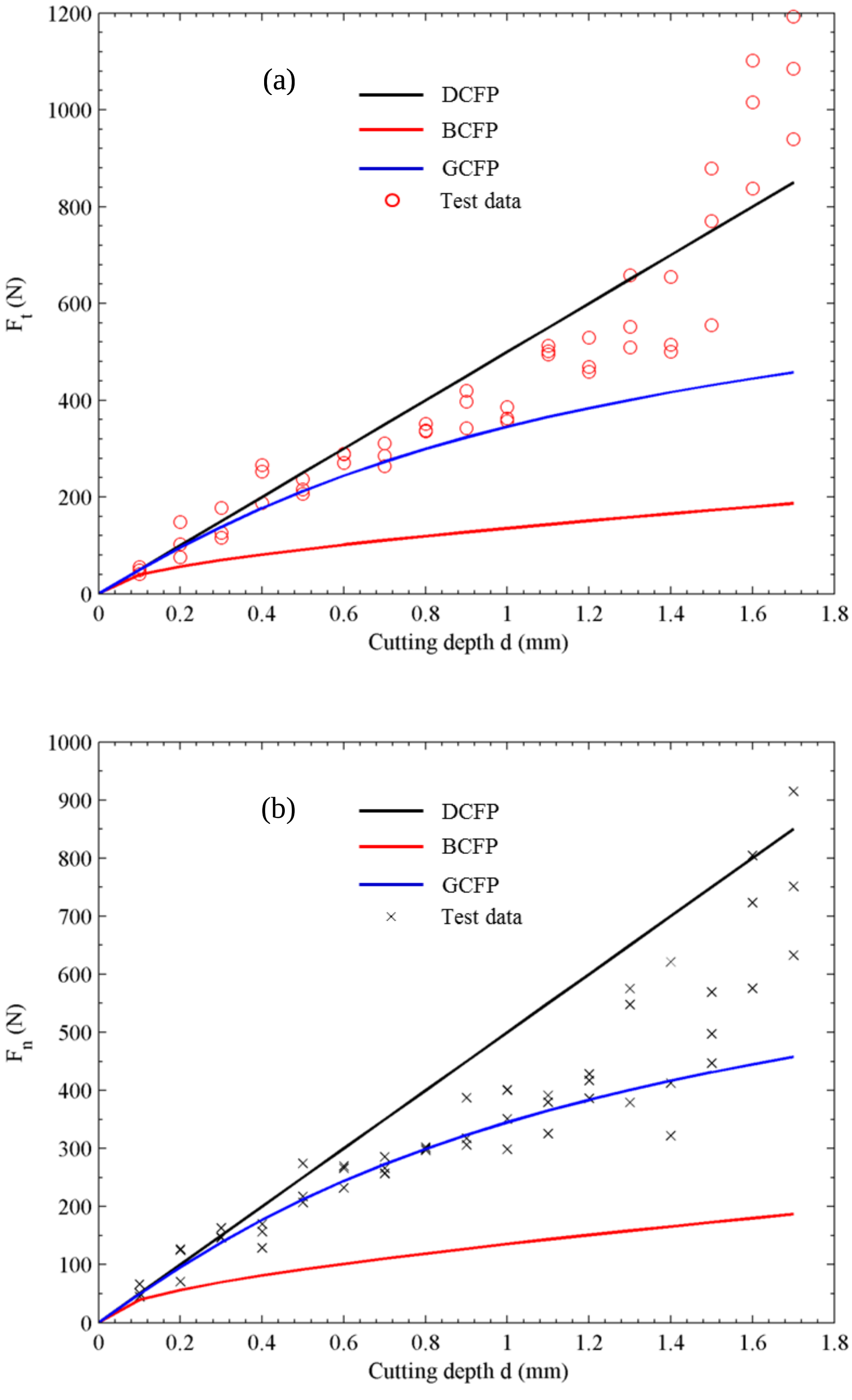

Fig. 5.12 Comparison of DCFP, BCFP and GCFP models for (a) tangential cutting force F_t and (b) normal cutting force F_n on SL sample with α=45°.

5.4.4 Discussion of the scratch tests results

From the tests results, it is clear that there are some similarities and discrepancies in cutting forces for the two types of rocks used in the cutting experiment. Similarities can be summarised as follows. Firstly, both rocks displays a non-linear increase of the cutting forces with increasing depth of cut. Secondly, at the same back rake angle, Tuffeau and Savonnières limestones have roughly the same tangential to normal cutting force ratio. Thirdly, the increase in cutting depth produces more scattered data for both rocks, suggesting the changing of cutting mode from ductile failure dominated process to the more unpredictable brittle failure dominated process.

In terms of discrepancy, subtle differences can be found in the raw force profiles for TL and SL rocks measured under the same operational parameters, i.e., the same depth of cut and the same back rake angle. As shown in Fig. 5.6, TL rock has some portion of the force profile resembling the saw tooth pattern while the force profile of the SL rock maintains its random noise pattern. As suggested in Richard et al. (2012), the random noise pattern implies the cutting in progress is associated with ductile failure while the sawtooth-like fluctuation indicates the brittle failure is taking place. Therefore, it might be appropriate to assume that the cutting is mainly brittle failure dominant for TL rock when the depth of cut is at 0.6 mm (Fig. 5.6) while for the SL rock the cutting is mainly ductile failure dominant at the same depth.

The GCFP model shows its potential in predicting the cutting forces, especially when the back rake angle is at 15°. However, as the back rake angle increases, the GCFP model becomes ineffective in predicting the cutting forces at large cutting depths. This could be attributed to that the brittle fracture failure during rock cutting may occur in a combination of two major fracture modes, i.e., crack opening mode (Mode I) and crack sliding mode (Mode II), but only K_{IC} is considered in the GCFP model. The pattern of fracturing during brittle regime cutting is still an issue with ongoing debates. Cherepanov and Cherepanov (1990) considered fracture propagation ahead of the cutter to be controlled by Mode II. Akono and Ulm (2011), on the other hand, suggested that brittle cutting to be a Mode I fracturing process. Further studies in Akono and Ulm (2014) and Akono et al. (2014) indicated that the rock cutting involves both Mode I and Mode II and which crack mode is dominant depends on the back rake angle.

Assuming that cutting at α=30° is under a mixed mode loading condition, the effective mixed mode I/II fracture toughness (K_{eff}) controls the cutting forces with $K_{eff} = \sqrt{K_I^2 + K_{II}^2}$. According to Ayatollahi and Aliha (2008), the ratio of K_{eff} to K_{IC} for the tested limestone is 1.49. The values of K_{eff} for TL and SL rocks can be derived based on this ratio and results are listed in Table 5.2. The predicted forces by replacing K_{IC} with K_{eff} in Eqs. (5.16) and (5.17) are shown in Fig. 5.13 and Fig. 5.14. It can be seen that predictions using the GCFP model with K_{eff} for cutting at α=30° performs much better compared with the original model using only K_{IC}. This in a way suggests that the fracturing of the brittle failure cutting is more likely to be in the mixed mode (I and II) condition.

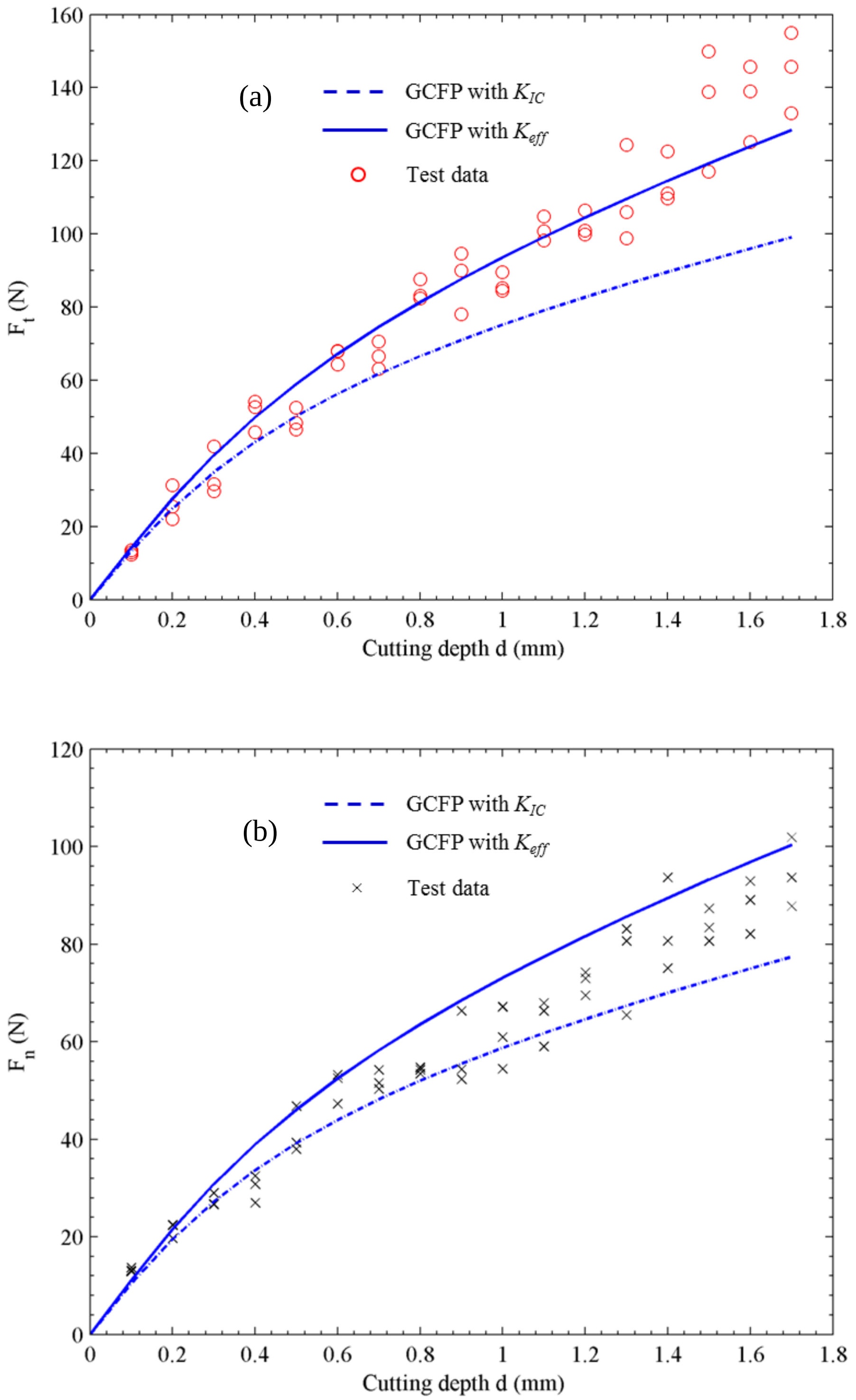

Fig. 5.13 Comparison the prediction of GCFP model with K_{IC} and K_{eff} for (a) tangential cutting force F_t and (b) normal cutting force F_n on TL sample for α=30°.

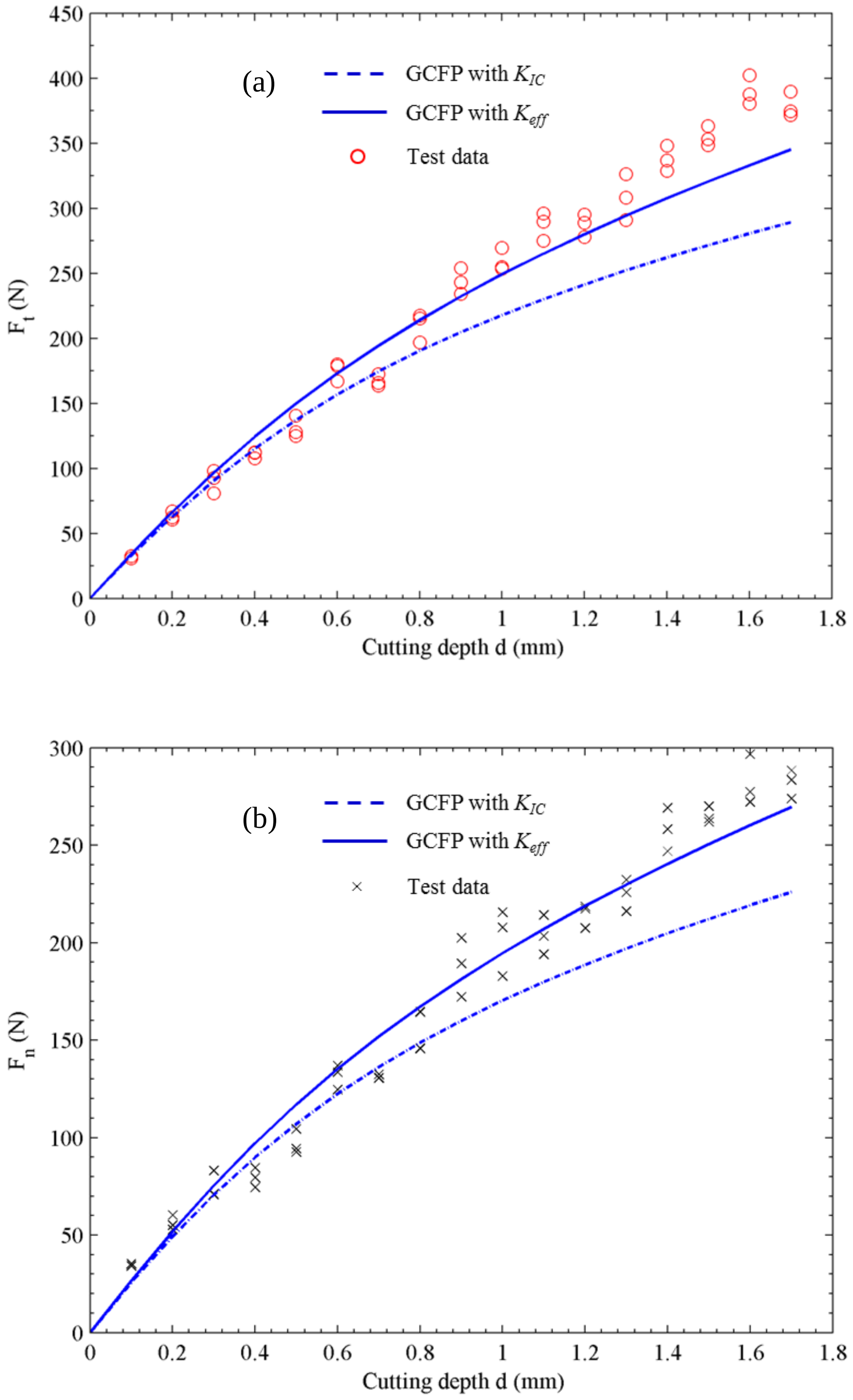

Fig. 5.14 Comparison the prediction of GCFP model with K_{IC} and K_{eff} for (a) tangential cutting force F_t and (b) normal cutting force F_n on SL sample for α=30°.

5.5 Conclusions

There exist two distinct material removal mechanisms in rock cutting, ductile and brittle failure modes, whose occurrence depends on rock properties, the depth of cut and the back rake angle. At shallow depth of cut and large back rake angle, ductile-mode cutting dominates and the cutting forces are mainly controlled by the uniaxial compressive strength of the rock. On the other hand, at large depth of cut and small back rake angle, brittle failure is dominant and the fracture toughness becomes the main rock property to control the cutting force responses. In this study, a new generalised cutting force prediction model is proposed, taking into account the fact that both the ductile and brittle failure modes generally coexist in rock cutting. To validate the model, experiments are carried out on Tuffeau and Savonnières rocks at different depths of cut for different back rake angles. The main conclusions based on the comparison study are summarised below:

Tangential and normal cutting forces increase with cutting depth and back rake angle. The normal cutting force has a higher increasing rate compared to the tangential cutting force with respect to the increase in back rake angles and, as a result, the ratio of tangential to normal cutting force decreases. This is mainly caused by the change in the material flowing direction from upward to downward as the back rake angle increases.

The experimental cutting data fall within the region bounded by the DCFP and the BCFP models, which can be viewed as an evidence to support the argument that rock cutting process is a combined action of both ductile and brittle failures and the dominant mode depends on rock properties and the operating parameters such as the cutting depth and the back rake angle.

The DCFP model is only valid for shallow cutting where rock failure is dominated by the ductile failure regime. The DCFP model overestimates the cutting forces for large cutting depth when the brittle failure mode is dominating. The BCFP model, on the other hand, always underestimates the true cutting forces for large cutting depths. Since the rocks used in this study are quasi-brittle material, using the BCFP model that is based on LEFM theory to predict the cutting forces might not be appropriate.

The newly proposed GCFP model gives a very good prediction of the cutting forces at the back rake angle of 15°. For large back rake angles, the predictability of the model deteriorates but its performance is still much better compared with the other two models. If the brittle failure is assumed to take place in mixed-mode (I and II) fracturing, the predictability of the GCFP model can be improved. It can be concluded based on the comparison study that the GCFP model developed in this study is more appropriate compared with the other two models for the prediction of cutting forces in rock cutting.

Note that the GCFP model is dependent on the critical failure transition depth as it is expressed effectively as a weighted average of forces of the two failure regimes using a failure-mode mixture ratio. A versatile equation for the critical transition depth prediction is required for the application of the GCFP model for different cutting conditions. Therefore, more extensive experiments are needed to derive such a model for a broader range of rocks under different cutting operational parameters.

The scope of this study is limited due to the fact that only two types of rocks are tested. However, it demonstrates the necessity of considering the coexistence of both the ductile and brittle failures when describing the force responses in rock cutting or scratching. It is expected that the approach developed in this study can be equally applicable for other types of cutting applications as long as there is a failure mode transition during the cutting process.

Acknowledgement

The work has been supported by the Deep Exploration Technologies Cooperative Research Centre whose activities are funded by the Australian Government's Cooperative Research Centre Programme. This is DET CRC Document. The authors would like to give special thanks to Luiz Franca for his generous support and constructive suggestions when performing the tests at CSIRO.

References

Akono A-T, Ulm F-J (2014) An improved technique for characterizing the fracture toughness via scratch test experiments. Wear 313:117-124 doi:10.1016/j.wear.2014.02.015

Akono A-T, Ulm F-J, Bažant ZP (2014) Discussion: Strength-to-fracture scaling in scratching. Engineering Fracture Mechanics 119:21-28 doi:10.1016/j.engfracmech.2014.02.025

Akono AT, Reis PM, Ulm FJ (2011) Scratching as a fracture process: From butter to steel. Physical Review Letters 106:204302

Akono AT, Ulm FJ (2011) Scratch test model for the determination of fracture toughness. Engineering Fracture Mechanics 78:334-342

Akono AT, Ulm FJ (2012) Fracture scaling relations for scratch tests of axisymmetric shape. Journal of the Mechanics and Physics of Solids 60:379-390

Ayatollahi MR, Aliha MRM (2008) On the use of Brazilian disc specimen for calculating mixed mode I–II fracture toughness of rock materials. Engineering Fracture Mechanics 75:4631-4641 doi:10.1016/j.engfracmech.2008.06.018

Barletta M, Gisario A, Lusvarghi L, Bolelli G, Rubino G (2008) On the combined use of scratch tests and CLA profilometry for the characterization of polyester powder coatings: Influence of scratch load and speed. Applied Surface Science 254:7198-7214 doi:10.1016/j.apsusc.2008.05.315

Bieniawski ZT, Bernede MJ (1979) Suggested methods for determining the uniaxial compressive strength and deformability of rock materials: Part 1. Suggested method for determining deformability of rock materials in uniaxial compression. International Journal of Rock

Mechanics and Mining Sciences & Geomechanics Abstracts 16:138-140 doi:http://dx.doi.org/10.1016/0148-9062(79)91451-7

Bieniawski ZT, Hawkes I (1978) Suggested methods for determining tensile strength of rock materials. International Journal of Rock Mechanics and Mining Sciences & Geomechanics Abstracts 15:99-103 doi:http://dx.doi.org/10.1016/0148-9062(78)90003-7

Bilgin N, Demircin MA, Copur H, Balci C, Tuncdemir H, Akcin N (2006) Dominant rock properties affecting the performance of conical picks and the comparison of some experimental and theoretical results. International Journal of Rock Mechanics and Mining Sciences 43:139-156 doi:10.1016/j.ijrmms.2005.04.009

Che D, Ehmann K (2014) Experimental study of force responses in polycrystalline diamond face turning of rock. International Journal of Rock Mechanics and Mining Sciences 72:80-91 doi:http://dx.doi.org/10.1016/j.ijrmms.2014.08.014

Cherepanov AG, Cherepanov GP (1990) Cutting resistance of rocks. Strength of Materials 22:1626-1645 doi:10.1007/bf00767151

Detournay E, Defourny P (1992) A phenomenological model for the drilling action of drag bits. International Journal of Rock Mechanics and Mining Sciences & Geomechanics Abstracts 29:13-23 doi:10.1016/0148-9062(92)91041-3

Ersoy A, Buyuksagic S, Atici U (2005) Wear characteristics of circular diamond saws in the cutting of different hard abrasive rocks. Wear 258:1422-1436 doi:10.1016/j.wear.2004.09.060

Evans I (1965) The force required to cut coal with blunt wedges. International Journal of Rock Mechanics and Mining Sciences & Geomechanics Abstracts 2:1-12 doi:http://dx.doi.org/10.1016/0148-9062(65)90018-5

Germay C, Denoël V, Detournay E (2009) Multiple mode analysis of the self-excited vibrations of rotary drilling systems. Journal of Sound and Vibration 325:362-381 doi:http://dx.doi.org/10.1016/j.jsv.2009.03.017

Göktan RM (1990) Effect of cutter pick rake angle on the failure pattern of high-strength rocks. Mining Science and Technology 11:281-285 doi:http://dx.doi.org/10.1016/0167-9031(90)90981-W

He X, Xu C (2015a) Discrete element modelling of rock cutting: from ductile to brittle transition. International Journal for Numerical and Analytical Methods in Geomechanics doi:10.1002/nag.2362

He X, Xu C (2015b) On the critical failure mode transition depth for rock cutting with different back rake angles. Journal of the Mechanics and Physics of Solids (under review)

He X, Xu C (2015c) Specific Energy as an Index to determine the Critical Failure Mode Transition Depth in Rock Cutting. Rock Mechanics and Rock Engineering doi: 10.1007/s00603-015-0819-6

Huang H, Lecampion B, Detournay E (2013) Discrete element modeling of tool-rock interaction I: rock cutting. International Journal for Numerical and Analytical Methods in Geomechanics 37:1913-1929 doi:10.1002/nag.2113

Kaitkay P, Lei S (2005) Experimental study of rock cutting under external hydrostatic pressure. Journal of Materials Processing Technology 159:206-213 doi:10.1016/j.jmatprotec.2004.04.418

Klecka M, Subhash G (2008) Grain size dependence of scratch-induced damage in alumina ceramics. Wear 265:612-619 doi:10.1016/j.wear.2007.12.012

Kuru E, Wojtanowicz AK (1992) An Experimental Study of Friction Induced By PDC Cutters During Rock Cutting. Paper presented at the Annual Technical Meeting, Calgary, Alberta, Jun 7 - 10, 1992 1992

Kuruppu MD, Obara Y, Ayatollahi MR, Chong KP, Funatsu T (2014) ISRM-Suggested Method for Determining the Mode I Static Fracture Toughness Using Semi-Circular Bend Specimen. Rock Mechanics and Rock Engineering 47:267-274 doi:10.1007/s00603-013-0422-7

Lin J-S, Zhou Y (2013) Can scratch tests give fracture toughness? Engineering Fracture Mechanics 109:161-168 doi:http://dx.doi.org/10.1016/j.engfracmech.2013.06.002

Nicodeme P (1997) Transition between ductile and brittle mode in rock cutting. Ecole Polytechnique, Paris

Nishimatsu Y (1972) The mechanics of rock cutting. International Journal of Rock Mechanics and Mining Sciences 9:261-270

Rajabov V, Miska SZ, Mortimer L, Yu M, Ozbayoglu ME (2012) The Effects of Back Rake and Side Rake Angles on Mechanical Specific Energy of Single PDC Cutters with Selected Rocks at Varying Depth of Cuts and Confining Pressures. Paper presented at the IADC/SPE Drilling Conference and Exhibition, San Diego, California, USA, 6-8 March 2012

Randall NX, Favaro G, Frankel CH (2001) The effect of intrinsic parameters on the critical load as measured with the scratch test method. Surface and Coatings Technology 137:146-151 doi:10.1016/s0257-8972(00)01097-5

Rice JR (1968) A Path Independent Integral and the Approximate Analysis of Strain Concentration by Notches and Cracks. Journal of Applied Mechanics 35:379-386 doi:10.1115/1.3601206

Richard T (1999) Determination of rock strength from cutting tests. Master thesis, University of Minnesota

Richard T, Dagrain F, Poyol E, Detournay E (2012) Rock strength determination from scratch tests. Engineering Geology 147-148:91-100 doi:10.1016/j.enggeo.2012.07.011

Richard T, Detournay E, Drescher A, Nicodeme P, Fourmaintraux D (1998) The Scratch Test As A Means To Measure Strength of Sedimentary Rocks. Paper presented at the SPE/ISRM Rock Mechanics in Petroleum Engineering, Trondheim, Norway, 8-10 July 1998

Roxborough FF Research in mechanical rock excavation: progress and prospects. In: Proceedings of the Rapid Excavation and Tunneling Conference, 1985. pp 16-20

Su O, Akcin NA (2011) Numerical simulation of rock cutting using the discrete element method. International Journal of Rock Mechanics and Mining Sciences 48:434-442 doi:10.1016/j.ijrmms.2010.08.012

Tan Y, Jiang S, Nie S, Yang D, Zhang G, Peng R (2012) Prestress Scratching on SiC Ceramic. International Journal of Applied Ceramic Technology 9:322-328 doi:10.1111/j.1744-7402.2011.0202726.x

Tönshoff HK, Hillmann-Apmann H, Asche J (2002) Diamond tools in stone and civil engineering industry: cutting principles, wear and applications. Diamond and Related Materials 11:736-741 doi:10.1016/s0925-9635(01)00561-1

Verhoef PNW (1997) Wear of rock cutting tools: Implications for the site investigation of rock dredging projects. PhD, Technical University Delft

Chapter 6

Conclusions and recommendations

6.1 Overall conclusions

This thesis presents a framework to characterise the rock/cutter interaction by quantitatively modelling the cutting forces and the critical failure mode transition depth with respect to varying cutting conditions. DEM modelling tool was employed to study the rock failure mechanism during cutting process, with emphasis on the identification of major rock properties that affect the failure transition from ductile to brittle mode. A comprehensive set of laboratory rock cutting tests were carried out to provide the data to explore the following topics: the influences of rock properties and cutting geometry on rock cutting mechanisms; the influences of varying cutting combinations on the failure mode transition; and the development of a robust generalised cutting force prediction model. Based on the outcomes of these research works, the following overall conclusions can be drawn:

1. The DEM modelling has successfully reproduced an important feature commonly observed in laboratory cutting tests, namely, the ductile-to-brittle cutting mode transition as the depth of cut increases. The critical transition depth is found to be proportional to DEM particle size and inversely proportional to the square of rock brittleness, suggesting that the critical transition depth is dependent on rock grain size, rock compressive strength as well as rock tensile strength, which was ignored in most previous numerical modelling investigations.

2. Results from the cutting tests conducted show that cutting force is insensitive to cutting velocity but the force increases when the back rake angle increases. As the specific cutting energy is proportional to the cutting force, it also follows the same trend with regard to the changes in cutting velocity and back rake angle.

3. The specific cutting energy transition model underestimates the critical failure mode transition depth compared with the size effect law model derived based on Bažant’s theory. The size effect law model fits the cutting data well and can give more accurate estimate of the critical transition depth.

4. The failure mode transition for Savonnières is shown to occur at greater depth of cut compared with that for Tuffeau under the same cutting conditions. Considering the fact that both rocks have approximately the same value of brittleness but Savonnières has coarser grains, the results confirm the findings from the DEM simulations that the critical transition depth is proportional to the mineral grain size in rocks.

5. The generalised cutting force prediction model is a significant advance towards better characterisation of the rock-cutter interactions. As most existing models are either focusing on ductile failure mode or brittle mode, their scope of applications is normally limited. In general, they can only provide good estimate for certain conditions but fail to give reasonable predictions over a wide range of cutting parameters. It was demonstrated that the proposed generalised model can give much more accurate predictions for cutting forces in vastly different rock cutting scenarios where both ductile and brittle failures commonly coexist.

6.2 Limitations and future perspectives

Similar to any other research, there are limitations in the current study and recommendations for future works. They are summarised below:

1. For the DEM rock cutting simulation, the synthetic rock sample was represented by an assembly of limited discrete elements (particles), far less than the number of mineral grains contained in real rocks. This would pose restrictions on the interpretation of the simulation results and one should be cautious when making comparison with results from laboratory rock cutting tests. A large scale model would be helpful to provide more realistic analysis so more reliable results can be derived.

2. The experimental results have shown that cutting forces and rock failure mechanism are sensitive to the back rake angle. Some numerical investigations using DEM in this aspect would be very useful to provide further insights into the relationship between the cutting mechanism and different back rake angles, particularly to understand the crack initiation, propagation and calescence leading to chip formations.

3. In the current study, when calculating the specific cutting energy, the volume of the removed material was taken as the product of projected contact area and the cutting distance. This is only an approximation to calculate the volume of materials being removed. A more accurate model is needed for the volume estimation, particularly for cases of brittle-dominant cutting where there are significant side chips formed along the cut groove walls due to lateral crack propagations.

4. For cutting at large back rake angle (e.g., 45°), the cut debris accumulate ahead of the cutter and cannot be removed easily. This leads to debris re-crushing and additional resistance to cutter movement and therefore the cutting forces recorded are not the truce

forces used for cutting the fresh rock. One way to potentially solve this problem is to perform the slab cutting where the width of the rock sample is smaller than the cutter width, instead of groove cutting.

5. The crack propagation in rocks under cutting is an extremely complex problem. It is still uncertain if the brittle-mode rock cutting is progressing with fracturing the rock in opening mode, sliding mode or the mixture of both. Therefore, the assumption that the fracture mode changes from opening mode to sliding mode at large back rake angle, made in the proposed generalised force prediction model, remains questionable. This uncertainty could not be eliminated until the stress or strain field around the cutting-induced crack tip is fully understood, which remains extremely challenging.